Nordic Seas Heat Loss, Atlantic Inflow, and Arctic Sea Ice cover over the last century

Lars H. Smedsrud [1]*, Morven Muilwijk [1]*, Ailin Brakstad [1]*, Erica Madonna [1]*, Siv K. Lauvset [2]*, Clemens Spensberger [1]*, Andreas Born [3]*, Tor Eldevik [1]*, Helge Drange [1]*, Emil Jeansson [2]*, Camille Li [1]*, Are Olsen [1]*, Øystein Skagseth [4]*, Donald A. Slater [5], Fiamma Straneo [6], Kjetil Våge [1] * and Marius Årthun [1]*.

[1] Geophysical Institute, University of Bergen, Norway.

[2] NORCE Norwegian Research Centre, Bergen Norway.

[3] Department for Earth Science, University of Bergen, Norway.

[4] Institute for Marine Research, Bergen, Norway.

[5] St. Andrews or University of Edinburg, Scotland, United Kingdom.

[6] Scripps Institution of Oceanography, UCSD, USA.

* Bjerknes Centre for Climate Research

Corresponding author: Lars H. Smedsrud (Lars.Smedsrud@uib.no)

Key Points:

- Nordic Seas heat loss dominates the mean Arctic Ocean heat loss and its variability.
- Atlantic Water volume and heat transport has increased over the last century consistently with increased wind forcing and heat loss.
- Ocean heat transport anomalies affect Greenland melting, Arctic sea ice, water transformations, and Arctic CO_2 uptake.

Abstract

Poleward ocean heat transport is a key process in the earth system. We detail and review the northward Atlantic Water (AW) flow, Arctic Ocean heat transport, and heat loss to the atmosphere since 1900 in relation to sea ice cover. Our synthesis is largely based on a sea ice-ocean model forced by a reanalysis atmosphere (1900-2018) corroborated by a comprehensive hydrographic database (1950-), AW inflow observations (1996-), and other long-term time series of sea ice extent (1900-), glacier retreat (1984-) and Barents Sea hydrography (1900-). The Arctic Ocean, including the Nordic and Barents Seas, has warmed since the 1970s. This warming is congruent with increased ocean heat transport and sea ice loss and has contributed to the retreat of marine-terminating glaciers on Greenland. Heat loss to the atmosphere is largest in the Nordic Seas (60% of total) with large variability linked to the frequency of Cold Air Outbreaks and cyclones in the region, but there is no long-term statistically significant trend. Heat loss from the Barents Sea (~30%) and Arctic seas farther north (~10%) is overall smaller, but exhibit large positive trends. The AW inflow, total heat loss to the atmosphere, and dense outflow have all increased since 1900. These are consistently related through theoretical scaling, but the AW inflow increase is also wind-driven. The Arctic Ocean CO2 uptake has increased by ~30% over the last century - consistent with Arctic sea ice loss allowing stronger air-sea interaction and is ~8% of the global uptake.

Plain Language Summary

The major flow to and from the Arctic Ocean occurs across the Greenland-Scotland Ridge. The inflow is mostly warm Atlantic Water (AW) flowing northwards and cooling gradually. After completing different loops within the Arctic Ocean, portions of this water eventually flows south as cold freshened Polar Water at the surface and cold, dense Overflow Water at depth. We review and synthesize how the AW cooling evolved over the last century in relation to the Arctic sea ice cover. In the mean 60% of the heat loss occurred in the Nordic Seas, 30% in the Barents Sea, and only 10% in the Arctic seas further north. Arctic sea ice decrease the last century created more open water and permitted stronger ocean heat loss. The ocean volume and heat transport also increased, consistently with increased heat loss, and increased wind forcing. Ocean temperatures have generally increased in many areas during the last 50 years, and on Greenland this drove the retreat of marine-terminating glaciers. Variability in ocean heat loss to the atmosphere was primarily driven by Cold Air Outbreaks and cyclones in the Nordic and Barents Seas, and explain variability in Arctic Ocean CO_2 uptake, being ~8% of the global uptake.

1 Introduction and focus

The individual seas of the Arctic all lose heat to the atmosphere when the yearly average is calculated. The heat loss and associated Atlantic Water (AW) circulation (Fig. 1) have been widely studied due to their important consequences for each regional sea, the Arctic climate as a whole, and the Global Ocean circulation. The actual surface heat flux is only measured in short periods over a limited area and varies over time and region in profound ways. The main goal of this paper is to quantify and describe this heat loss, why it has increased over the last century, and how it relates to sea ice cover, CO_2-uptake, and atmospheric circulation, as well as the general warming trend from climate change. While it has been known for more than 100 years that AW is the primary heat source for the Arctic Ocean (Helland-Hansen and Nansen, 1909), much of the variability, trends, and related consequences are still undetermined.

A most important consequence of ocean heat loss is that when sea water cools, it becomes denser. The heat loss in the Arctic Ocean is thus the primary driver of the transformation of the warm inflowing water into dense water that fills the North Atlantic at depth (Mauritzen 1996; Pemberton et al., 2015; Gebbie & Huybers, 2011; Chafik & Rossby, 2019;). The cooling also increases the CO_2 solubility, such that the Arctic Ocean is an important sink of CO2 (Takahashi et al., 2009). If the water column is strongly stratified or the surface water sufficiently fresh, cooling leads to sea ice formation, which dramatically changes energy, momentum, and biogeochemistry fluxes between the ocean and the atmosphere. So the heat loss dictates variability in the Arctic sea ice cover, but it also works the other way with sea ice regulating the heat loss. If less heat is lost to the atmosphere, the heat remaining in the ocean can result in increased melting of sea ice further downstream or increased melting of marine-terminating glaciers with potential implications for ice discharge from the Greenland Ice Sheet (e.g., Lindeman et al., 2020; Mouginot et al., 2015). Ocean temperatures on the Greenland shelf are above 0°C, and variability in ocean temperature drives the advance and retreat of marine-terminating glaciers (Straneo & Heimbach, 2013). Finally, the heat loss itself is driven by atmospheric conditions, which are clearly modulated by temporal and spatial changes of the wind field in different regions (Simonsen & Haugan, 1996). We hereafter use the term ‘heat loss’ for the spatially integrated surface heat flux over a region like the Nordic Seas in TW (terawatt = 10^{12} W), and use the term ‘heat flux’, meaning the specific value at the surface for a smaller area or an observation in the unit W/m² (Table 1).

Our region of interest is the interconnected ocean north of the Bering Strait and the Greenland-Scotland Ridge (GSR), the Arctic gateways to the Pacific and Atlantic oceans, respectively. We prefer to term this collection of seas the Arctic Ocean (Fig. 2), which is consistent with the official Arctic Ocean definition of the International Hydrographic Office (IHO 1953; Jakobsson & Macnab, 2006). We divide the Arctic Ocean into three regional seas that have fundamentally different behavior when it comes to heat loss and ocean transport; the Nordic Seas, the Barents Sea, and the remaining area termed the Polar Sea (Hopkins, 1991). The Nordic Seas include the Greenland, Iceland, and Norwegian Seas. The Polar Sea covers the Beaufort, Chukchi, East Siberian, Laptev and Kara Seas, as well as the two main deep Arctic basins (Canadian and Eurasian Basin, Fig. 2). Some authors use the term 'Central Arctic Ocean' for what is termed the Polar Sea here. We thus exclude the Baffin and Hudson Bays west of Greenland as they are not well connected with the remaining Arctic Ocean (Hopkins, 1991). The name 'Arctic Mediterranean' has also been used for what we term the Arctic Ocean here, especially in oceanographic literature, starting with Sverdrup et al. (1942).

The Arctic Ocean acts like a double estuary (Fig. 1). This implies that AW is the main inflow and two major outflows: fresh Polar Water (PW) at the surface and dense Overflow Water (OW) in the deep (Eldevik & Nilsen, 2013). The concept of the Arctic Ocean as a double estuary dates back to Stigebrandt (1981), who also estimated the two main outflows across the GSR. From observations of the AW inflow, a total (net) transport of 8.0 ±0.7 Sv across the GSR has been estimated (between 1993 and 2017; Østerhus et al., 2019; Tsubouchi et al., 2020). The two secondary inflows are relatively minor, bringing 0.8 Sv through the Bering Strait (Woodgate et al., 2006), and ~0.1 Sv from river runoff (Carmack et al., 2016). The total inflow is balanced by a net southward flow of PW through the Canadian Archipelago and the southward flow of both PW and OW across the GSR (Fig. 1). A recent estimate (1993-2016) indicates 2.7 Sv outflow of PW and 5.6 Sv of OW (Tsubouchi et al., 2020).

As will be shown, one of our main findings is that the Arctic Ocean heat loss and the Ocean Heat Transport (OHT) into the Arctic Ocean were smaller in the early part of the last century than in recent decades. The following increase in heat loss to the atmosphere has occurred in parallel with the overall warming trend and loss of Arctic sea ice. What has caused the heat loss and transport to increase, and what are the consequences? Our focus here is to review current knowledge of the variability and influences of AW inflow. We are guided by a century-scale model simulation corroborated by observations, and synthesize to what extent the inflow trend and variability from 1900 to present influences Nordic Seas heat loss,

properties of the deep water properties and outflows, Arctic CO_2 uptake, Greenland Glaciers, and Arctic sea ice cover (Fig. 1).

To determine these possible influences, we need to establish the relevant long-term means and trends and then investigate the physical mechanisms contributing to the simulated and observed changes. We start with a review of relevant conditions in Section 2. Realizing we need to examine the variability over the last century in a consistent way, we next describe the methods used to do this (Section 3). Naturally, observational coverage has increased over time, and only a few time series go back to the early 1900s, so simulations must be used the further back one goes. Section 4 presents our new estimates of the centennial mean values (1900–2000), before we dive into the variability and trends over time. The new results are discussed in Section 5 in light of existing knowledge (Section 2). We conclude on the implications of the Arctic Ocean heat loss variability in Section 6 and speculate about present trends persisting into the future.

2 Review of relevant processes and conditions

Over the last 100 years, estimates of Arctic Ocean heat loss to the atmosphere have evolved substantially. Thanks to the early Arctic explorer-oceanographers and a long history of fishery-related surveys, there are century-long observational records in the region that document how these waters have changed over time. Mosby (1962) reported the mean hydrographic properties, volume, and heat budgets of the regional seas based on observations from the Maud Expedition (1918-1925) onwards. Many estimates were close to present values, and the AW inflow was identified as the largest heat source. However, as we will present here, the AW inflow volume estimate of 3.6 Sv across the GSR was probably about half of the correct value, and the 90 TW heat loss of the Polar Sea much too high (Mosby 1962). Bjerknes (1964) documented the existence of large year-to-year fluctuations in the North Atlantic and Nordic Seas temperature related to radiation, air-sea heat fluxes, and OHT. Bjerknes (1964) found that the atmosphere generally forces the ocean via the exchanges of heat and momentum, but also that ocean temperatures can influence the thermodynamics of the atmosphere.

It has also been evident for a long time that the North Atlantic dominates northward OHT in a global perspective. This dominance was consistently quantified to be 15 Sv and ~600 TW across 45°N based on global hydrographic data by Ganachaud & Wunsch (2000). Recently

Lozier et al. (2019) found that a similar volume makes it as far north as 58°N, but the OHT has here lowered to ~450 TW, and there is substantial wind-driven variability.

2.1 Atmospheric forcing of heat loss

The general regional circulation within the Arctic Ocean is driven by wind stress (Timmermanns & Marshall 2020). We focus on the AW inflow and transformation by surface heat loss for this review (Fig. 1), and not the internal circulation. In the annual mean, the atmosphere north of 60°N loses about 2500 TW of heat to space (Trenberth & Fasullo 2017; Trenberth et al., 2019). This loss is balanced by northward heat transport in the atmosphere and ocean. The bulk of the heat transport happens in the atmosphere, while the OHT is on the order of 500 ±100 TW or 20% (Trenberth & Fasullo 2017, Trenberth et al., 2019). The AW OHT variability since 2000 across 26°N is about ±20%, and uncertainties are thus large for this OHT estimate (Trenberth & Fasullo 2017). The possibility of large variability across multiple time scales, sparked interest in this review. A large portion of the OHT is lost to the Arctic atmosphere, mostly in the Nordic and Barents Seas (Serreze et al. 2007). On long time scales, when the climate is at equilibrium, the OHT and ocean heat loss to the atmosphere will balance.

There is a pronounced seasonal cycle in the ocean heat loss around the annual mean, driven predominantly by radiation (Serreze et al., 2007). Indeed, it is only from September to March that the ocean loses heat to the atmosphere (Serreze et al., 2007; Mayer et al., 2019); from April to August, the ocean gains heat on average. The downward surface heat flux peaks in July at around 100 W/m² (Serreze et al. 2007), while the upward heat loss is more evenly distributed throughout winter. In addition to the seasonal cycle, ocean heat loss exhibits variability on a range of other time scales. There are large year-to-year (interannual) variations, owing mainly to the large internal variability of atmospheric heat transport (Fan et al., 2015; Mayer et al., 2019). On decadal scales, Bjerknes (1964) hypothesized that there is strong compensation between the ocean and atmospheric heat transport. This mechanism, called Bjerknes compensation, was later confirmed for decadal and even longer time scales (e.g., Shaffrey & Sutton 2006; Outten et al., 2018), but on year-to-year time scales, the

192 atmosphere and ocean heat transports vary relatively independently (Shaffrey and Sutton
193 2006).

194 The reason for the large variability in atmospheric heat transport is that much of it is
195 associated with weather events (Overland et al. 1996), reflecting the chaotic nature of the
196 atmosphere. Weather dominates the mid-latitude atmospheric variability on times scales from
197 daily to interannual, causing fluctuations in the position and strength of the North Atlantic jet
198 stream and storm track (e.g., Woollings et al., 2010). From a synoptic perspective, the
199 importance of single weather events for the atmospheric heat transport to high latitudes is
200 best demonstrated by the phenomenon known as warm moist intrusions (e.g., Woods et al.,
201 2013). These intrusions are relatively narrow and predominantly meridional air streams that
202 transport warm and moist airmasses into the Arctic. Such air streams are typically associated
203 with atmospheric blocking events (Woods et al., 2013), or sequences of extratropical
204 cyclones (Binder et al., 2018; Messori et al., 2018). However, the exact relationship between
205 the synoptic and large-scale circulation features that drive heat and moisture transport to the
206 Arctic remains a topic of active research (Papritz & Dunn-Sigouin 2020, Madonna et al.
207 2020). Consequently, the atmospheric meridional heat transport distribution is strongly
208 skewed, with a few intense events contributing a considerable fraction of the seasonal
209 average transport (Messori et al., 2017).

210 Analogous to the meridional heat transport, much of the ocean heat loss is also associated
211 with individual weather events. For this reason, time-mean surface flux values can be
212 misleading in the mid and high-latitudes, because much of the time-mean exchange occurs in
213 brief bursts, and winds during these events differ considerably from the time average (Ogawa
214 & Spengler 2019). For example, Condron & Renfrew (2013) show that bursts in surface
215 fluxes associated with polar lows contribute substantially to the climatological water mass
216 transformation, although they are both small scale (typically < 300 km) and short-lived
217 (typically < 24h). Polar lows are often embedded in cold-air outbreaks (CAOs, Terpstra et al.,
218 2021) that move polar air masses off the sea-ice or cold continents and over relatively warm
219 water, leading to locally intense ocean cooling (Papritz & Spengler 2017). Further, CAOs are
220 often linked to extratropical cyclones (Kolstad et al., 2009; Fletcher et al., 2016; Papritz

2017) that have strong winds and are generally hotspots of air-ice-sea interactions (Sorteberg & Kvingedal 2006; Sampe & Xie 2007).

Slower modes of atmospheric variability also influence day-to-day weather and heat loss (Lorenz & Hartmann 2003). This variability can, to some extent, be captured by slower varying components of the atmosphere, such as the North Atlantic Oscillation (NAO) or the Pacific North America pattern (PNA). The NAO represents a latitudinal shift of the North Atlantic storm track (Hurrell 1995; Woollings et al. 2010). This shift is only weakly related to the atmospheric heat transport towards high latitudes (Ruggieri et al., 2020), but it captures the variability in the occurrence of pertinent weather events, such as CAOs (Kolstad et al. 2009, Papritz 2017). The PNA is associated with atmospheric blocking over the eastern North Pacific (Renwick & Wallace 1996, Moore et al., 2010), and thus represents variations in the occurrence of warm moist intrusions into the Arctic from the Pacific side (L'Heureux et al., 2008). These variability indices capture a considerable fraction of the atmospheric variability from monthly to multidecadal scales, but trends remain difficult to assess (Woollings et al., 2014).

Given the relevance of both the NAO and the PNA for air-ice-sea interactions in the Arctic, it is tempting to consider their combined effects using the dominant pattern of atmospheric variability over the entire northern extratropics, the Arctic Oscillation or Northern Annular Mode. However, the NAO and the PNA are largely uncorrelated and physically unrelated, making their combination of limited use when trying to understand regional climate (Deser 2000; Ambaum et al. 2001; Huth & Beranová 2021).

2.2 Cryospheric links towards ocean heat anomalies

Arctic sea ice loss is now apparent throughout the year, but the amount of loss varies depending on season and region (Onarheim et al., 2018). Diminishing sea ice has a number of important consequences for marine ecology and navigation (Meier et al., 2014; Stocker et al., 2020; Lannuzel et al., 2020), plays a part in Arctic Amplification (Pithan & Mauritsen 2014), and, by decreasing surface albedo, acts as a positive feed-back on global warming (Pistone et al., 2019). To first order, there is a nearly linear relationship between the global atmospheric CO_2 concentration, increased long-wave radiation and Arctic sea-ice extent (Notz & Stroeve, 2016) appearing in both observations and coupled climate simulations. During late spring, summer, and early fall, the largest ice loss is found inside the Polar Sea, causing a profound change in surface fluxes there (Perovich et al., 2007). The additional solar heat gained by the

ocean during this time of year is lost to the atmosphere before and during sea ice formation in the cold seasons, resulting in a small net change in the annual mean heat fluxes. So there is an increase in the annual cycle of summer heat gain and winter heat loss within the Polar Sea, but there has until today been little change in the net annual heat loss (Onarheim et al., 2018). This is different for the regions experiencing reduced winter sea ice, which up to now has mostly occurred in the Greenland and Barents Seas (Onarheim et al., 2018).

Large changes in annual mean heat loss in the regions experiencing reduced winter sea ice cover may be expected – both for trends and inter-annual variability. A clear relationship between OHT and sea ice cover variability has been established for the Barents Sea (Årthun et al., 2012, Smedsrud et al., 2013, Muilwijk et al., 2019). Here an increased OHT leads to reduced winter sea ice cover, stronger ocean heat loss, and increased dense water production. There is evidence that a similar mechanism is now at play north of Svalbard (Ivanov et al., 2016) and in the Eastern Eurasian Basin (Polyakov et al., 2017). Increased AW inflow leads to less sea ice cover also in the western Nordic Seas, based on simulations (Årthun & Eldevik 2016) and observations covering the last decades (Selyuzhenok et al., 2020). As a result, the East Greenland Current flowing southward along the Greenland slope is now partially exposed to the atmosphere in winter so that water mass transformation directly within the boundary current may occur (Våge et al., 2018). These new areas of open water allow for more local heat loss and dense-water formation and may alter the properties and composition of the OW at depth. However, while the loss of winter sea ice may cool the ocean more locally, it also stops brine from being released during ice growth. The overall and net effect of less winter ice on dense-water formation is thus not obvious. Deep convection will only occur under strong heat loss if the surface is sufficiently saline and is thus dependant on stratification often reflected in winter Sea Surface Salinity (SSS).

Northeastern Greenland forms the western boundary of the Nordic Seas. Numerous tidewater glaciers here are in contact with the ocean in narrow fjords that connect to the continental shelf (Straneo et al., 2012). These marine-terminating glaciers deliver both liquid freshwater and icebergs to the ocean. In the northeast region of the Greenland Ice Sheet, the annual flux of ice into the ocean is estimated to be approximately 35 x 10^{12} kg (Mouginot et al., 2019), equivalent to around 0.001 Sv of freshwater. This ice either melts near the glacier calving front (including underneath any remaining ice shelf) or as icebergs close to the coast. The bulk of the heat needed to melt this ice is supplied by the Nordic Seas. Based on the above annual ice flux (Mouginot et al., 2019), an estimate of the ocean heat needed to melt the

annual ice flux is less than 1 TW. This is small relative to the overall cooling of the AW within the Nordic Seas. To obtain the total freshwater input from Greenland, this ice discharge must be added to the liquid freshwater discharge from the net surface melt.

Over the 1960-1990 period, the total (liquid plus solid) freshwater discharge from Greenland into the Nordic Seas has been estimated to be 107±8 km^3/yr (~0.003 Sv) (Bamber et al., 2012). In recent years (2007-2016), this has increased by approximately 24 km^3/yr (i.e., an additional 0.008 Sv each year; Bamber et al., 2018). It remains an active area of research to assess the potential impact of this freshwater on the shelf and large-scale ocean dynamics (e.g., Gillard et al., 2016). Greenland's tidewater glaciers also respond dynamically to the ocean through the melting of their calving fronts and floating ice shelves. Recent decades have seen widespread retreat and increased sea level contribution from Greenland's tidewater glaciers. Numerous processes may contribute to this retreat, but the current consensus suggests that the dominant driver is ocean warming (Straneo & Heimbach, 2013). In northeast Greenland specifically, variability in AW properties is understood to control the melting of Greenland's largest remaining ice shelf at 79 °N (Wilson & Straneo, 2015; Schaffer et al., 2020) and has been implicated in the recent collapse of the adjacent ice shelf at Zachariae Isstrom (Mouginot et al., 2015). Quantifying past variability in the Nordic Seas thus provides essential context for understanding northeast Greenland ice sheet dynamics.

2.3 Ocean

The Arctic Ocean can largely be viewed as an enclosed basin – the Arctic Mediterranean (Eldevik, T. & Nilsen, 2013) – with the GSR as the gateway to the Atlantic in the south (Fig. 2). Consequently, the oceanographic conditions in the Nordic Seas are heavily influenced by the northward-flowing Norwegian Atlantic Current transporting warm, saline AW across the GSR (Orvik & Niiler, 2002; Østerhus et al., 2019). The Norwegian Sea accordingly exhibits pronounced variability in ocean heat content on interannual to decadal timescales associated with changes in the properties and transport of AW into the region (Mork et al., 2014; Yashayaev & Seidov 2015; Asbjørnsen et al., 2019).

2.3.1 Atlantic inflow to the Nordic Seas

The atmospheric forcing is instrumental in driving the ocean circulation in two ways. Firstly, heat loss to the atmosphere cools the AW inflow within the enclosed Arctic Ocean and densifies the water as it progresses northward on the eastern side of the Nordic Seas and circulates cyclonically in the Arctic boundary current (Mauritzen et al., 1996; Eldevik et al.,

2009). This cooling thus contributes to the mean circulation, but variability in cooling may consequently also drive variability in flow. Secondly, surface wind stress both drives the mean cyclonic circulation (Nøst & Isachsen, 2013; Timmermans & Marshall, 2020) as well as inflow variability. Wind forcing clearly influences the short-term AW inflow variability across the GSR (Nilsen et al, 2003; Bringedal et al, 2018). Interannual variability in the Nordic Seas inflow has also been linked to large-scale wind forcing associated with the North Atlantic Oscillation (NAO; e.g., Zhang et al., 2004; Sandø et al., 2012; Muilwijk et al., 2018 Bringedal et al., 2018). The relationship between AW inflow and NAO also holds for longer timescales, an increasingly positive phase of the NAO related to increased AW inflow from 1965-1996 (Dickson et al., 2000). Several studies have also demonstrated the importance of North Atlantic gyre dynamics in affecting the properties and transport of AW across the GSR (Hatun et al., 2005; Langehaug et al., 2012; Kenigson & Timmermans 2021; Asbjørnsen et al., 2021). A weak subpolar gyre is associated with a northwestward shifted subpolar front, higher poleward transport of subtropical waters in the North Atlantic Current, and a warmer and more saline GSR inflow. In the real world and climate model simulations, wind forcing and heat loss combine to drive the full variability of the flow and water mass transformations in the region.

2.3.2 Heat fluxes and cooling of the Atlantic inflow

Our understanding of the cooling of AW as it circulates the Arctic Ocean has improved over the last decades. Using re-analysis of the atmosphere, Simonsen & Haugan (1996) highlighted the Barents Sea as an area of effective heat loss to the atmosphere (42–162 TW) in addition to the Nordic Seas (220–250 TW) but also documented large uncertainties in the parameterizations used to determine the surface fluxes. There have been quite limited efforts on how the heat loss has developed over decades. Dickson et al. (2000) found some downstream consequences of increased AW inflow in terms of sea ice loss and increased ocean temperature. Mork et al. (2014) found a Nordic Seas warming of 0.3 W/m² since 1950 and argued that air-sea heat fluxes explained about half of the interannual variability in ocean heat content in the Atlantic domain of the Nordic Seas. This was supported by Muilwijk et al. (2018), who further showed that the heat fluxes effectively damp OHT anomalies, but also that the wind-forced AW volume transport change in relationship with the NAO, especially in the 1930s. Yashayaev & Seidov (2015) summarized variability after 1950 from observed hydrography in the Nordic and Barents Seas, and found that fluctuations in AW properties dominate on decadal and longer time scales. NAO and the Atlantic Multidecadal Oscillation

(AMO) correlate, with low AMO values forced by high NAO and a related high heat loss in the Labrador Sea, and the AW temperature and salinity signals are lagged along the Nordic Seas inflow path (Yashayaev & Seidov, 2015). Asbjørnsen et al. (2019) documented that the AW inflow is the primary contributor to heat content variability within the Nordic Seas after the 1990s and highlighted the possibility for related long-term predictions. The above described AW variability further propagates from the Nordic Seas and through the Barents Sea into the Polar Sea, as Polyakov et al. (2004) and Polyakov et al., (2009) described. Despite well-documented spatial and temporal variations of AW properties, an overview of 20th century variability of AW flow, properties, and consequences concerning ongoing global warming is not established. New relevant results will therefore be presented in section 4.

2.3.3 Analytical AW inflow and relation to surface heat fluxes

A central question for the regional dynamics and thermodynamics is the relationship between the Arctic Ocean heat loss and the mass, heat and fresh water flows in the region. Pemberton et al. (2015) analyzed a steady-state numerical solution and found that large surface heat fluxes (~70 W/m²) in the southwestern Barents Sea is key for water mass transformation within the Polar Sea. They concluded that surface freshwater is important for transformations occurring below salinities of 30 g/kg but that the net transformation at such low salinities is negligible. Spall (2004) presented an analytical solution based on an idealized circular basin with sloping bottom, resembling the real Arctic Ocean with the main inflow across the GSR (Fig. 2) - forced by heat loss only. He found that in the absence of topographical or far-field (AW inflow) temperature changes, the overturning, inflow volume, and heat transport all scale with the overall mean heat loss Q at the surface. The Arctic Ocean heat flux is on the order of 15 W/m² (Table 1), yielding a heat loss of about 200 TW over the total area of 12.3 mill km² (Fig. 3, Table 1).

The inflow volume across the GSR can be directly expressed using the mean velocity V_{in} over the $H_{in} = 500$ m deep sill and the $L = 105$ km wide slope. We generally expect an increase in OHT with more heat loss over the Arctic Ocean, and Spall (2004) finds that the inflow (in m^3/s) can be expressed as

Eq (1) $$V_{in} * L * H_{in} = \frac{H_{in}}{\rho_0} \sqrt{\frac{R\, L\, \alpha\, g\, Q}{2\, f\, c_p\, c}}.$$

Here R is the Arctic Ocean radius, f the Coriolis parameter, α the thermal expansion coefficient, c_p the specific heat capacity, g gravitational acceleration, c an empirical eddy mixing efficiency and ρ_0 a mean density. Because the slope and the sill depth, together with the other parameters, are constant in time, the inflow volume and speed are solely dependent on the density in the basin, through the thermal wind relationship and governed by Q. Representative values for the Arctic Ocean are a radius $R = 2000$ km (Fig. 1), and a Coriolis parameter f for 80°N. Physical constants are the thermal expansion coefficient $\alpha = 0.2\ kg/(m^3°C)$, the specific heat capacity $c_p = 3985\ J/(kg°C)$, the gravitational acceleration $g = 9.8$ m/s^2, an empirical eddy mixing efficiency $c = 0.025$, and a mean density $\rho_0 = 1027\ \frac{kg}{m^3}$. These values give a total inflow of 8.5 to 11.5 Sv for the range of Q between 10 and 20 W/m², equivalent to a change in integrated heat loss from 125 TW to 250 TW (Eq. 1). A similar dependency between AW inflow and mean heat loss results from the analytical diagnostic by Eldevik & Nilsen (2013) who also accounted for the freshwater budget. In their solution, an increased heat flux of 10 W/m² results in +4 Sv of increased AW inflow.

The AW inflow is gradually cooled and densified as it progresses northward with the rim current system in the Arctic Ocean (Mauritzen et al., 1996; Eldevik et al., 2009). As the AW flows around the basin, downwelling occurs along the boundary current, and much of the volume leaves the basin as OW at depth. The remaining volume exits at the surface on the western side as freshened PW. Spall (2004) concluded that in high latitude regions, and in particular in small basins, the majority of the heat is transported by the near-surface gyre circulation while deep overturning plays a smaller role. The division between the horizontal gyre and vertical overturning circulation is more equal further equatorward in the subpolar North Atlantic (Böning & Bryan 1996; Lozier et al., 2019).

The AW inflow downstream of the GSR is thus a warm boundary current that cools as it travels northward (Spall 2004), but in nature, it also freshens along the perimeter of the Arctic Ocean (Mauritzen 1996). Given that vertical profiles of density are available, the speed of the baroclinic component of such a boundary current V_{bc} in one location can be found following Jakhelln (1936) and Werenskiold (1935):

Eq (2) $$V_{bc} = \frac{g}{f\,\rho_{ref}} \int_{-h}^{o} \int_{-h}^{z} [\rho(-h) - \rho(z)]\ dz'\ dz$$

Here ρ_{ref} is a reference density, and the integration depth is h. Repeated CTD observations within the boundary current can be used to estimate the baroclinic transport strength as has been demonstrated for the northward AW flow across the Svinøy section just north of the GSR (Orvik et al., 2001). An AW inflow that is less dense (i.e., warmer and/or fresher) or deeper would thus lead to a stronger boundary current.

2.3.4 Transformation of AW into OW and PW

The AW inflow across the GSR may undergo a variety of transformations within the Arctic Ocean before returning south. Some AW returns southwards without undergoing much cooling, forming what is known as the AW outflow (Table 3). Rossby et al. (2018) observed ~3 Sv of AW returning south between Iceland, the Faroes and Shetland. A small amount of AW also flows south in the eastern part of Denmark Strait (Mastropole et al., 2017). The remaining GSR outflow is either fresh and cold PW in the East Greenland Current, or the denser OW spilling across the ridge between Greenland and Shetland (Østerhus et al. 2019). Dense OW is transported towards the GSR along different pathways. To the Denmark Strait the OW comes with the East Greenland Current (Mauritzen, 1996) and the North Icelandic Jet flowing westward along the north slope of Iceland (Jónsson & Valdimarsson 2004; Våge et al., 2011; Semper et al., 2019). The Faroe-Shetland Channel OW has a contribution flowing southward from the Norwegian Sea (Eldevik et al. 2009; Chafik et al., 2020) and the Iceland Faroe Slope Jet arriving from the west (Semper et al., 2020). Much of the dense OW experiences the final heat loss in the interior Iceland and Greenland Seas (Swift & Aagaard 1981; Marshall & Schott 1999), with recent studies pointing more towards the Greenland Sea as the active region (Våge et al., 2015; Huang et al., 2020).

Deep convection in the Greenland Sea used to produce the coldest and densest bottom waters in the Arctic Ocean due to the combined effect of severe winter cooling and sea ice formation (Helland-Hansen & Nansen, 1909; Aagaard et al., 1985). However, since the early 1980s, only convection to intermediate depths (<2000 m) has been observed (Karstensen et al., 2005; Latarius & Quadfasel, 2016; Lauvset et al., 2018; Brakstad et al., 2019). A main reason for this change is the retreat of the sea ice edge toward Greenland (Visbeck et al., 1995). The retreating sea ice has led to reduced brine release over the central Greenland Sea since the late 1970s, and in combination with reduced atmospheric cooling, this may limit the formation of intermediate water masses and OW supply (Moore et al., 2015). This has not yet occurred because a concurrent increase in salt advected in with the AW has increased upper ocean density (Glessmer et al. 2015; Lauvset et al., 2018; Brakstad et al., 2019). The salt

444 increase has resulted in enhanced ventilation of intermediate waters in the Greenland Sea
445 since the mid 1990s (Lauvset et al., 2018). In the last 10 years, the trend has reversed (Mork
446 et al., 2019), and convection in the Greenland Sea could become increasingly vulnerable to
447 inter-annual changes in ocean heat loss.

448 Consistent with this study's focus on ocean heat loss, we mostly analyze the Atlantic sector
449 of the Arctic and explicitly leave out many of the processes and variations on the Pacific side.
450 There are indeed wind-related changes within the Beaufort Gyre that have prominent effects
451 on freshwater storage (Johnson et al., 2018), but there is little variability in heat loss and
452 storage. The Beaufort Gyre is characterized by anti-cyclonic ocean circulation and sea ice
453 drift (Timmermans & Marshall, 2020), but the heat loss is small because it is ice-covered
454 throughout winter (Fig. 4). For the main heat-loss region, the Nordic Seas (Fig. 2), Glessmer
455 et al. (2015) inferred from observations and model simulations (1950–2010) that anomalous
456 freshwater content is relatively unaffected by what is transported southward with the East
457 Greenland Current but rather relates to salinity anomalies arriving with the Atlantic inflow.

458 2.4 CO_2 Uptake in relation to heat loss

459 Arctic Ocean CO_2 uptake was first determined by Lundberg & Haugan (1996). Based on
460 volume flows and inorganic carbon observations, they inferred a net uptake of 110 Mt C/yr.
461 Similar approaches have subsequently been applied to the individual seas based on more
462 recent data. Based on observations from the late 1990s and early 2000s, MacGilchrist et al.
463 (2014) inferred a net uptake in the Polar Ocean and the Barents Sea of 166 Mt C/yr, while
464 Jeansson et al. (2011) determined a net Nordic Seas uptake of 190 Mt C/yr. The CO_2 uptake
465 has also been estimated from observations of the CO_2 partial pressure in the ocean surface,
466 which allows for direct computation of the air-sea CO_2 flux as described by e.g., Takahasi et
467 al. (2009). For the Barents sea, Omar et al. (2007) determined flux densities in the range of
468 3.4 mmol C/(m²d) (winter) to 21 mmol C/(m²d) (fall), these estimates were extrapolated to
469 the entire Barents Sea by Kivimäe et al., (2010) yielding a net uptake of 58 Mt C/yr. East of
470 the Barents Sea, CO_2 outgassing may occur, a consequence of the decomposition of terrestrial
471 organic matter supplied by the large Siberian rivers (Anderson et al., 2009). Across the
472 Bering Strait, however, the Chukchi sea is highly undersaturated in summer because of ample
473 biological productivity, and the uptake of CO_2 has been estimated to 13 Mt C/yr over the ice-
474 free season (Pipko et al., 2015), much of which is exported to the halocline and deeper waters
475 over the winter. Air-sea fluxes over the western Arctic coastal ocean, including the Chukchi

476 and Beaufort Seas were recently estimated by Evans et al. (2015). They found the region to
477 be a sink of approximately 11 Mt C/yr, with flux densities ranging from 3 mmol C/(m²d) in
478 winter, to 20 mmol C/(m²d) in summer. While sea-ice cover restricts the winter uptake, Evans
479 et al. (2015) observed that the waters were nevertheless only modestly undersaturated in this
480 season, such that disappearance of the sea ice might not lead to ample uptake of CO_2 in
481 winter in these regions. Towards the east, on the other hand, over the Eurasian basin and into
482 the Barents Sea, waters beneath the sea ice are strongly undersaturated (Fransson et al.,
483 2017), and here the uptake will increase as the sea ice extent decreases. We thus speculate
484 that the CO_2 uptake in the west and east Polar Sea may show contrasting responses to sea ice
485 loss.

486 Reviewing available literature at the time, Bates and Mathis (2009) determined net
487 annual air-sea flux in the Polar and Barents seas to between 66 and 199 Mt C/yr. Recently,
488 Yasunaka et al. (2018) mapped all available pCO_2 observations in this region and determined
489 an annual uptake of 180 ±130 Mt C/yr over 1997-2014, including also the Bering Sea. We
490 extracted fluxes for the Polar Sea and Barents sea as defined here (Fig. 1) from the mapped
491 data published by Yasunaka et al. (2018) and obtained a mean flux of 149 ±107 Mt C/yr.

492 For the Nordic Seas, the maps presented by Yasunaka et al. (2018) show annual
493 average flux densities 8-16 mmol C/(m²d) in the west, while they are a bit lower in the east,
494 4-8 mmol C/(m²d). This is in agreement with flux densities reported by Skjelvan et al. (1999)
495 based on pioneering pCO_2 measurements conducted in the mid-1990s: 15-19 mmol C/(m²d)
496 in the Greenland Sea, and 9 mmol C/(m²d) in the Norwegian Sea. A total Nordic Seas uptake
497 of 90±10 Mt C/yr was estimated by Skjelvan et al. (2005) based on available literature and
498 data then. This is in good agreement with an estimate obtained for this region by extracting
499 data from Yasunaka et al. (2018): 98 ± 71 Mt C/yr for 1997-2014. The uncertainty was
500 derived by assuming the same signal-to-noise ratio as derived for the Polar and Barens seas
501 by Yasunaka et al. (2018). This gives a total uptake of (149+98=) 247 Mt C/yr for the Arctic
502 Ocean as defined here. This is quite a bit less than the sum of the estimates by MacGilchrist
503 et al. (2014) and Jeansson et al. (2011) mentioned above, 300 Mt C/yr, reflecting the ample
504 uncertainties in all of these numbers.

505 Many processes influence the Arctic Ocean CO_2 uptake, primary production and organic
506 matter remineralization (Arrigo & van Dijken, 2015); biogeochemical processes during sea-
507 ice formation and melting (Rysgaard et al., 2013); and the delivery of excess alkalinity with
508 riverine run-off (Olafsson et al., 2021). However, the most important process is the heat loss,

509 which cools the water and increases CO_2 solubility. Watson et al. (1995) stated this
510 relationship between heat loss and CO_2 uptake as:

511 Eq (3) $$\mathrm{CO_2\ uptake} = \frac{-Q\ DIC\ \tau}{c_p\ R_f},$$

512 where DIC is Dissolved Inorganic Carbon concentration, τ is the isochemical pCO_2
513 temperature dependency (Takahashi et al, 1993), and R_f the Revelle factor. Q is the heat loss
514 and c_p the heat capacity as in Eq (1). We return to this way of estimating the CO_2 uptake
515 when we have derived the centennial heat loss values. For now, we simply evaluate the
516 theoretical and observed increase in *DIC* that occurs as the AW cools and overturns in the
517 Arctic Ocean. The temperature of inflowing AW is ~7.5 °C at the GSR, while the
518 temperature of the OW is ~0.5°C. This cooling can increase the *DIC* solubility of about 60
519 µmol/kg. Such an increase in *DIC* is present in available observations: Using the *DIC*
520 concentrations of the inflowing AW and outflowing OW tabulated by Jeansson et al. (2011)
521 and correcting for their anthropogenic carbon content and dilution as the salinity declines
522 from ~35.2 (AW inflow) to ~34.9 (OW), we find a difference in DIC of 61 µmol/kg. This is
523 not associated with a large gradient in nutrients (only ~0.1 µmol/kg in phosphate), and as
524 such, it mostly reflects uptake of CO_2 from the atmosphere. If this solubility-generated *DIC*
525 increase is combined with a present-day inflow of AW and outflow of colder OW and PW
526 of ~8 Sv, this amounts to a total uptake of ~200 Mt C/yr, and can explain most of Arctic
527 Ocean CO_2 uptake as reviewed above. The present-day uptake as estimated from
528 observations is thus consistent with simple analytical scaling, but the longer-term changes of
529 the CO_2 uptake are unknown and therefore a primary focus in section 4.

530

531 **3 Methods**

532 **NorESM simulations:** Many of our new results stem from simulations with the Norwegian
533 Earth System Model (NorESM). The main set of simulations analyzed are the global ocean-
534 ice fields of the NorESM forced by a reanalysis atmosphere from 1900-2018. The general
535 model description is provided by Bentsen et al. (2013), while the specific forcing-setup for
536 1900-2009 is described in He et al. (2016). The ocean model BLOM (an extensively updated
537 version of the Miami Isopycnic Coordinate Model, MICOM, Bleck et al., 1992) is isopycnic
538 with 51 interior layers, referenced to a pressure of 2000 dbar, and a surface mixed layer
539 divided into two non-isopycnic layers. The sea ice component is CICE4 (Hunke et al., 2008).

A tripolar grid is used, which allows for higher spatial resolution in high latitudes. At the equator, the grid resolution is one degree zonally and 1/4 degree meridionally. The grid gradually becomes more isotropic as latitude increases: the typical horizontal resolution in the Nordic Seas is approximately 40 km. This limited resolution means that eddies are not resolved, and the width of a slope current will be larger in the simulations than in nature. The ocean-ice model is forced by the 20th century atmospheric reanalysis forcing (20CRv2; Compo et al., 2011), which was adjusted by satellite observations and corrected using the Coordinated Ocean-ice Reference Experiments phase-II (He et al. 2016). The forcing consists of momentum fluxes (wind stress), heat fluxes (radiative and turbulent components), and fresh water fluxes (precipitation, evaporation, and river runoff). The wind stress, heat (latent and sensible), and moisture (evaporation) fluxes are computed using bulk formulas (Large & Yeager 2004) and the 20CRv2 air and surface temperature, humidity, winds, air density, ocean current, and fractional sea-ice cover (He et al., 2016). No restoring is applied to SST, but salinity in the mixed layer is relaxed towards a monthly-mean SSS climatology (He et al., 2016). The ocean model is initialized with zero velocity, and the initial potential temperature and salinity are taken from the January-mean climatology of the World Ocean Atlas (Levitus et al. 1998), with the modified data of the Polar Science Center Hydrographic Climatology (PHC3.0; updated from Steele et al., 2001) in the Arctic. The model forcing started in 1871, and the first 30 years until 1900 is considered a spin-up period.

An updated version of NorESM (NorESM2-LM, Bentsen et al., 2019) forced by the Japanese Re-Analysis (JRA55-do; Tsujino et al., 2018) is available for 1958-2018 and is used for the years after 2010. These updated simulations are provided as part of the CMIP6 contribution for the OMIP2 (Ocean Model Intercomparison Project; Griffies et al., 2016) experiments. The NorESM simulations were already evaluated towards hydrography along the AW inflow path (Ilicak et al., 2016). Overall, the simulation captures the observed variability well (Muilwijk et al., 2018), with further evaluation presented here.

The overturning and horizontal gyre contributions to the OHT across the GSR were calculated based on the NorESM simulated velocity and temperature. The overturning part is the circulation related to the deep overflows, while the horizontal gyre circulation encompasses both PW and AW surface layer outflow. The decomposition was done by calculating the overturning part of OHT using along-section averages of across-section velocity and temperature. This analysis follows the GSR along the model grid of NorESM and is equivalent to zonal averages in the more common calculation of meridional heat

transport (Bryden & Imawaki, 2001). Our results are thus more representative for the GSR but are not directly comparable with previous estimates using zonal averages that cut across the GSR (e.g., Li & Born, 2019). The results shown here are based on monthly average values of temperature and across-section flow, so that heat flux on shorter time scales, from transient eddies, is neglected. From this data, we calculated both the total OHT and the overturning component as mentioned above, while defining the difference between the two as the gyre component. Thus, our gyre component can be further decomposed and also includes diffusive transports, which we expect to be very small (Fanning & Weaver, 1997).

Diagnostics to capture variability in atmospheric forcing: The 20CRv2 reanalysis is also analyzed directly for detecting weather events such as cyclones and CAOs. Extratropical cyclones are a key component of the atmospheric dynamics in the mid- and high latitudes, while CAOs are important for heat exchanges between the ocean and the atmosphere. We use feature detection algorithms to identify these features. Cyclones are detected as closed contours of SLP minima using the detection scheme of Wernli & Schwierz (2006). For detecting CAO events, we use the definition of Papritz and Spengler (2017) and require at least a "moderate" intensity according to their classification ($\theta_{SST} - \theta_{850\,hPa} > 4$ K). We remove the linear trend and select the 15 highest and lowest years of Nordic Seas heat loss from the reanalysis for further analysis. In a first step, we analyze the relation between ocean heat loss and the occurrence of these weather events. As a second step, we embed these feature-based results in the context of atmospheric variability patterns. We derive these variability patterns through an analysis of Empirical Orthogonal Functions (EOF's) of monthly mean sea level pressure for the North Atlantic sector (90°W-40°E, 20-80°N) and the extended winter season November through April. The first three EOF's correspond to the NAO, the East Atlantic pattern, and the Scandinavian pattern as expected and shortly described in section 2.1. All analyses are performed separately for each ensemble member of the 20CRv2, and there are 56 ensemble members.

Available observations: We employ hydrographic observations (temperature and salinity profiles) from 1950 to 2019 from two different data sets. The first data set, used in Huang et al. (2020), covers the period 1980-2019 and is a collection from various archives, including the Unified Database for Arctic and Subarctic Hydrography (UDASH, Behrendt et al., 2018). The second data set, called NISE (Norwegian Iceland Seas Experiment, Nilsen et al., 2008), is a combination of data from several archives from 1900 to 2006. Due to very few observations in the first half of the 20th century, we restricted our observational analysis to

1950 onwards. Duplicates between the two databases are removed for the overlapping time period. To look at how thermohaline water mass properties transform within the Nordic Seas, we extracted profiles from various standard sections following the cyclonic boundary circulation (see Fig. 6) and from the Iceland and Greenland Sea gyres (defined according to Moore et al., 2015). Various water masses were identified using the following criteria: Atlantic Water (AW) and Returning Atlantic Water (RAW) by the depth of maximum temperature below 100 m (± 50 m); Overflow Water (OW) by density above 27.8 kg/m³ and above the sill depths (650 m for the Denmark Strait and 840 m for the Faroe Shetland Channel); Intermediate Water (IW) by the typical mixed-layer depths 150-350 m in the Iceland Sea (Våge et al., 2015) and 500-1500 m in the Greenland Sea (Brakstad et al., 2019). Timeseries of annual mean temperature and salinity for each geographical region and water mass were then used to estimate linear trends.

Additionally, we use available observations from the Svinøy section in the Norwegian Sea between 1996 and 2018 (NMDC, 2020), the Kola section in the Barents Sea (ICES, 2020, location shown in Figure 4), and wind observations from the Norwegian Climate Service Centre (NCSC, 2020). The simulated sea ice cover is compared to Arctic sea ice reconstructions from HadISST (Rayner et al., 2003), NSIDC (Walsh et al., 2017), and PIOMAS-20C (Schweiger et al., 2019).

CO_2 observations and new estimates: There are few observations of CO_2 and CO_2 fluxes in the Arctic Ocean, and the only available observations-based gap-filled data product covers 1997-2017 (Yasunaka et al., 2018). In addition, the NorESM simulations used in this study do not include biogeochemistry. Because we expect CO_2 fluxes to be proportional to both heat loss and sea ice loss, we overcome this challenge by using basin-wide annual averages of simulated heat loss and sea ice concentration (SIC) as predictors to extrapolate the basin-wide CO_2 fluxes back to 1900 (Table 2, Sec. 2.4). Given that there is only a 12-year overlap between the observation-based CO_2 fluxes and the centennial NorESM run forced with 20CRv2, we additionally use the simulation forced by the JRA55-do reanalysis product for the period 1958-2018 to determine regression coefficients. These simulations compare well without significant biases, supporting a combination of the two. The analysis shows that CO_2 fluxes in the Nordic Seas scale with the heat flux, in the Polar Sea the CO_2 fluxes scale with the sea ice concentration, while in the Barents Sea, a combination of sea ice concentration, sea surface salinity, and heat flux is necessary to explain the CO_2 flux. Other factors than these also have importance for CO_2 fluxes. Previous work (e.g., Lauvset et al., 2013; Chierici

et al., 2009) shows that it can be useful to include chlorophyll as a proxy for biological production. Without including such biological or biogeochemical predictors, we find that our algorithms only explain 42-48% of the total variance (Table 2). It should also be noted that there is a known, observable interannual to multidecadal variability in the ocean carbon sink (e.g. Landschützer et al., 2016; Fröb et al., 2019), the drivers of which are not fully understood or explained (DeVries et al., 2017; McKinley et al., 2020). However, because we can only explain about half the variance in the observations we make no attempt to use our extrapolated data to describe long-term variability in CO_2 flux, but focus on regional differences and trends.

Ocean-Ice Sheet interaction: The heat lost to melting Greenland's marine-terminating glaciers and icebergs is not directly represented in NorESM in the absence of an interactive ice sheet model. The freshwater fluxes from Greenland are thus prescribed in a similar manner as Arctic rivers using mean values before 1958, and values from Bamber et al. (2018) onwards. The modest magnitude of this heat loss (~1 TW) suggests that the direct impact of the ice sheet on the Nordic Seas heat budget is small. Importantly, the Nordic Seas heat content impact on the ice sheet may be significant and has been quantified using simulated ocean temperatures over the NE Greenland continental shelf. We use the parameterization described by Slater et al. (2019) to quantify the advance and retreat of Greenland's glaciers driven by oceanic forcing. The parameterization utilizes a summer liquid freshwater flux per glacier (F) from the regional climate model MAR (Fettweis et al., 2017) together with mean annual ocean thermal forcing (TF), calculated as the ocean temperature above the in-situ freezing point between 200 and 500 m depth. Glacier terminus change is then calculated as $\Delta L = \kappa \Delta(F\ 0.4\ TF)$, where κ is a sensitivity parameter (Slater et al., 2019). The projections of terminus position are compared with a compilation of observations since 1984 from King et al. (2020).

4 Results

We first present the baseline centennial mean values of the Arctic heat transport and air-sea exchange of heat. Then we proceed with the trends and variations following the AW flow from the Nordic Seas and onwards to the Barents and Polar Seas, where it meets the sea ice. The AW has cooled around 6°C at this stage, and it is still sufficiently saline to yield high-density water masses that eventually flow southwards back to the Atlantic Ocean across the

GSR as OW or RAW. Some of the AW has contributed to the melting of sea ice and glaciers, or it is mixed with river water becoming sufficiently fresh to exit the GSR at the surface in the East Greenland Current as fresher PW. Observations are included to the extent available, complementing and providing evaluation of the simulations.

4.1 The Centennial Means (1900 – 2000)

Surface cooling: The warm northward-flowing AW is cooled by the overlying atmosphere. The heat is transferred to the atmospheric boundary layer as sensible, latent, and radiative fluxes and ultimately radiates out to space as long-wave radiation. Because the winter season is generally colder and longer the higher the latitude, one might expect the heat fluxes to be larger in the Polar Sea than further south. This is not the case. Heat loss from the Polar Sea is effectively restricted by the nearly permanently ice-covered sea. The Nordic Seas lose the most heat with a centennial annual mean of 115 TW (Fig. 2) based on an average surface heat flux of 45 W/m² (Table 1; all the heat loss and surface flux values presented here are simulated annual means, unless otherwise specified). The Barents Sea has a smaller surface area and a lower surface heat flux (38 W/m²), so the centennial mean heat loss adds up to 57 TW. Furthermore, the much larger area of the Polar Sea has a surface flux of fewer than 2 W/m², resulting in a heat loss of only 16 TW (Fig. 2).

Sea ice prevents heat loss in two ways. Firstly it forms an effective insulating layer by its low thermal conductivity. Secondly, when sea ice forms at the surface, the latent heat is released into the atmosphere, and is entirely used to grow the sea ice. This means that the ocean temperature only decreases at the time and location where the sea ice melts. In the Polar Sea surface layer during winter, the temperature is already at the freezing-point, and cannot get colder. A volume flux of about 2000 km³/yr of the Polar Sea ice drifts southward through the Fram Strait into the Nordic Seas with the East Greenland Current and melts there; a process termed sea ice export. The simulated exported annual sea ice area is close to 1 mill km^2 (indicated in Fig. 2), about 10% higher than the area export estimated from pressure observations over the last 80 years (Smedsrud et al. 2017). The heat gained by the Polar Sea atmosphere during this sea ice formation thus cools the Nordic Seas when it melts. The heat transport carried by this sea ice export is estimated to approximately 17 TW, so the exported latent heat and the direct Polar Sea heat loss are comparable in magnitude. The atmosphere above the Polar Sea thus gains about 33 TW; the exported 17 TW of sea ice in addition to the 16 TW directly lost from the ocean. In the centennial mean the Nordic Seas are additionally

cooled by the melting of this imported sea ice (Fig.2), adding to the heat extracted by the local Nordic atmosphere. Regionally in the Nordic Seas, the heat flux is larger in the east in the region of the warm AW inflow than in the west over the colder PW outflow (Fig. 4), consistent with warmer or more voluminous currents giving up more heat in general (Mauritzen 1996; Eldevik et al. 2009), and what, e.g., Segtnan et al. (2011) found for the 1990s.

The Nordic Seas heat loss has remained quite constant over time, with a small, insignificant long-term trend (Fig. 3, Table 1). In contrast, large increases in heat loss have occurred since 1900 in the Barents and Polar Seas and are addressed in section 4.2. Such simulated heat loss values are essentially not possible to evaluate towards the short-term and small-scale observations. This does not imply that they are fundamentally more uncertain than the simulated temperature or SIC that can be evaluated – just that we do not have a perfect grip of that uncertainty. Based on comparisons for the present day (2002-2017) between NorESM and the Arctic subpolar gyre state estimate (Nguyen et al., 2021) we estimate the heat loss uncertainty to be of order ±10 TW, similar to that found in Smedsrud et al. (2013). The simulations reflect AW inflow and water mass transformation well. The integrated heat loss values and trends must also be close to that of the real world, although the spatial distribution could be shifted because of a cold ocean bias discussed later. We mostly present long-term trends of annual mean properties, so the uncertainties of these means are substantially lower than the monthly mean values in any smaller area.

Ocean Temperature and Sea Ice Extent : The temperature of the AW inflowing across the GSR is close to 8 °C, and clearly the warmest water in the Arctic Ocean. The highest AW temperature is found at the surface in the Nordic Seas, but inside the Polar Sea, the maximum is located below the fresher and colder surface layer. The two AW branches entering the Polar Sea are clearly visible in the SST (not shown) and the surface heat flux (Fig. 4) fields, with one branch flowing eastwards into the Barents Sea and one flowing northwards west of Svalbard (West Spitsbergen Current). The only other poleward-flowing water mass is the Pacific Water in the Bering Strait, but temperatures are much lower, and the surface is sea ice-covered in the centennial mean (Fig. 4). On the Pacific side, the centennial mean sea ice edge is located at 60°N, well south of the Bering Strait. On the Atlantic side, it ranges from 60°N in the west to 80°N near Svalbard and about 70°N in the Barents Sea (Fig. 4). This

737 enormous latitudinal range has a dynamical explanation: the unevenly distributed poleward
738 transport of ocean and atmospheric heat.

739 **The Ocean Heat Transport (OHT):** The OHT towards the Arctic Ocean (179 TW) is close
740 to that of the surface cooling (187 TW), and is dominated by the net heat transport across the
741 GSR (172 TW). The centennial mean AW volume inflow across the GSR is +9.5 Sv (Fig. 2,
742 Table 3). The Pacific inflow is +0.7 Sv, and most of this leaves the Arctic Ocean through the
743 Canadian Archipelago, which has a net southward volume transport of -1.7 Sv. The volume
744 budget is closed by the net southward transport across the GSR of -8.5 Sv. With this closed
745 volume budget, a simulated Arctic OHT value of 179 TW is obtained (Fig. 5). This combined
746 OHT, independent of a reference temperature, is the heat flux convergence.

747 Heat transport for the individual straits requires, however, a reference temperature. Because
748 0°C is close to the simulated mean temperature of the Arctic Ocean (not shown) and a
749 representative temperature of the cold water flowing southward across the GSR (Fig. 9), we
750 adopt 0°C as our reference temperature. This follows e.g. Årthun et al., 2012 for Barents Sea
751 OHT and Rossby et al., 2018 discussing OHT across the GSR. We also use the term 'heat
752 transport' and the TW unit for the individual strait values (Table 3). Other authors, especially
753 those using observed values where a closed volume budget is more challenging, prefer to use
754 the term 'temperature flux' and the 'unit' [TW - equivalents]. Referenced to 0 °C the GSR
755 heat transport is +172 TW, the Bering Strait has a transport of +0.9 TW, and there is a net
756 positive contribution from the Canadian Archipelago of +6.6 TW (Fig. 5). About half of the
757 heat transport across the GSR is due to the overturning circulation related to the deep
758 overflows, with the remainder coming from the horizontal gyre circulation (Fig. 5). A
759 noticeable and important overall Arctic OHT increase from roughly 150 TW (1900-1920) to
760 200 TW (1980-2000) should be mentioned, mostly governed by the heat transport across the
761 GSR (Fig. 5). Further details about OHT within the Arctic Ocean, Fram Strait and the Barents
762 Sea Opening, are given by Muilwijk et al. (2018).

763 **Hydrography and dense water formation:** The inflowing AW is transformed into denser
764 but also fresher water. This means that cooling is the ultimate driver of densification. The
765 progressive observed cooling and freshening from AW to OW are clearly illustrated in Fig. 6.
766 The transformation falls along a close to the linear line in T-S space, showing a gradual
767 cooling and freshening along with the cyclonic flow of AW from the Faroe-Shetland Channel
768 towards Fram Strait and southwards again along the east coast of Greenland. By the time the

769 OW spills across the GSR, the water has cooled by roughly 7 °C compared to the AW inflow.
770 More than 60% of this cooling has occurred before the AW subducts beneath the fresh PW in
771 Fram Strait, and the transformed AW is sufficiently dense to contribute to the GSR overflow.
772 Dense water formed in the Iceland and Greenland Seas during winter additionally contributes
773 to the OW as described in Section 2.3.

774 The hydrographic properties at the GSR of both inflowing AW and outflowing OW are quite
775 well represented in NorESM (Fig. 6). In general, the largest bias is found in salinity. A
776 typical example after the completed AW transformation is the observed and simulated
777 Iceland Sea Intermediate Water that differ by about 0.15 in salinity but matches well in
778 temperature. We also note that the cooling of the AW as it progresses northwards appears to
779 be too strong in NorESM (Ilicak et al., 2016), but this bias only appears north of the GSR. At
780 the Barents Sea Opening, the simulated mean temperature is about 1.0 °C lower (Fig. 6) and
781 salinity 0.1 lower than observed values. A probable explanation for this deficiency is the
782 course resolution of the model leading to too much mixing with the colder and fresher coastal
783 waters (Docquier et al., 2020). A too slow (under-resolved) boundary current will also lose
784 too much heat. Ilicak et al. (2016) found that NorESM is too diffuse and loses the AW heat
785 and salt too quickly as it flows northwards, and conclude that is likely due to a lack of
786 parameterized physics in the vertical mixing process and/or description of water mass
787 exchange between the shelves and deep basins. North of the Fram Strait and the Barents Sea,
788 NorESM has excessive cold water spilling into the Polar Sea through the St. Anna Trough,
789 mixing extensively with the AW. Despite some regional biases, transformation from a density
790 of ~27.4 kg/m³ (inflowing AW) to ~28.0 kg/m³ (outflowing OW) is realistically captured, and
791 simulated trends and anomalies are independent of the mean state.

792 **The atmospheric circulation and heat loss:** The surface heat flux is largest over the
793 northward-flowing AW between the GSR and the sea ice (Fig. 4). The heat loss increases
794 towards the north in Fram Strait west of Svalbard and in the Barents Sea. The spatial pattern
795 of this heat loss north of 60°N is very similar between 20CRv2 and NorESM, and this is
796 reassuring as the two have quite different sea ice cover distributions. The annual mean heat
797 fluxes in the individual seas are somewhat different from the simulated heat loss (Fig. 3),
798 which is mainly caused by the active ocean and sea ice components of the NorESM (not
799 shown). The NorESM generally simulates higher Arctic sea ice concentrations in the period

prior to 1950, as we will later discuss for the Barents Sea. This is also the case for the Nordic Seas and the Polar Sea.

Given the inherent uncertainties when reconstructing the atmospheric state in the Arctic based on limited surface observations during the first half of the 20th century, we do not examine trends in atmospheric heat transport. Instead, we analyze which atmospheric features drive the ocean heat loss and contribute to its large interannual variations over the regional seas (section 4.2).

CO_2 uptake: Centennial mean CO_2 uptake for the Arctic Ocean (Table 1) is calculated based on the extrapolated basin-wide CO_2 fluxes (Table 2, Fig. 7). Just as for the heat loss, the Nordic Seas dominate the total Arctic Ocean CO_2 uptake, but the CO_2 uptake in the three basins becomes more similar with time. This is likely due to the strong influence of sea ice loss – more open water – on CO_2 uptake in the Barents and Polar Seas. The centennial mean CO_2 uptake in the Arctic Ocean (191 MtC/yr, Table 1) is consistent with the back-of-the-envelope calculation presented in Section 2.4 and previous estimates (Yasunaka et al., 2018). This suggests that heat loss is the major driver of the Arctic Ocean carbon sink and that biological drawdown plays a smaller role. The Arctic Ocean CO_2 uptake estimated here corresponds to ~8% of the global ocean CO_2 uptake of ~2500 MtC/yr (Friedlingstein et al., 2019). This is much larger than the area of 12.4 mill km² (3.4% of the total ocean area of 362 mill km²) would suggest, highlighting the importance of the Arctic Ocean as a major carbon sink during the last century.

4.2 Variability and Trends (1900 - 2000)

With the long-term means established for the Nordic, Barents, and Polar Seas (Fig, 2), we continue to describe variations and trends. We do this by first presenting the overall variability in atmospheric forcing over the larger Arctic Ocean region. Our main focus, as before, is on the Nordic Seas as the major heat loss variability occurs there (Fig. 3). After that, we describe the various consequences and related AW and heat variability elsewhere within the Arctic Ocean.

The atmospheric circulation and heat loss: Consistent with previous studies (e.g., Papritz & Spengler 2017), pronounced ocean heat loss over the Nordic Seas is associated with an increased frequency of CAOs (Fig. 8a). In absolute terms, the frequency of occurrence increases from 10-15% of the extended winter season for low heat flux years to 20-25% of

831 the time for high heat flux years. Because the heat loss takes place during winter presented
832 results are for an extended winter for each calendar year (January-April, November, and
833 December). However, results for consecutive extended winter seasons (November-April) and
834 core months (December - February) are very similar. This highlights that our results are
835 insensitive to the definition of winter.

836 CAOs over the Nordic Seas are associated with more cyclones than average over Scandinavia
837 and the eastern part of the Nordic Seas (Fig. 8b), in accordance with Papritz & Grams (2018).
838 This is because cyclones situated in this region have their cold sector situated over the Nordic
839 Seas. In the cold sector, they advect cold air masses from the central Arctic and through Fram
840 Strait over the relatively warmer ocean, yielding more CAOs (Fig. 8a). Further, the increase
841 in cyclone activity over Scandinavia indicates a reduced frequency of Scandinavian
842 anticyclones and blocks linked to the negative phase of the Scandinavian pattern. The relation
843 can be quantified by the negative correlation between a Scandinavian pattern index time
844 series and the ocean heat loss of r = -0.48 (not shown).

845 While the Nordic Seas heat loss is related to more cyclones over Scandinavia, it is also
846 related to fewer cyclones between Greenland and Iceland (Fig. 8b). The reduction in cyclone
847 occurrence here of ~7% represents about one-fourth of the climatology (30%, blue contours).
848 Accordingly, the heat loss is correlated with the East Atlantic pattern (r = -0.49), which in its
849 negative phase is associated with fewer cyclones over, and to the west of the British Isles.
850 The ocean heat loss in the Nordic Seas exhibits a negative correlation also with the NAO, but
851 it is comparatively weak (r = -0.15) and not statistically significant.

852 **Ocean Heat Transport:** The OHT of AW across the GSR has varied due to changes in
853 volume transport and temperature over the last century. The primary reason for the steady
854 increase in OHT from +150 TW to +200 TW over the last century (Fig. 5) is an enhanced
855 flow across the GSR of about +1 Sv, which on the outflow side is split into OW and PW into
856 equal parts (Fig. 9). The enhanced volume transport alone explains a linear trend of 28
857 TW/century while changes in temperature on their own would cause an increase of 17
858 TW/century. Both the overturning and gyre components contribute about equally to the
859 increase as expected from the similar trends in OW, and PW volume transports. No
860 significant trends in volume transport are found for the Canadian Archipelago and the Bering
861 Strait over the last century (not shown). The cause of this volume transport increase across
862 the GSR is attributed to Arctic Ocean heat loss and local wind forcing, as discussed in section
863 5. Both the OW and the PW have cooled slightly over the last century but appear to stabilize

or warm in recent decades (Fig. 9). For the AW returning south across the GSR, the AW outflow, there has been no trend in volume, but a general small long-term warming. The GSR AW outflow includes both AW flowing south in the Denmark Strait and recirculated in the Faroe-Iceland and the Faroe-Scotland channel, and is therefore relatively warm.

Nordic Seas heat loss: The Nordic Seas heat loss has remained quite constant (Fig. 3) despite a large increase in poleward OHT across GSR and a loss of Nordic Seas ice cover. The century long heat loss trend of +6.2 TW/century (Table 1) is only +5% of the total heat loss and thus quite small and not significant. This implies that the Nordic Seas have warmed or that heat now reaches further poleward. Consistently, the increased GSR OHT mostly continue into the Barents Sea with the retreating sea ice (not shown). Furthermore, there has been a systematic warming in the simulated Nordic Seas since the 1970s of about +0.5°C (volumetric mean, not shown). This warming is also consistent with a small reduction in the Nordic Seas heat loss to the atmosphere of about 10 TW over the last 50 years (Fig. 3) The reduced heat loss explains about half of the simulated warming.

The (annual mean) Nordic Seas ice cover dropped from ~700.000 km² around 1900 to ~500.000 km² in the late 1970s. The sea ice cover has been quite stable since the 1980s with values in the range 400.000 to 450.000 km². The main reason for the sea ice decrease is not a reduced heat loss - as this has remained fairly stable (Fig. 3). The annual changes of Nordic Seas heat loss are thus also unrelated to the sea ice area (r = -0.09); they are rather explained by variations in the atmospheric circulation as described above. This is consistent with most of the heat loss occurring away from the sea ice covered areas over the warm AW in the east (Fig. 4). There is only a small correlation between sea ice area and the net OHT (r = -0.27), but there is a much larger correlation between sea ice area and the inflowing OHT across the GSR (r = 0.77). The GSR OHT seems to drive a similar response for Nordic Sea ice as documented in the Barents Sea with 10 TW of OHT leading to an ice loss of 70.000 km² (Årthun et al., 2012**,** not shown). Reduced sea ice import from the Polar Sea has also contributed to the Nordic Seas ice loss. Over the 1920-1950 period, this import was as high as ~3000 km³/yr, largely caused by a thicker sea ice cover. The ice import dropped to ~2000 km³/yr towards 2000, and the correlation between sea ice import and the Nordic Sea ice area is r = 0.55. This decreased import of ice represents a drop in required heat for melting from 20 to 12 TW, a magnitude well within the range of annual variability of ±20 TW (not shown).

Barents Sea heat loss has increased steadily over time (Fig. 3), with a very systematic congruent increase in AW temperature and a decrease in sea ice cover (Fig. 10b). The

increased heat loss corresponds to an increase in the area-averaged surface heat flux from ~30 W/m² around 1900 to ~50 W/m² around 2000. This is first and foremost a consequence of sea ice retreat, as there is a high correlation between the Barents Sea open water area and heat loss (r = 0.86). Using a representative heat flux of the open water area (Fig. 4) of 100 W/m², most of the increased cooling (+30 TW between 1900 and 2000, Fig. 3) can be explained by the more extensive open water area (sea ice area of ~750.000 km² in 1900 decreasing to ~450.000 km² in 2000, Fig. 10). This further supports earlier findings (Årthun et al., 2012; Smedsrud et al., 2013, Muilwijk et al., 2019), concluding that the OHT is the main driver of sea ice and heat flux variability in the Barents Sea, with positive OHT anomalies preventing sea ice formation and letting the heat escape to the atmosphere; "The Barents Sea Cooler" (Skagseth et al., 2020). Consistent with Muilwijk et al. (2018), most of the increased Barents Sea OHT is related to an increase in volume transport of about +1 Sv over the last century (not shown). These changes occur at the same time as there are large observed changes in ocean temperature in the southern Barents Sea (Kola section, Fig. 10a). Additionally, a recent increase in AW inflow temperature has resulted in a steady increase of SST from the early 2000s (Barton et al., 2018). The NorESM simulations capture this ice-ocean variability well, although the mean temperature is too low.

Polar Sea heat loss also increases steadily over time, with a tripling from 7 TW in 1900 to around 21 TW in 2000. The annual mean heat flux remains below 3 W/m², mostly explained by a long-lasting sea-ice cover and net sea ice growth. Open water area increased from around 5% in the early period (1900-1920) to 20% after the 1990s; this corresponds to a loss of about 1 mill km² of sea ice area. In the annual mean, this sea ice loss occurs directly north of the land areas from Svalbard, along Siberia to Alaska (not shown). There is a small net increase in OHT for Bering Strait and the Canadian Archipelago (Fig. 5), as well the northward OHT through the Fram Strait and the Barents Sea (not shown).

Hydrography and dense water formation: The net AW-inflow increase across the GSR of about 1 Sv over the last century was compensated by an equally large increase in the southward outflow. Approximately 0.4 Sv of this increase can be assigned to the OW (Fig. 9), mainly to the OW spilling across the GSR in the Faroe Shetland Channel (not shown). The southward transport of cold low salinity PW in the Denmark Strait has increased by 0.6 Sv, while no significant trend was found in the AW outflow (Fig. 9, Table 3). The simulated positive trend in OW volume transport occurred together with a simulated negative trend in OW temperature until the 1980s that is comparable to observations after 1950 (Fig. 6, 9).

930 Systematic cooling was also evident in the simulated upstream intermediate waters during the
931 same period (not shown). The largest temperature decrease (1°C for the Iceland Sea and
932 0.5°C for the Greenland Sea intermediate water) occurred between 1920 and 1960. This is
933 consistent with the large increase in atmospheric heat loss over the same time period (Fig. 3).
934 After the 1980s, the intermediate water masses started to warm. This occurred concurrently
935 with both increased AW inflow temperature and reduced atmospheric heat loss. A small but
936 persistent warming has also occurred in the OW after around 2000.

937 **Greenland Ice Sheet melting:** Variability in ocean temperature adjacent to the Greenland ice
938 sheet is understood to drive the advance and retreat of marine-terminating glaciers (e.g.,
939 Straneo & Heimbach, 2013). Slater et al. (2019) developed a parameterization relating
940 tidewater glacier terminus position to ocean temperature on the continental shelf and to the
941 subglacial discharge of surface melt. The application of this parameterization to NE
942 Greenland allows us to quantify the impact of ocean variability on the regional ice sheet over
943 the past century.

944 The parameterization suggests there have been sustained periods of both advance and retreat
945 over the past century (Fig. 11). According to the proposed parameterization, sustained retreat
946 occurred during 1900-1925 (Fig. 11b) during a period of increasing subglacial discharge but
947 stable ocean temperature (Fig. 11a). This is followed by ~50 years of advance during a period
948 of cooler ocean temperature and reduced subglacial discharge. From 1980 to the present, a
949 sustained retreat is projected in response to both ocean warming and increased subglacial
950 discharge. The response of glaciers to the ocean alone (Fig. 11b, blue) can be isolated by
951 applying the parameterization while holding subglacial discharge constant (Slater et al.,
952 2019). Based on these results, the ocean variability alone explains about 50% of the marine-
953 terminating glacier advance and retreat in NE Greenland over the past century.

954 Observations of tidewater glacier terminus position from satellite imagery since 1984 (King
955 et al., 2020) also show sustained retreat during this period and agree well with the projections
956 (Fig. 11b). The longer-term projected trends are also very consistent with terminus position
957 changes observed in southeast Greenland since 1931 based on historical and satellite imagery
958 (Bjørk et al., 2012).

959 **CO_2 uptake:** The calculated CO_2 fluxes from 1900-2009 (Fig. 7) show a rather stable uptake
960 in the Nordic Seas, with no discernible trend. This is consistent with the small (not
961 significant) trend in heat loss over the Nordic Seas in this time period (Fig. 3). However, the

gradual sea ice loss results in essentially a doubling of the ocean CO_2 uptake (fluxes) in both the Barents and Polar Seas. According to our simple but physical extrapolations described in section 3 (Table 2) the Barents Sea mean CO_2 flux increased from 47 to 60 MtC/yr from 1900 to 2009, while the mean Polar Sea CO_2 flux increased from 36 to 61 MtC/yr. The much smaller Barents Sea has a larger overall uptake, reflecting both the larger areas of open water and the strong cooling, but the total uptake is similar between Barents Sea and Polar Sea from 1960-2000 (Fig. 7). Because our algorithms (Table 2) only explain 42-48% of the variance in observations, we make no attempt to use the extrapolated data to analyze variability in CO_2 uptake over this period.

4.3 The last decades (2000 - 2018)

Atlantic Water Inflow volume: There are no observed trends in AW inflow volume across the Svinøy section west of Norway between 1996 and 2018. This is nicely captured by the NorESM model (Fig. 12 b). The observed variability of the AW inflow in the eastern branch at the Svinøy section is presented in Fig. 12 b) and is ±0.5 Sv in the last 20 years. There is a low positive correlation with the local wind forcing, suggesting a contribution from simple Ekman transport dynamics towards the Norwegian coast. The baroclinic transport of the western branch at the Svinøy section was calculated based on Eq (2) with Coriolis parameter f for 60°N, reference density $\rho_{ref} = 1027.5\ kg/m^3$, integrating to a depth h=500 m. The resulting mean baroclinic AW inflow value of this western branch was calculated from 123 CTD casts taken at one single location offshore of the slope current between 1996 and 2018. This AW inflow is 4.1Sv ±0.1 Sv and was added to the observed AW volume of the inner branch in Fig. 12 b). The de-seasoned standard deviation of the western branch baroclinic transport is 0.9 Sv and is likely mostly due to eddy variability.

The halting Barents Sea Cooling Machine: New observations clearly indicate a major change in the Barents Sea over the last 20 years. Fig. 10 shows a continued loss of annual sea ice cover and continued warming. The sea ice loss has mostly occurred in the northeast, and in this region there has also been an increased heat loss (Skagseth et al. 2020). In the southwest, however, heat loss was substantially reduced in the 2000s, compared to the 1980s and 1990s, to the extent that total Barents Sea heat loss decreased in the recent decades (Fig. 3). This has created warming of the dense water that exits to the Polar Sea via the St. Anna Trough (Fig. 2). The major change is an increase in sensible heat flux over the southern Barents Sea, while there were minor changes in both latent, shortwave, and long-wave

surface fluxes, based on the ERA-interim re-analysis (Skagseth et al., 2020). Asbjørnsen et al. (2020) show that most of the recent change is caused by high AW OHT and reduced surface heat loss.

Hydrography and dense water formation: Since the 1980s there has been persistent warming in the interior Iceland and Greenland seas with a rapid increase of 0.5°C and 0.7°C from 2000 to 2018 (not shown). The long-term (1950-2019) trends for the OW are still showing cooling (Fig. 6), but there is a small sign of observed OW warming after 2000 that is also partly simulated by the NorESM. One main reason for this warming is the increased temperature of the AW inflow. The co-variability between the AW inflow and OW properties was thoroughly investigated by Eldevik et al. (2009) based on observations up to 2005, and our updated time series supports their main findings. They found that anomalies in temperature and salinity exiting the Denmark Strait have travelled along the rim of the Nordic Seas from inflow to overflow, and concluded that the AW circulating in the Nordic seas is the main source for changes in OW. Additionally, Lauvset et al. (2018) found a strong correlation (r=0.72) between the AW temperature in the Faroe Shetland Channel and the near-surface temperature in the central Greenland Sea 3 years later. A similar correlation (r=0.80) was found for salinity, which further supports that AW anomalies transfer into the Greenland Sea through lateral mixing or direct advection. The other main reason for the observed intermediate water warming is a reduced wintertime heat loss. Moore et al., (2015) showed that the magnitude of the winter heat loss in the central Iceland and Greenland Seas has declined by 20% since 1979, mainly because the ice edge and the cold winds are further away. There are thus different rates of warming in the atmosphere and ocean that at present may affect the Greenland Ice sheet.

Greenland ice sheet: Simulated subsurface ocean temperature on the NE Greenland continental shelf has increased consistently since approximately 1980, but a particularly rapid increase of >0.75°C occurs between 2000 and 2017 (Fig. 11 a). The simulated subsurface ocean temperature exceeded +1°C in 2017 for the first time in over a century, and the mean temperature post-2000, at 0.63°C, is higher than during any 20-year period since 1900. The tidewater glacier response has been a sustained retreat (Fig. 11 b), with a particularly rapid retreat of 0.48 km post-2000. Even if ocean temperatures now stabilize, tidewater glaciers in NE Greenland may continue to retreat due to the long response time of tidewater glaciers to climate forcing. As such, in the absence of ocean temperatures returning to pre-2000 values,

tidewater glaciers in NE Greenland are likely to remain in a retreated or further retreated state over the next decades.

The Arctic sea ice loss and CO_2 impact. The gap-filled data product for Arctic Ocean CO_2 fluxes over the period 1997-2018 (Yasunaka et al., 2018) shows no significant trend in the Polar Sea CO_2 fluxes. However, in the Nordic Seas and the northern Barents Sea these estimates show that CO_2 uptake has strengthened. Interestingly the fluxes have weakened in the southern part of the Barents Sea, consistent with the observed local warming and smaller heat loss (Skagseth et al., 2020). While both the Nordic Seas and the Barents Sea exhibit stronger CO_2 uptake, the mechanisms are different. In the Barents Sea, the increased CO_2 uptake is primarily a consequence of the sea ice loss (Fig. 10), and the present uptake has increased from the ~59 MtC/yr estimated in Smedsrud et al. (2013) to about 80 MtC/yr today (Fig. 7). In the Nordic Seas, the increasing CO_2 uptake is instead due to increasing disequilibrium between pCO_2 in the atmosphere and in the mixed layer. In the Polar Sea, impacts of the retreating sea-ice edge on the CO_2 flux is evident in all regions that have lost ice the past few decades. There is in general strong correlation between CO_2 uptake and the number of ice-free days, and this pattern is expected to spread northwards as the ice retreats further.

5 Discussion

Our review and analysis presented five main results over the last century, summarized with the simplified sketch in Fig. 1.; 1) A majority of the Arctic Ocean heat loss occurs in the Nordic Seas where the AW is warmest, and the variability is directly driven by the atmosphere. 2) Production of dense water flowing southwards towards the North Atlantic across the GSR has remained fairly stable, but there is a small volume increase and recent warming. 3) Increased Arctic Ocean heat loss has increased the overall CO_2 uptake. 4) Warming waters on Greenland's continental shelf affect melting of marine-terminating glaciers in NE Greenland. 5) The Arctic Ocean sea ice cover is shrinking and there is a related increase in OHT and ocean heat loss in the Barents and Polar Seas. We start by discussing the regional contrasts in the strongly coupled heat loss, OHT, and sea ice cover, before venturing into the temporal changes.

Regional Arctic Ocean heat loss: Generally, the heat flux is larger in the east than in the west, caused by the larger temperature contrast between the warm AW inflow and the cold Arctic atmosphere (Fig. 4, Mauritzen 1996; Segtnan et al., 2011). The heat loss values are

largely consistent with earlier estimates stating that the Nordic Seas dominate the heat loss but are in the lower range (Simonsen & Haugan 1996). Given that most earlier estimates are from recent decades and the large positive trends presented here - this is within expectations. The centennial mean values are, however, still consistent with new estimates from ocean re-analysis after 2001 (Mayer et al., 2019). These show consistent values with average heat fluxes of ~40 W/m² in the Barents Sea and values below 5 W/m² in the Polar Sea, similar to Table 1.

Temporal variability of heat loss: The overall Arctic heat loss increases over time (Fig. 3). The heat loss trends over the last century are mostly found in the Barents Sea and in the Polar Sea, reflecting the sea ice retreat and expansion of open waters there (Fig. 10). The generally increasing open water area in the Arctic Ocean thus generally allows a larger heat loss to the atmosphere, and the implied mean heat flux in the new open water area is 40 W/m² (not shown). There has also been a sea ice loss in the Nordic Seas - but only a small (and not significant) trend in heat loss. The major explanation for the different heat-loss and sea ice relationship in the Nordic Seas is that the sea ice loss occurred in regions with cold surface water. Regardless of the small heat loss trends in the Nordic Seas, it is here where the bulk of the heat loss takes place, as already suggested by Helland-Hansen & Nansen (1909). The Nordic Seas also dominate the year-to-year variability, directly forced by the atmospheric circulation (Fig. 8). Consistent with other recent work (e.g., Papritz & Grams 2018), we find that in the years with most heat loss in the Nordic Seas, more cyclones than usual occur over Scandinavia (a negative SCA pattern) and drive winter-time bursts of cold air over open water (CAOs).

Temporal variability of Arctic Sea ice cover: The NorESM sea ice loss is similar to observation-based Arctic sea ice reconstructions (Walsh et al., 2017; Brennan et al., 2020) for the time period after 1960. We focused on the Barents Sea ice cover variability (Fig. 10 b) as it is the region that mostly affects the heat loss trends. For the period before 1960, the NorESM Barents Sea ice cover has similar variability but overall larger values. These annual values are mostly reflecting the winter sea ice, as there is not much summer sea ice in the Barents Sea (Onarheim et al., 2018). The observational coverage in winter is also relatively scarce prior to the 1960s (Walsh et al., 2017), and these values are at least in part reflecting the use of low climatic mean values from recent decades. As the NorESM values reflect atmospheric forcing from the 20CRv2 that incorporate observations from available weather

stations, it is not clear which of the sea ice estimates best reflect "observations". The NorESM fields are at least from simulations that conserve energy between the OHT, the sea ice, and the heat loss , but there are also uncertainties in parametrizations of surface fluxes. The decreasing Barents sea ice cover is consistent with the available atmospheric forcing, and the ocean variability appears well captured as the independent temperatures of the Kola section reflect (Fig. 10a). We also know that there is a physical link between the strength of the AW inflow, Barents Sea temperature, sea ice cover and heat loss (Smedsrud et al., 2013). The Barents Sea ice decline between 1900 and 1950 is thus consistent with the observed increasing temperatures (Fig. 10a) that provides confidence in the simulated sea ice cover. The cold bias in the model described in Section 4.1 does not affect the variability. The simulated Barents sea ice loss is also consistent with new Arctic estimates over the last century (Schweiger et al., 2019), who found a significant decline in sea ice volume in the Atlantic sector from 1900 - 1940 related to early-twentieth-century warming. Muilwijk et al. (2018) found that this early warming was more related to a warm temperature anomaly in contrast to the AW volume anomalies dominating later in the century.

Heat loss and Ocean Heat Transport: The overall Arctic heat loss variability contributes to variations in OHT over time. The analyzed NorESM forced ice-ocean simulations apply both wind and buoyancy forcing to drive the inflows and outflows, so we attempt to extract the heat loss contribution using a simplified analytical Arctic Ocean model (Eq. 1, Spall 2004). Figure 12 a) shows that the heat loss explains a large portion of the variability since 1900. A close to 50% increase of the overall Arctic heat loss Q is a close match to the simulated increase onwards from 1900 (150 ⇒ 225 TW, Fig. 3 or 12 ⇒ 18 W/m², Fig. 12 a). These heat flux values lead to a surprisingly good fit with the NorESM values with an increased AW inflow from 9.5 to 11.0 Sv. An increase in the AW OHT has been found as a consequence of increased CO_2 forcing using a fully coupled climate model and could thus be expected (van der Linden et al., 2019).

It may appear surprising that the simple relationship by Spall (2004) can explain much of the variability in a forced complex climate model like the NorESM. Given these limitations such as the assumption of a perfectly circular basin, the representativeness of this relationship is spanned out using a range of plausible values: the radius of the basin $R = [1900, 2100]$ km, slope width $L = [90, 120]$ km, thermal expansion $\alpha = [0.18, 0.22]$, eddy mixing efficiency $c = [0.22, 0.28]$, and the depth of the GSR $H = [400, 600]$m. The overall relationship

between the heat loss and the overall volume inflow remains clear and is also consistent with first order analytical diagnostic of the volume, heat, and salt budget (Eldevik & Nilsen 2013). The inflow strength is governed by the thermal wind equations and is a steady-state solution. Consistently there is a better fit for the Spall (2004) line with the 5-year means than the annual values (Fig. 12 a). There is indeed some volume flow variability of order ±1Sv that is away from the expected heat loss (flux) relationship, especially on the year-to-year basis. We, therefore, turn to the wind-driven variability below.

As discussed above, a majority of the OHT increase over the last century is explained by an increased AW volume inflow, as temperature changes were minor and the OHT across the other Arctic straits remained stable. This is consistent with new short-term results from farther south in the subpolar North Atlantic, which also find the OHT to be primarily dictated by AW inflow (Lozier et al, 2019). Recent work confirms a high OHT northwards through the Nordic Seas over the last decades. Eldevik & Nilsen (2013) estimated an Arctic Ocean heat loss of 282 TW based on observed mean inflow and outflow temperature and volume. They ignored the contributions from the Bering Strait and Canadian Archipelago, so this is broadly in line with our values after the 1990's (up to 250TW). Based on moored observations across the Arctic gateways and an inverse calculation, Tsubouchi et al. (2020) estimated an increased Arctic OHT from ~ 290 TW in the 1990s to ~310 TW in the 2000s carried by both increased AW volume and temperature. Most of this heat (281 ±24 TW) is transported across the GSR. The NorESM numbers are lower, but consistent with a new state estimate for 2002-2017, suggesting a mean OHT of 223 TW across the GSR and a total Arctic Ocean heat loss of 239 TW (Nguyen et al 2020). Using primarily shipboard temperature and velocity measurements since 2008, Chafik & Rossby (2019) estimated a heat transport of 273 ±27 TW across the GSR. These numbers are ~50 TW higher than the comparable simulated northward OHT across the GSR (Fig. 5). So while the NorESM has inflowing AW transporting 285 TW, there is also ~100 TW transported out by the-−3.3 Sv of AW outflow (Table 3), making the net long-term mean OHT as low as 172 TW. About -1.6 Sv of the AW outflow occurs in the Faroe-Shetland channel (Fig. 2). This is twice the amount found by Berx et al.(2013) from 1994-2011 but comparable to the estimate from Rossby et al. (2018) here. The rest of the outflowing AW is distributed in the Denmark Strait and east of Shetland . The separation used between southward flowing AW and OW does influence the volume of outflowing AW, and some authors appear to vary this separation between the straits (Østerhus et al., 2019). We classified water denser than 1027.8 kg/m³ as OW (Fig. 9).

Rossby et al., (2020) suggests that the OHT northwards across the GSR peaked in 2010 at ~270 TW, and predicts that it will reduce to ~210 TW in the decades ahead based on Atlantic SST variability 0-60°N (Atlantic Multidecadal Variability, Trenberth & Shea, 2006). Chafik & Rossby (2019) and Tsubouchi et al. (2020) thus both find that the overall OHT in recent decades is substantially larger than the simulated net OHT of ~200 TW (Fig. 5). Despite this disparity, we may conclude that the OHT has increased over the last century and appears to have peaked temporarily. This points to the importance of a continuous monitoring of this inflow.

Wind forcing of the AW inflow variability: Several studies show a strong link between the AW inflow and the large-scale wind forcing in the region. For example, Muilwijk et al. (2019) showed a clear relationship between NAO-type wind forcing in the Greenland Sea and the AW volume transport northward. Also, Bringedal et al. (2018) analyzed AW inflow across the GSR over the instrumented period (1996-2016). They found that wind forcing drives much of the seasonality and also interannual variability, but here overturning and buoyancy forcing must also be considered as the time scale increases. For monthly time scales, there is a connection to the NAO for the inflow along the Norwegian coast over these 20 years, where the along-coast wind stress drives an Ekman transport towards the coast that piles up water locally and drives a barotropic inflow (Eq. 2. in Bringedal et al., 2018). We have tested this relationship for the 1900-2000 period and find a consistent response of the simulated GSR inflow to the along-coast wind strength (Fig. 12 b). The correlation is high in the NorESM simulations (r=0.78), but lower and not significant for our new available observations in the Svinøy section (1996 - 2018). The increasing wind forcing thus partly explains the increased volume inflow across the GSR. There is no correlation between the (annual mean) GSR wind forcing and the ocean heat loss north of the GSR, so these are independent drivers of the inflow. Orvik et al. (2001) calculated the mean value of the outer (western) branch at Svinøy based on hydrography and found a (1995-1998) mean of 3.4 Sv. An updated baroclinic estimate of this branch is 4.14 Sv. The observed values in Fig. 12 b) show variability of the eastern inner branch with +5.14 Sv added to represent this outer branch and the +1 Sv inflow around Iceland.

Several studies have documented an increase in wind speed in some regions of the world ocean. A small overall increase in surface ocean flow speed of +1 cm/(s yr) was also found for the 1992 to 2015 period (Wunsch, 2020) based on satellite sea level data. Young & Ribal

(2019) documented an increase in wind speed between 1985 and 2018 of about ~2 cm/(s yr) in the Southern Ocean and of about 1 cm/(s yr) in the North Atlantic. These values are comparable to the +2 m/s increase over the last 100 years in the 20CRv2 reanalysis west of Norway (Fig. 12 b). A long-term increased wind forcing for many locations in the Norwegian Sea was also documented by Vikebø et al. (2003) for 1900-2000. They also found a consistent increase in wave height in this area but also noted a reduced wind forcing between 1880 and 1900. Wind observations were very limited before the 1950s, but we analyzed available observations from an island west of Bergen (Utsira) that is consistent with the overall increase (Fig. 12 b), although there are some substantial data gaps. However, wind increases are not visible in recent reanalysis (e.g., ERA5) for the last 40 years (1979-2019), and thus trends arise mainly from the early part of the century. The increase in wind speed along the Norwegian Sea and the related wind stress forcing on the ocean can thus explain part of the observed increase in the AW inflow and the OHT (Fig. 5). For the future, there is little consensus regarding expected changes in wind forcing, so we take this driver of OHT variability as natural climate variability. There are, for example, large inter-model differences in projected wind speed for the North Atlantic region, but also some consistent strengthening and squeezing of the zonal flow (Oudar et al., 2020).

Implications of Arctic heat loss, sea ice, and OHT: The discussion above summarized the combined consistent relationship between Arctic heat loss, the OHT, and the sea ice cover. Over the last century, the heat loss and OHT increased while the sea ice cover decreased. This relationship was perhaps expected based on analytical models and previous analysis but was quantified and presented in a consistent model framework here. Clearly, the inflowing AW OHT anomalies are not fully escaping to the atmosphere through cooling in the Nordic Seas, but some surplus heat is left and continues onwards into the Barents and Polar Seas. Our main hypothesis listed in the introduction was that the inflowing OHT AW anomalies influence the; **1) Ocean heat loss 2) deep and intermediate water properties 3) Arctic Ocean CO2 uptake, 4) Greenland's marine-terminating glaciers, and 5) Arctic sea ice cover** (Fig. 1). We established that there is an analytical relationship between the Arctic sea ice cover, ocean heat loss and OHT; less sea ice allows a larger heat loss and accommodates a stronger OHT by the AW. Arctic sea ice loss is one of the well-established consequences of global warming and increased CO_2 levels in the atmosphere (Notz & Stroeve, 2016), and the ocean heat loss and OHT, therefore, also change with global warming.

1219 How would this 'heat-loss\sea-ice\OHT' relationship have played out in the absence of global
1220 warming? As natural climate variability is strong in the Arctic - Atlantic sector, we speculate
1221 that the wind forcing would then have dominated the variability. AW inflow is partly wind-
1222 driven, and we found an increased wind-driven AW inflow (Fig. 12 b). This increased OHT
1223 would then alone also have contributed to ice loss, especially in the Barents Sea, as outlined
1224 by Smedsrud et al. (2013).

1225 **Warming AW and melting of Greenland marine-terminating glaciers:** The warming on
1226 the NE Greenland shelf of about +0.5°C since the 1970s (Fig. 11 a) is quite typical for the
1227 other Arctic shelf seas. In the Barents Sea, the warming has been twice as large (Fig. 9), but
1228 similar warming is otherwise simulated for all the Arctic shelf seas (not shown). The
1229 warming is also comparable to observations of AW temperature in the Fram Strait (79°N)
1230 and in the West Spitsbergen current (76°N) indicating that AW is the advective source
1231 (Muilwijk et al., 2018). There is a large re-circulation of AW in the Fram Strait (Hatterman et
1232 al., 2016), a water mass termed Return AW, and this has warmed about +1°C since the 1950s
1233 (Fig. 6). The simulated warming on the shelf (Fig. 11 a) is similar to that observed at the
1234 margins of the largest ice shelf in NE Greenland (Nioghalvfjerdsfjorden; Lindeman et al.,
1235 2020; Mouginot et al., 2015). The warming of AW inflow at the GSR is smaller than the
1236 warming in Fram Strait (Fig. 6). This suggests that the relatively low Nordic Seas heat loss
1237 since 2000 has played a role (Fig. 3). The simulated +0.5°C warming since the 1970s has
1238 clearly driven increased melting of marine-terminating glaciers, and the inferred retreat of
1239 ~0.5 km is substantial and about 50% of that observed (Fig. 11 b), consistent with additional
1240 retreat resulting from dynamic thinning of the glaciers in response to the forced retreat. The
1241 atmospheric warming, dictated by the 20CR forcing, is a clear manifestation of global
1242 warming. It too, contributes to driving glacier retreat through the enhanced submarine
1243 melting associated with an increased release of surface melt at depth (Jenkins, 2011; Slater et
1244 al., 2016). According to the employed data-constrained parameterization (Slater et al., 2019),
1245 the ocean and atmospheric variability contribute in approximately equal parts to the glacier
1246 retreat (Fig. 11).

1247 **Heat fluxes and CO_2 uptake:** The relationship between CO_2 flux and heat transport and loss
1248 is a consequence of the increased CO_2 solubility in colder waters, i.e., the larger the heat loss,
1249 the larger the CO_2 uptake. Using Eq (3) (Watson et al. 1995) and representative numbers for
1250 the early 20th century Arctic Ocean ($Q = 160$ TW; Atlantic inflow DIC = 2070 μmol kg^{-1}

and $R_f = 11$) we find a heat loss driven CO_2 uptake of 120 Mt C yr^{-1}. This increases to 160 Mt yr^{-1} for $Q = 210$ TW, which has been the value reached in the last decades (Fig. 3). The magnitude and increase of this heat loss inferred flux are somewhat smaller than the ~170 Mt yr^{-1} increasing to ~230 Mt yr^{-1} (Fig. 7). This might be related to the large uncertainties involved in this calculation; it is for example, highly sensitive to the exact heat flux value used and also the complete neglect of biological and anthropogenic fluxes. Naturally also the regressions in Fig. 7 (Table 2) have their uncertainties. Nevertheless, the results from the three lines of evidence presented the solubility considerations (Sec. 2.3), Fig. 7, and Eq. (3) with the simulated heat loss, give results of the same order of magnitude. Together theyshow that the bulk of the CO_2 uptake in the Arctic Ocean is driven by ocean cooling and that the increased cooling has caused a larger CO_2 uptake.

One might ask whether the difference between the increase in annual CO2 uptake derived from the heat fluxes here (40 Mt yr^{-1}) and that derived from the regressions earlier (60 Mt yr^{-1}) is a consequence of the fact that the increased heat loss has occurred in the Barents and Polar Sea associated with the retreating sea ice. This exposes waters undersaturated with CO_2 to the atmosphere and enables primary production, which leads to a larger CO_2 uptake than anticipated from heat loss increases alone (Anderson & Kaltin, 2001). This might be the reason why the changes in Polar and Barents seas' CO_2 uptake since 1998 relates more strongly to sea-ice cover than heat loss (Fig. 7). Disentangling the impacts of each specific process is best done with a fully coupled model, including carbon cycle components. Such studies should also consider the potential impacts of variations in the horizontal ocean carbon transports on the air-sea carbon flux in the Arctic Ocean; as these fluxes are much larger than the air-sea flux (Jeansson et al., 2011). More explicit accounting of changes in natural vs. anthropogenic carbon fluxes would also be worthwhile.

Heat transport anomalies and production of Overflow Water (OW): NorESM simulates mean properties and long-term trends of the dense waters flowing southward across the GSR reasonably well (Fig. 6). Since the mid-1990s, the observed OW transport has remained steady, but the temperature has increased (Hansen et al., 2016; Jochumsen et al., 2017; Mastropole et al., 2017; Østerhus et al., 2019), this is well captured by the NorESM (Fig. 9). Between 1998 and 2002, the observed AW inflow temperature and volume transport increased, resulting in a 7% increase in OHT (Tsubouchi et al., 2020), qualitatively similar but not identical to the NorESM simulations (Fig. 5). The recent interior warming in the

Iceland and Greenland Seas after 2000 is also partly captured by NorESM (Fig. 6). The density of the intermediate waters has been stable over the same time period due to a compensating increase in salinity (Lauvset et al., 2018). This balance may imminently change as a result of the pronounced freshening of the inflowing AW (Mork et al., 2019), especially if the heat loss continues to decrease as could be expected in a warming climate (Moore et al., 2015). On the other hand, may the sea ice retreat lead to more favorable conditions for dense water formation at new locations (Lique & Thomas, 2018), as recently observed in the Barents Sea (Skagseth et al., 2020), along the East Greenland Current (Våge et al., 2018), and north of Svalbard (Pérez-Hernández et al., 2019; Athanase et al., 2020).

6 Conclusion

Global Warming and Arctic sea ice loss have been ongoing and well documented for at least 30 years. The Arctic sea ice loss is consistent with a larger loss of heat from the ocean to the atmosphere, mostly in the Barents and Polar Seas. This increased heat loss from the inflowing Atlantic Water (AW) is in itself connected to a larger inflow of AW. However, there has additionally been an increased wind forcing of the AW inflow in the Nordic Seas, and the two together explain the long-term AW increase of about +1 Sv over the last century. This increased AW volume inflow is the main explanation for the increased heat transport to the Arctic Ocean from about 150 TW in 1900 to 200 TW today. The partitioning between overturning (dense water and Overflow Water (OW) formation) and the horizontal boundary current (Polar Water (PW) formation) has remained roughly equal over the last century, but temperature variability plays a larger role in the overturning part.

The gradual cooling of the AW as it circulates the Arctic Ocean from its entry across the Greenland-Scotland Ridge (GSR) mostly occurs in the Nordic Seas. The year-to-year variability of this (winter) cooling is dictated by the atmospheric forcing manifested in the variability of occurrence of low-pressure systems over Scandinavia, which drive Cold Air Outbreaks (CAOs) with strong winds off the sea ice in the Polar Sea. The AW cooling in the Nordic Seas explains about 50% of the CO2 uptake of the entire Arctic Ocean, but the contribution from the Barents and Polar Seas is increasing with the diminishing sea ice cover.

The sea ice cover of the Arctic is set to further decrease in the future. This will contribute to more open water and a larger ocean heat loss. Such an increased heat loss – unless compensated elsewhere – will again require a larger (baroclinic) inflow of AW and a larger Ocean Heat Transport (OHT). This heat transport takes place mostly in the horizontal inflow

of AW on the eastern side of the GSR, and there has been a consistent increase in this boundary flow of about + 1 Sv over the last century, which is thus expected to continue to increase. Consistently we expect that the main processes illustrated in Fig. 1 are all set to increase; warming on the Arctic shelves, the ocean contribution to melting of glaciers on Greenland, melting of sea ice, and the future Arctic Ocean CO2 uptake.

The future production of dense water is more uncertain, as it is wedged between the increased heat transported in and the larger heat loss at the surface. There is in addition, the natural climate variability exemplified here by the wind forcing of the AW and the CAOs. These fluctuations remain hard to dissect – not to say predict, and a century of variability may not be long enough to properly disentangle the governing mechanisms.

Acknowledgments

This work was supported by the Bjerknes Center for Climate Research, the Norwegian Research Council through the Nansen Legacy Project (Grant#276730) and the U.S. Norway Fulbright Foundation. L. H. Smedsrud particularly thanks the Foundation for the Norwegian Arctic Chair grant 2019-20 that made much of this work possible.

We acknowledge the World Climate Research Programme, which, through its Working Group on Coupled Modelling, coordinated and promoted CMIP6. We thank the NorESM Consortium for producing and making available their simulations, the ESGF for archiving and providing access, and the multiple funding agencies who support CMIP6 and ESGF. We would also like to thank all those who collected valuable observations over the last century that made this study possible.

Data Availability Statement

Monthly fields from the NorESM2-LM for the period 1958-2018 (Bentsen et al., 2019) have been provided through the Ocean Model Intercomparison Project Phase 2 (OMIP2) experiment as part of the Coupled Model Intercomparison Project Phase 6 (CMIP6, Eyring et al., 2016), and are available for download on the Earth System Grid Federation (ESGF) website: https://esgf-node.llnl.gov/search/cmip6/. Monthly fields of NorESM for the time period 1900-2009 are available upon request. 20CRv2c reanalysis data are freely available for download at https://portal.nersc.gov/project/20C_Reanalysis/. Kola section data is from the Knipovich Polar Research Institute of Marine Fisheries and Oceanography available through ICES (International Council for Exploration of the Seas; https://ocean.ices.dk/core/iroc)

Abbreviations

20CRv2 - 20th Century atmospheric Reanalysis forcing, AMO - Atlantic Multidecadal Oscillation, AW - Atlantic Water, CAO – Cold Air Outbreaks, DIC – Dissolved Inorganic Carbon, EOF – Empirical Orthogonal Functions, GSR - Greenland-Scotland Ridge, IW – Intermediate Water, NAO - North Atlantic Oscillation, NorESM - Norwegian Earth System Model, OHT - Ocean Heat Transport, OW - Overflow Water, PNA - Pacific North America pattern, PW - Polar Water, RAW - Return Atlantic Water, SIC - Sea Ice Concentration, SSS - Sea Surface Salinity, SST - Sea Surface Temperature.

1355

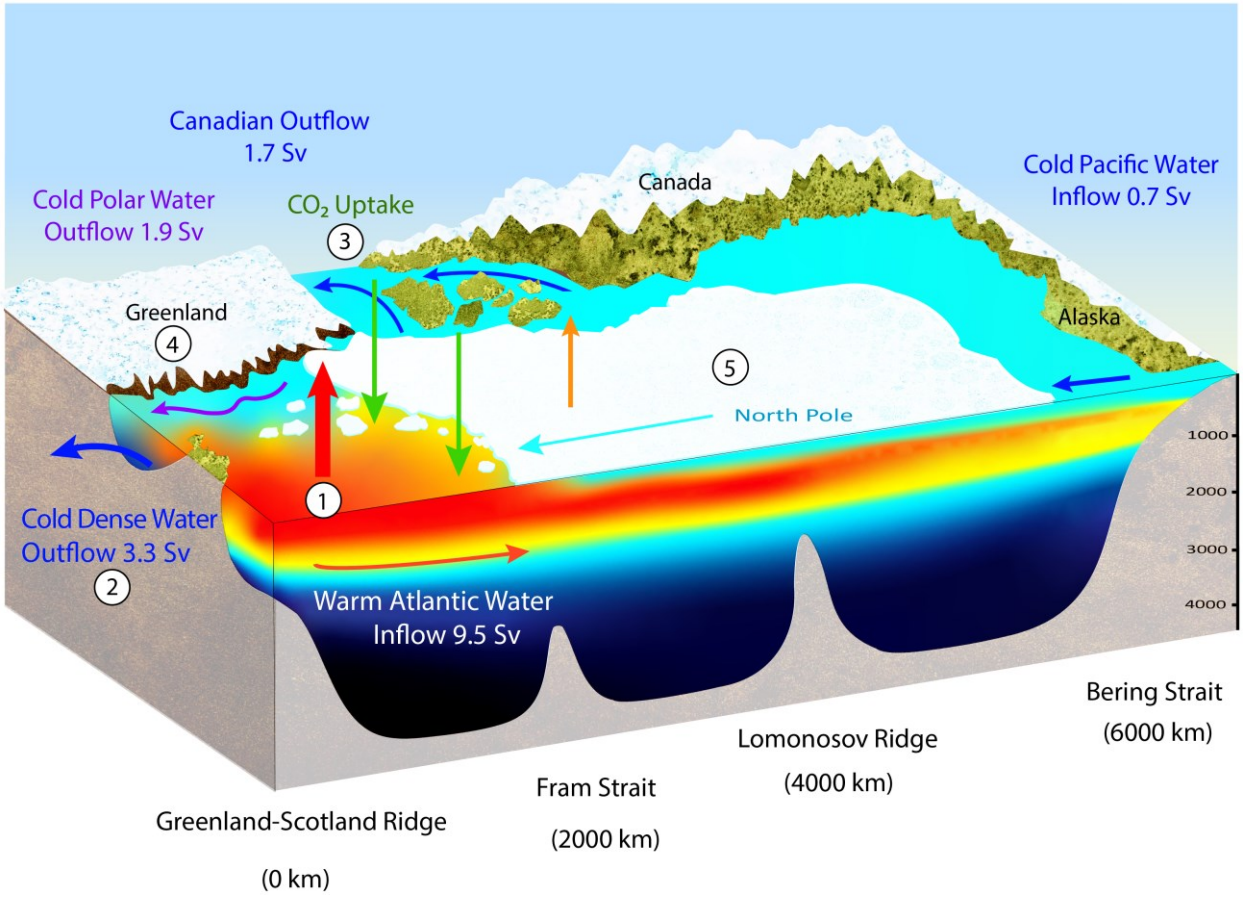

1356

1357 **Figure 1:** Schematic overview of the relationship between the warm Atlantic Water inflow
1358 across the Greenland-Scotland Ridge and its influence on 1) Nordic Seas heat loss, 2) deep
1359 and dense water outflow, 3) CO_2 uptake, 4) Greenland melting, and 5) Arctic sea ice cover.
1360 The vertical red arrow illustrates the large cooling in the Nordic Seas, and the orange arrow
1361 the smaller cooling in the Polar Sea. The eastern half of the Arctic Ocean and the Barents Sea
1362 is not shown, but the area and bathymetry is correctly scaled. The cyan arrow represents the
1363 systematic sea ice drift towards the Fram Strait.

1364

1365

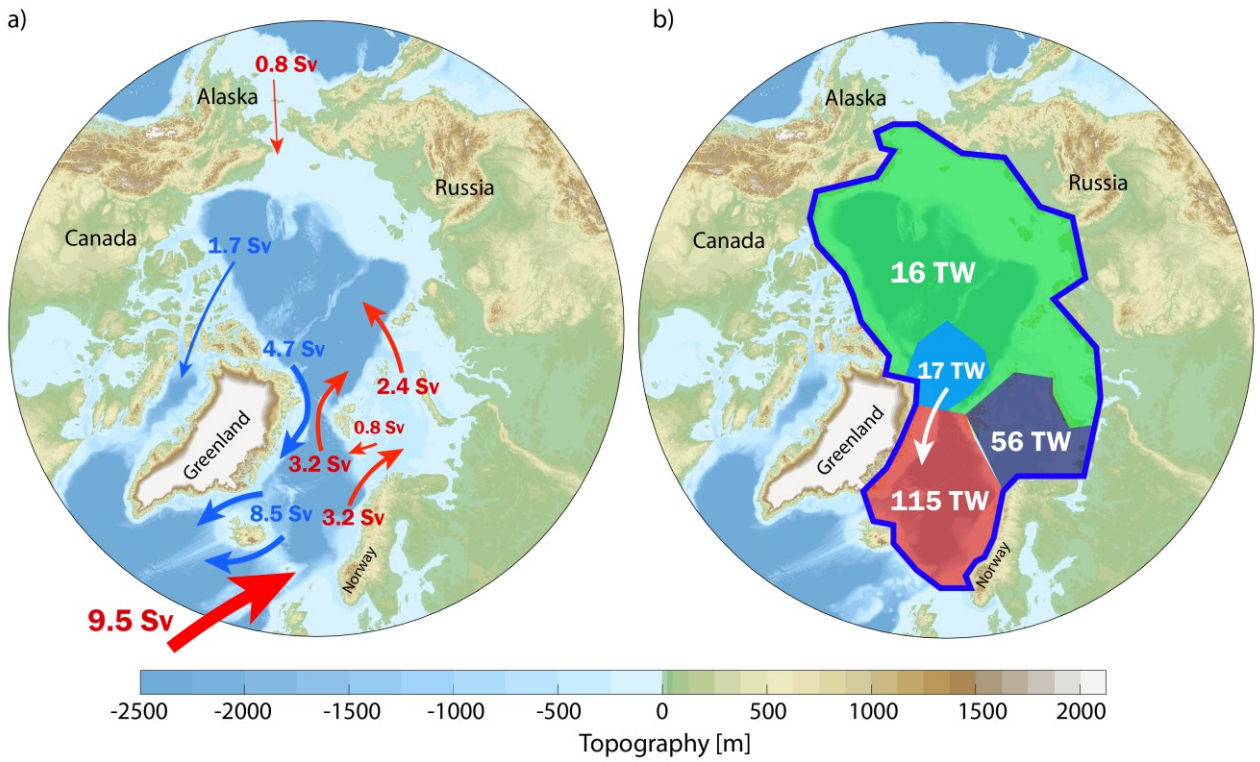

Figure 2: The mean simulated Arctic Ocean volume transport (Table 3) and heat loss. a) The northward (red arrows) and southward flows (blue arrows) are scaled so that the width represents volume transports in Sv. b) The heat loss in the Nordic Seas (red, area of 2.5 mill km²), the Barents Sea (black, 1.5 mill km²) and the Polar Sea (Green, 8.4 mill km²) in Tera Watts (1 TW = 1×10^{12} W). The cyan region represents the annual mean sea ice area export (~1 mill km²) from the Polar Sea to the Nordic Seas (white arrow). This heat is released to the Polar Sea atmosphere when the sea ice forms, with subsequent loss of heat from the Nordic Seas when the sea ice melts, contributing to the 115 TW cooling indicated in the figure. The Arctic Ocean is outlined (dark blue line) and is the sum of the colored regions. The division lines between the individual seas follow standard oceanographic sections.

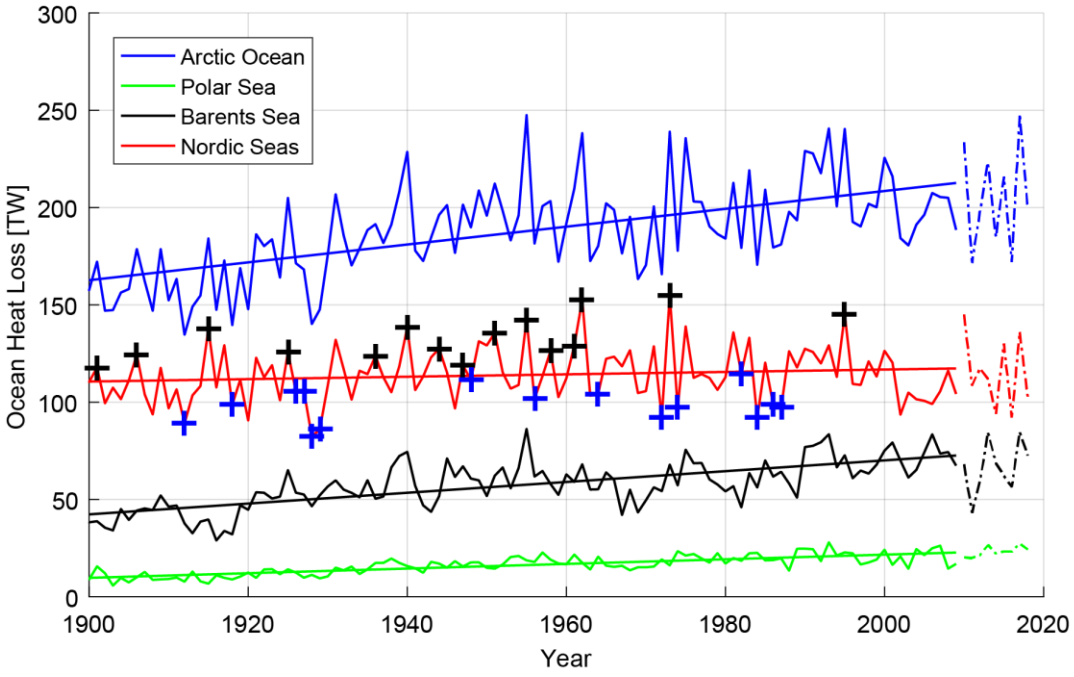

Figure 3: The simulated total annual heat loss of the Arctic Ocean (blue) and the three subdomains (green, black and red) by NorESM.

The simulated, annual mean ocean heat loss (TW) from the 20CR (1900-2009; solid lines) and the JRA forced (2010-2018; dashed lines) runs, with colors from Fig. 2b. The mean cooling of the Arctic Ocean is 187 TW (Table 1). For the Nordic Seas the 15 years of highest (black crosses) and lowest (blue crosses) annual de-trended heat losses are indicated.

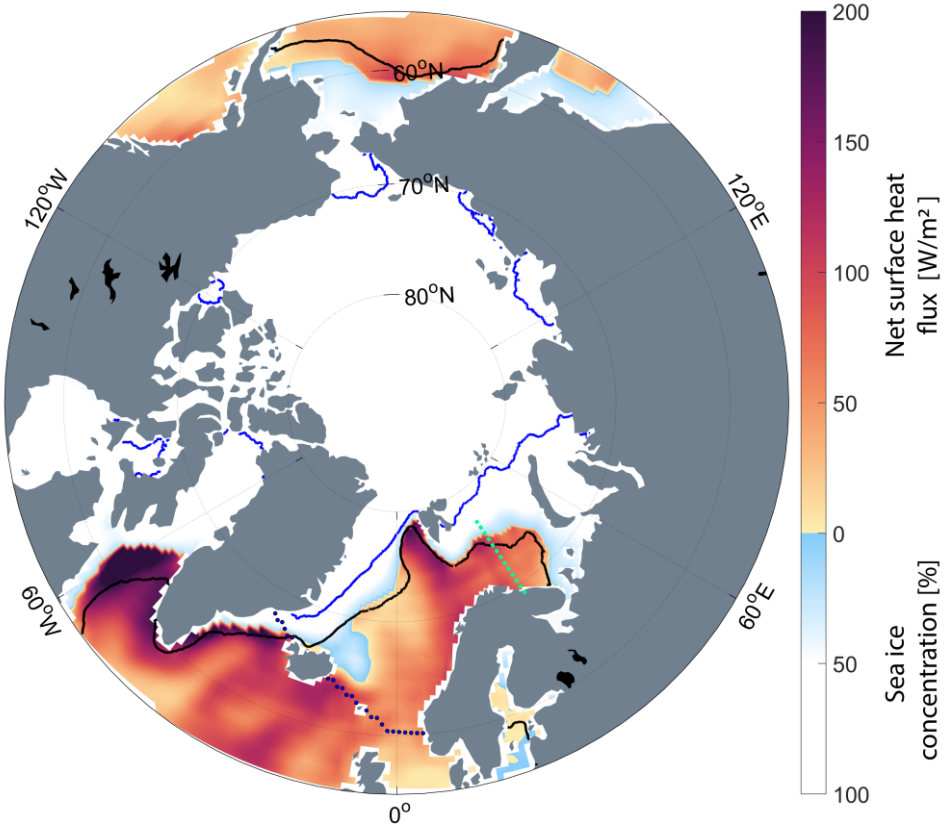

Figure 4: The simulated annual mean surface heat flux (W/m^2, warm colors) and Sea Ice Concentration (SIC, percentage, cold colors) between 1900-2000.

The centennial mean observed sea ice extent for September (blue line) and March (black line) has been added from Walsh et al. (2017). The dotted blue line shows the location of the Greenland-Scotland Ridge (GSR) as used here and extended directly east along 60 °N from Shetland to Bergen. The dotted green line shows the location of the Kola Section as used in Figure 10 (ICES, 2020).

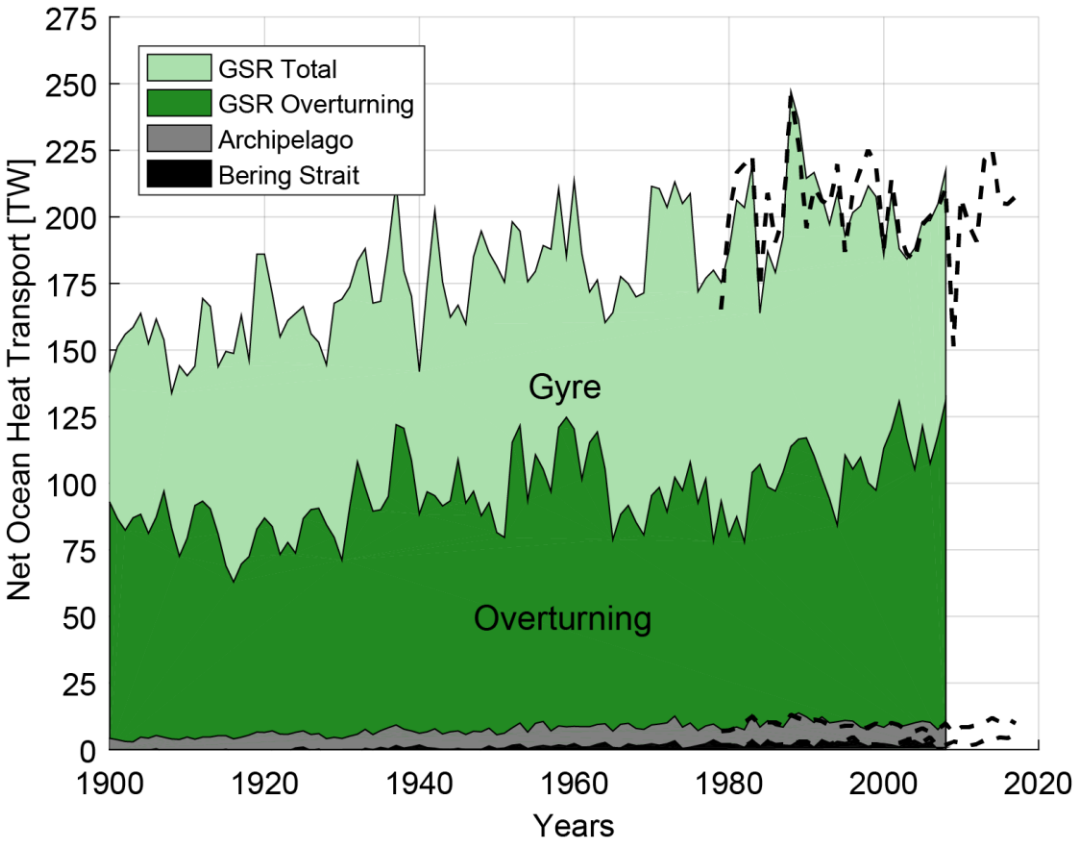

Figure 5: The simulated, annual mean Arctic Ocean heat transport.

The contributions from the individual straits are calculated using 0 °C as reference, and show the Bering Strait inflow, the outflow through the Canadian Archipelago, and the inflow and outflow across the Greenland-Scotland Ridge (GSR). The centennial mean Arctic Ocean heat transport is 179 TW. The top line shows the Arctic Ocean total independent of a reference temperature. The dashed line is the total NorESM JRA forced version updated to 2018. The heat transport across the GSR has been decomposed into a horizontal gyre and a vertical overturning contribution.

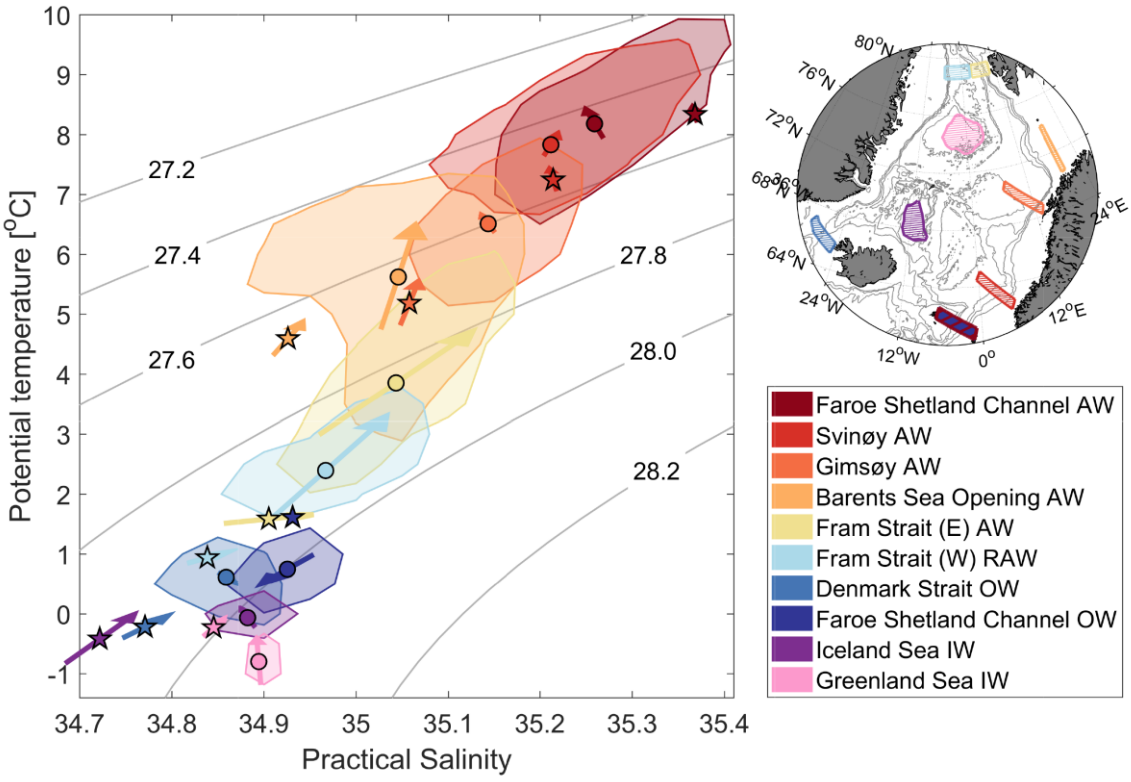

Figure 6: Observed and simulated Nordic Seas thermohaline water mass properties since 1950.

Geographical regions, with color coding, are marked on the map. The TS-range of each water mass is based on the frequency of occurrence and indicated by the colored patches outlining 60 percent of the observations. Color-filled dots show observed median values, and related arrows show the linear trends (1950-2019). Similarly, colored stars show simulated NorESM median values and the related arrows the linear trends (1950-2009). Vertical constraints for defining the water masses are as follow: Atlantic Water (AW) and Returning Atlantic Water (RAW) by the depth of maximum temperature below 100 m (± 50 m); Overflow Water (OW) by density above 27.8 kg/m³ and above the sill depths (650 m for the Denmark Strait and 840 m for the Faroe Shetland Channel); Intermediate Water (IW) by the typical mixed-layer depths 150-350 m in the Iceland Sea and 500-1500 m in the Greenland Sea. Observations from Brakstad et al. (In Prep).

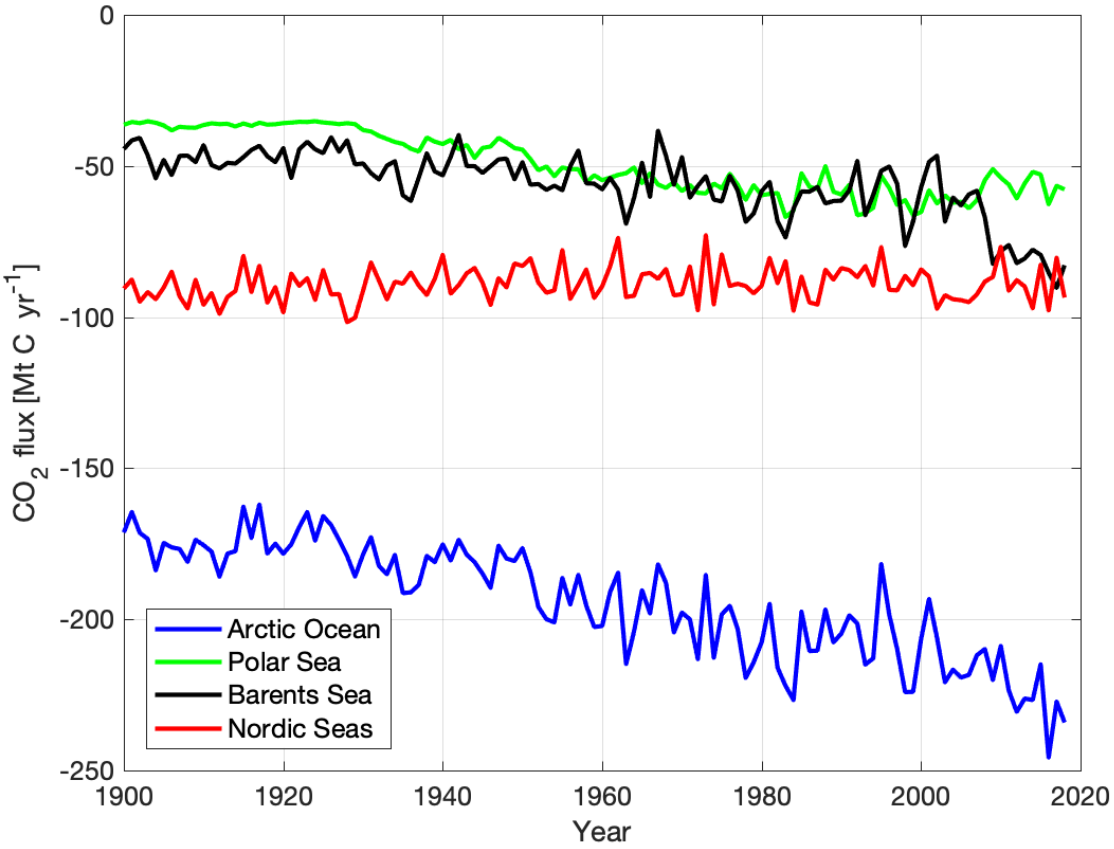

Figure 7: CO_2 uptake (Mt C/yr) as a function of simulated (NorESM) surface forcing. For the Barents and Polar Seas the most important parameter is the sea ice cover, whereas in the Nordic Seas heat loss is best at explaining observed variability. The negative values show ocean uptake of CO_2. Areas used to convert fluxes into Mt C are from Table 1.

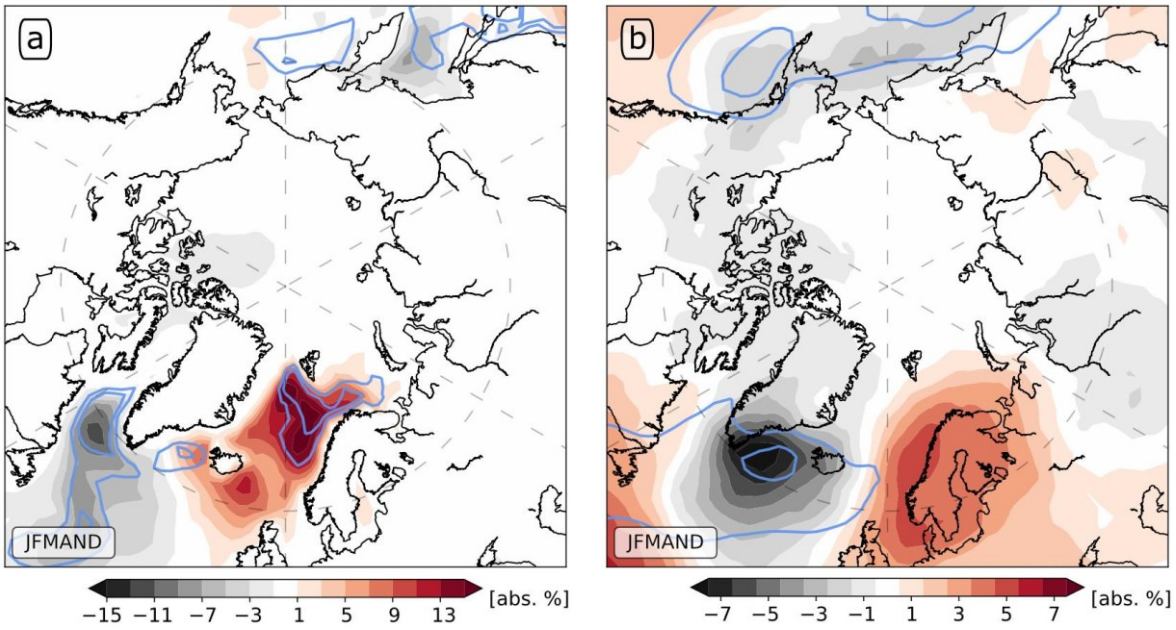

Figure 8: Anomalous frequency of occurrence (%) of (a) cold air outbreaks (CAOs) and (b) extratropical cyclones.

Plots show the 15 years with the largest versus smallest Nordic Seas heat loss based on the detrended centennial time series (black and blue symbols in Fig. 3). Contour lines show the respective climatology with contours at 20 and 30 absolute % frequency of occurrence. The anomalies are based on 20CRv2c and for the extended winter season within the same calendar year (January through April, and then November and December).

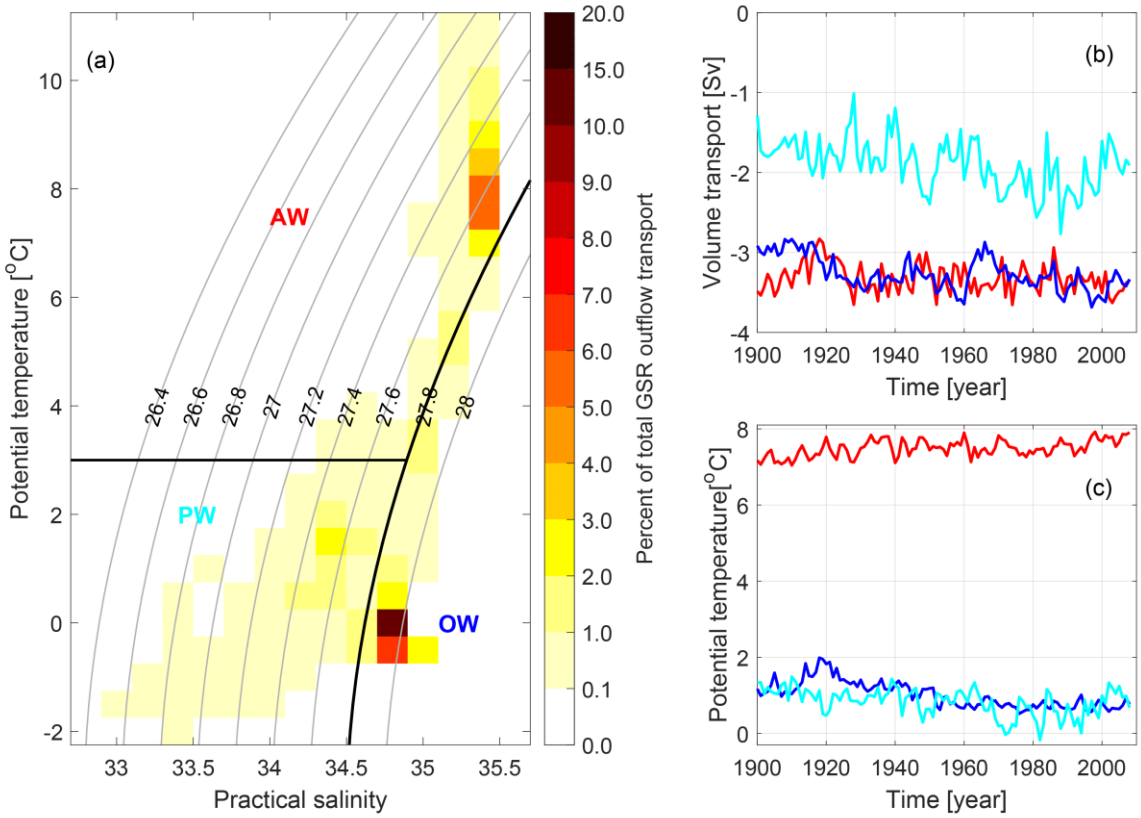

Figure 9: Simulated properties of the Greenland-Scotland ridge (GSR) outflow. a) shows the contribution (%) to GSR outflow as a function of temperature and salinity. The outflow is divided into three main water masses: Overflow Water (OW), Polar Water (PW) and outflowing Atlantic Water (AW), b) shows annual mean volume transport (Sv) and c) potential temperature (°C) for each water mass, with color coding as in a).

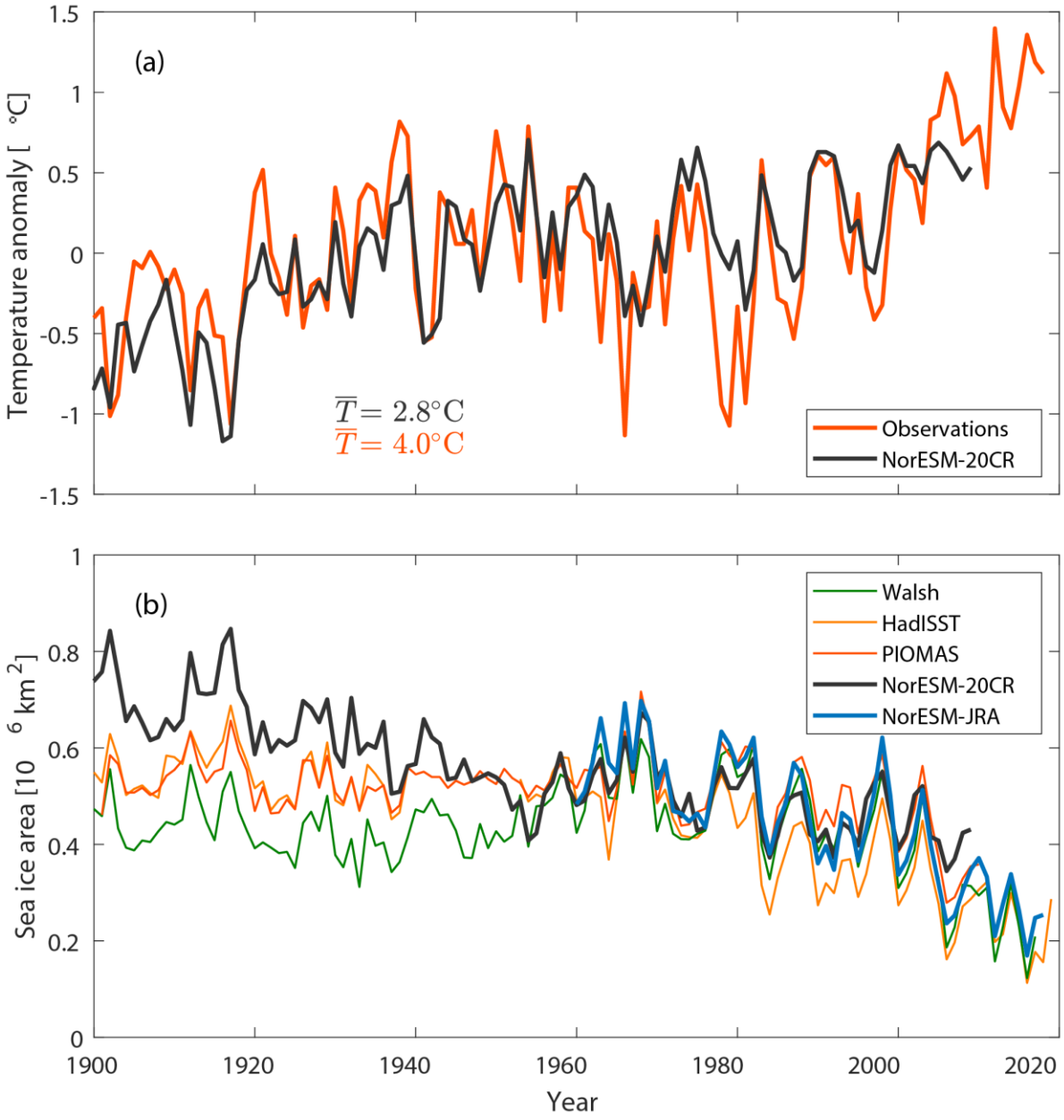

1443

1444 **Figure 10:** Simulated and observed Barents Sea temperature and sea ice variability since
1445 1900.

1446 (a) Observed (orange; ICES 2020) and simulated (black) annual mean temperature anomalies
1447 (°C) relative to the 1900-2009 mean temperature of respectively 4.0 °C and 2,8 °C along the
1448 Kola Section (Figure 4). (b) Annual mean sea ice area (10^6 km^2) in the Barents Sea from
1449 NorESM and reconstructions based on observations or simulations (HadISST; Rayner et al.
1450 2003, Walsh et al. 2017, and PIOMAS-20C; Schweiger et al. 2019).

1451

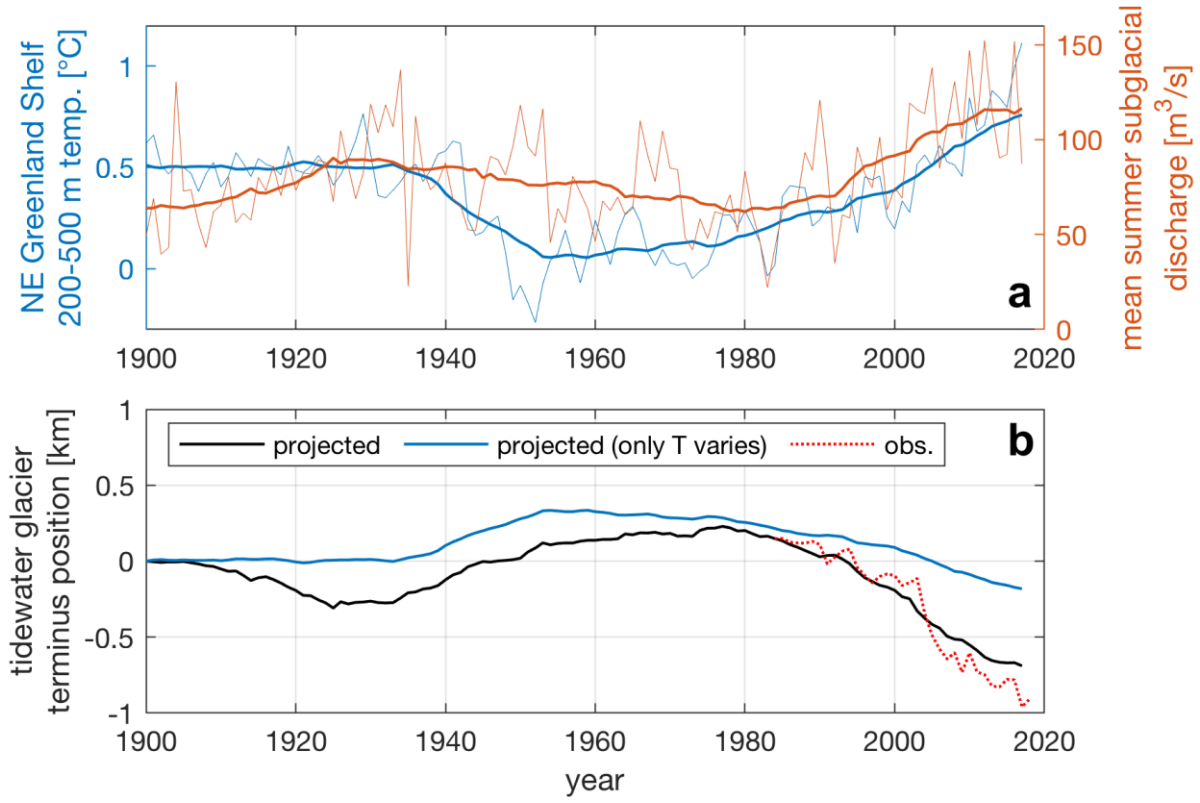

Figure 11: Impact of ocean changes on the NE Greenland ice sheet.

(a) NorESM-simulated ocean temperature averaged over the NE Greenland continental shelf between the depths of 200 and 500 m (°C, blue, left axis) and simulated summer liquid freshwater flux (subglacial discharge) from NE Greenland's marine-terminating glaciers (m^3/s, red, right axis; Fettweis et al., 2017). (b) Simulated advance or retreat of NE Greenland's marine- terminating glaciers. The projected terminus position (km, black) is based on the parameterisation described by Slater et al. (2019), using the NorESM ocean temperature and subglacial discharge shown in (a) as inputs. The blue line shows the projected terminus position when subglacial discharge is held constant at its mean 1900-2017 value, and thus isolates the impact of the ocean on the glaciers. The red dashed line shows the observed terminus positions since 1984 (Slater et al. 2019). All values are averaged over all glaciers in the region and more negative position values indicate a more retreated glacier.

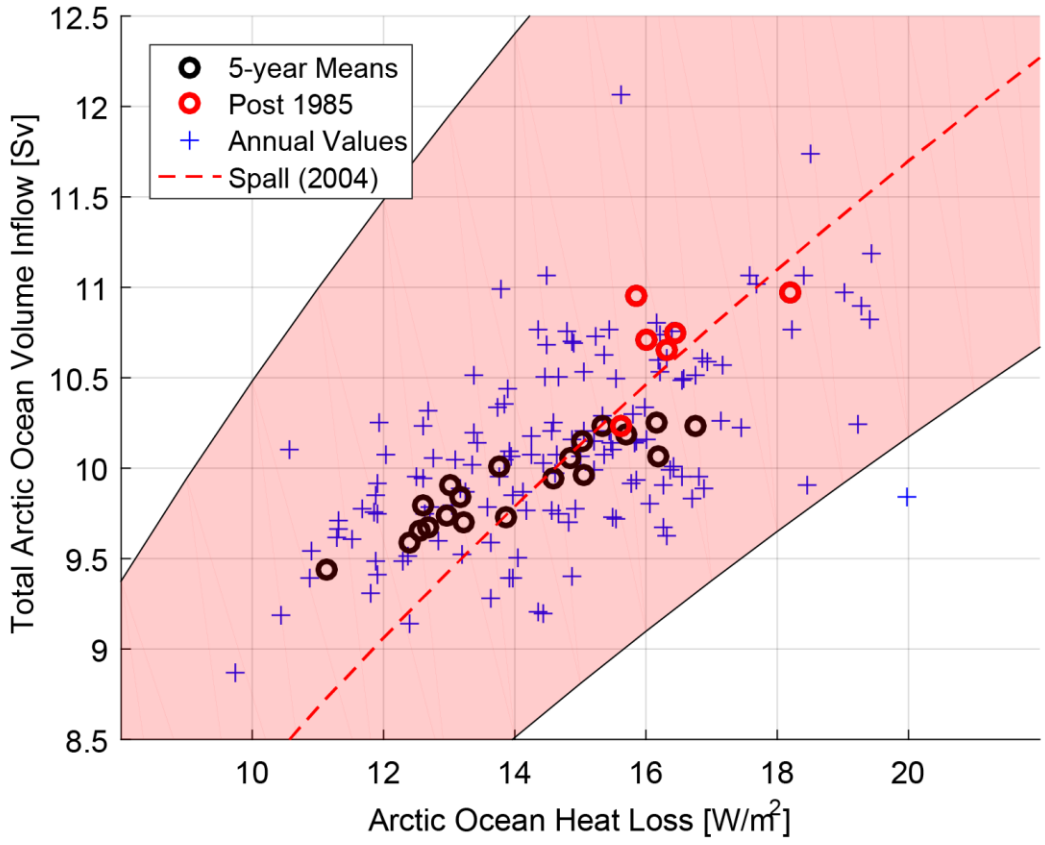

1467

1468 **Figure 12 a):** Inflow towards the Arctic Ocean as a function of heat loss.

1469 Simulated (NorESM) annual values and the 5-year means of the inflow (Sv) towards the
1470 Arctic Ocean across the Greenland Scotland Ridge and the Bering Strait. The dashed line is
1471 from Spall (2004), analytically derived from the heat loss (abscissa) and representative values
1472 of the basin radius, Coriolis parameter, the slope width, and the 500 m inflow depth of the
1473 GSR. The red envelope spans out inflow values based on varying these parameters as
1474 explained in the text.

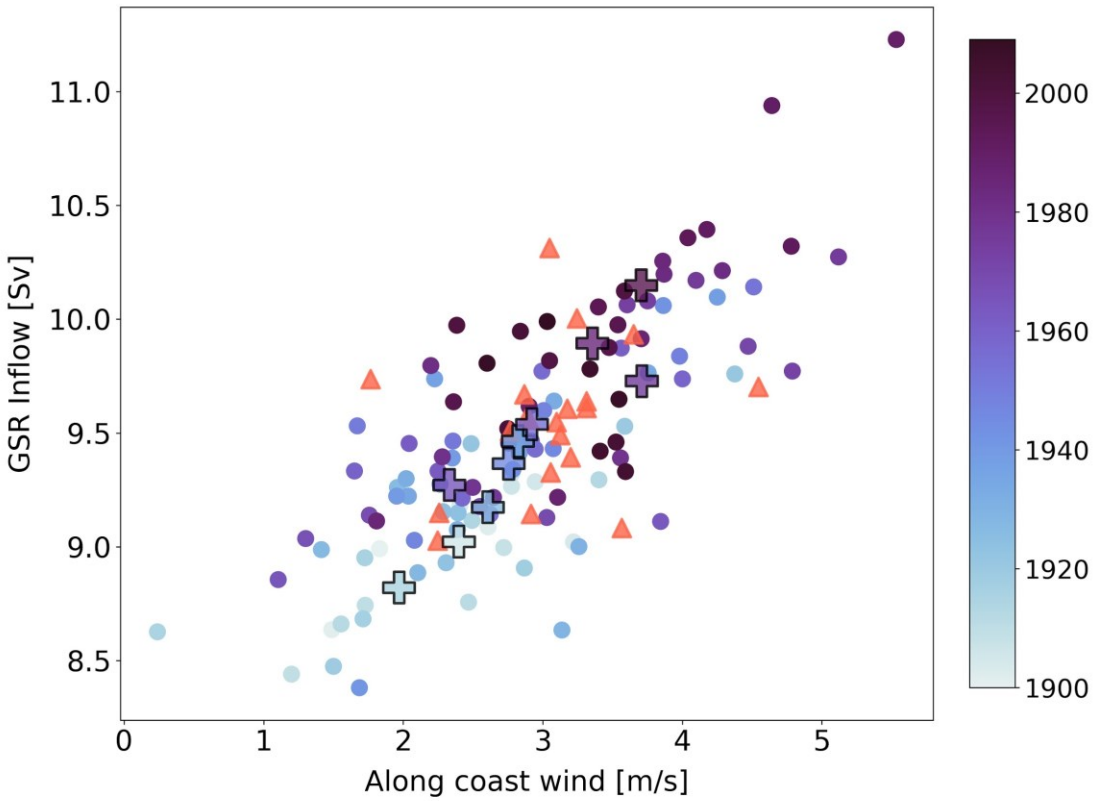

Figure 12 b): Inflow and wind forcing.

Circles show the simulated annual (spatial) mean values of along-coast wind speed (m/s) between the Faroes-Shetland and the Svinøy sections off the Norwegian west coast, and the overall poleward flow (Sv) across the GSR. The correlation coefficient is r=0.78. Larger crosses show decadal means. Color coding represent the simulation year. Observed volume transport from the eastern Svinøy branch (NMDC 2020, 1996-2016) and observed (bias-corrected) wind speed from Utsira (NCSC 2020) are included as orange triangles, using a constant addition of +5.14 Sv representing the outer branch (value of +4.14 Sv) and inflow west of Iceland (+1 Sv).

1493

1494 **List of Figures**

1495 1. Schematic overview
1496 2. The Arctic Ocean Bathymetry + mean transport + heat loss
1497 3. The surface heat loss over time
1498 4. The centennial mean heat loss spatially + SIC
1499 5. Heat Transport Convergence and warming of Nordic Seas
1500 6. Observed and simulated Hydrography
1501 7. Simulated CO2 uptake
1502 8. Atmospheric circulation patterns
1503 9. Simulated changes in OW and PW waters
1504 10. Evaluation in the Barents Sea (AW mean temperature + Kola section + ice)
1505 11. Changes in Greenland glaciers due to AW temperature
1506 12. AW inflow as forced by heat loss and wind
1507
1508

1509 **Table 1.** Simulated centennial annual mean properties for the Arctic Ocean and the three
1510 subdomains from the NorESM for 1900-2009. The heat loss is the heat flux multiplied by the
1511 area of each sea. The CO_2 uptake is estimated as described in the methods based on heat flux
1512 and Sea Ice Concentration (SIC). All values, including Sea Surface Temperature (SST) and
1513 Sea Surface Salinity (SSS) are averages over the seas shown in Fig. 1. Heat loss trends that
1514 are significant at the 95% level is indicated by a (*) $p < 0.05$. TW (Tera Watt = 10^{12} W).

1515

	Area	Heat Loss	Heat Flux	SIC	SST	SSS	CO_2 Uptake	Heat Loss Trend/Century
Unit	[10^6 km²]	[TW]	[W/m²]	[%]	[°C]	[g/kg]	Mt C/yr	TW/100 yr
Polar Sea	**8.36**	**15.89**	**1.90**	**94.8**	**-1.6**	**31.3**	**55.7**	**11.9***
Barents Sea	**1.47**	**56.54**	**38.10**	**52.8**	**0.9**	**34.2**	**66.7**	**27.7***
Nordic Seas	**2.54**	**114.75**	**45.08**	**28.0**	**3.0**	**34.5**	**88.3**	**6.2**
Arctic Ocean	**12.38**	**186.80**	**15.08**	**75.7**	**-0.3**	**32.3**	**209.9**	**45.8***

1516

Table 2. Applied regressions and associated statistics for calculating ocean CO2 uptake.

Region	Parameter	Function	R^2	p value
Nordic Seas	Heat flux (HF)	F=0.0355*HF – 12.0352	0.44	0.018
Barents Sea	HF+SSS+SIC	F=–0.0479*HF + 13.603*SSS + 0.2004*SIC – 479.556	0.42	0.024
Polar Sea	SIC	F=0.0516*SIC – 6.0082	0.48	0.000

SSS = sea surface salinity SIC = Sea ice concentration

Table 3. Mean ocean transports in relevant Arctic sections (1900-2000). Positive volume transport values are northward. The Ocean Heat Transport (OHT) is relative to 0 °C for all sections. A positive OHT with a negative (southward) volume transport implies that the temperature is lower than 0 °C. Numbers are rounded to the closest 0.1 Sv.

	Volume	OHT
Unit	[Sv]	[TW]
Bering Strait net	**+0.7**	**+0.9**
Canadian Archipelago net	**-1.7**	**+6.6**
GSR net transport	**+1.0**	**+172**
Arctic Ocean net	**0.0**	**+179**
GSR AW Inflow	**+9.5**	**+285**
GSR total outflow	**-8.5**	**-113**
GSR OW	**-3.3**	**-9**
GSR PW	**-1.9**	**-3**
GSR AW outflow	**-3.3**	**-101**

References

Aagaard, K., Swift, J. H., & Carmack, E. C. (1985), Thermohaline circulation in the Arctic Mediterranean Seas, *J. Geophys. Res.*, 90 (C3), 4833– 4846, doi:10.1029/JC090iC03p04833.

Ambaum, M. H., & Hoskins, B. J. (2002). The NAO troposphere–stratosphere connection. Journal of Climate, 15(14), 1969-1978, doi:10.1175/1520-0442(2002)015

Anderson, L. G. & Kaltin, S. (2001) Carbon fluxes in the Arctic Ocean - potential impact by climate change, Polar Res, 20, 225-232, doi:10.3402/polar.v20i2.6521

Anderson, L. G., Jutterstrom, S., Hjalmarsson, S., Wahlstrom, I., & Semiletov, I. P. (2009) Out-gassing of CO2 from Siberian Shelf seas by terrestrial organic matter decomposition, Geophys Res Lett, 36, doi:10.1029/2009GL040046

Arrigo, K. R., & G. L. van Dijken (2015), Continued increases in Arctic Ocean primary production, Progress in Oceanography, 136, 60-70, doi:10.1016/j.pocean.2015.05.002.

Asbjørnsen, H., Årthun, M., Skagseth, Ø., & Eldevik, T. (2019). Mechanisms of ocean heat anomalies in the Norwegian Sea. J. Geophys. Res. Oceans, 124, 2908–2923, doi:10.1029/2018JC014649

Asbjørnsen H., Årthun, M., Skagseth, Ø., & Eldevik, T. (2020). Mechanisms underlying recent Arctic Atlantification. Geophysical Research Letters, 47, e2020GL088036, doi:10.1029/2020GL088036

Asbjørnsen, H., Johnson, H. L., & Årthun, M. (2021). Variable Nordic Seas inflow linked to shifts in North Atlantic circulation. Journal of Climate, 1-50, doi:10.1175/JCLI-D-20-0917.1

Athanase et al. (2020) Atlantic Water Modification North of Svalbard in the Mercator Physical System From 2007 to 2020. Journal of Geophysical Research: Oceans, 125, 10, doi:10.1029/2020JC016463

Barton, B. I., Lenn, Y. D., & Lique, C. (2018). Observed Atlantification of the Barents Sea causes the polar front to limit the expansion of winter sea ice. *Journal of Physical Oceanography*, *48*(8), 1849-1866, doi:10.1175/JPO-D-18-0003.1

Barnston, A. G., & Livezey, R. E. (1987) Classification, seasonality and persistence of low-frequency atmospheric circulation patterns. Mon. Wea. Rev., 115:1083–1126, doi:10.1175/1520-0493(1987)115<1083:CSAPOL>2.0.CO;2

Bamber, J., van den Broeke, M., Ettema, J., Lenaerts, J., & Rignot, E. (2012) Recent large increases in freshwater fluxes from Greenland into the North Atlantic. Geophysical Research Letters, 39, L19501, doi:10.1029/2012GL052552

Bamber, J. L., Tedstone, A. J., King, M. D., Howat, I. M., Enderlin, E. M., van den Broeke, M. R., & Noel, B. (2018). Land ice freshwater budget of the Arctic and North Atlantic Oceans: 1. Data, methods, and results. Journal of Geophysical Research: Oceans, 123, 1827–1837, doi:10.1002/2017JC013605

1570 Bates, N. R., & J. T. Mathis (2009), The Arctic Ocean marine carbon cycle: evaluation of air-
1571 sea CO2 exchanges, ocean acidification impacts and potential feedbacks, Biogeosciences,
1572 6(11), 2433-2459, doi:10.5194/bg-6-2433-2009.

1573 Behrendt, A., Sumata, H., Rabe, B., & Schauer, U. (2018). UDASH – Unified Database for
1574 Arctic and Subarctic Hydrography, Earth Syst. Sci. Data, 10, 1119–1138, doi:10.5194/essd-
1575 10-1119-2018.

1576 Bentsen, M. et al. (2013). The Norwegian Earth System Model, NorESM1-M - Part 1:
1577 Description and basic evaluation. Geoscientific Model Development Discussions, 5, 2843–
1578 2931, doi:10.5194/gmdd-5-2843-2012

1579 Bentsen, M. et al. (2019) NCC NorESM2-LM model output prepared for CMIP6 OMIP
1580 omip2. Version 20200401. Earth System Grid Federation, doi:10.22033/ESGF/CMIP6.8089

1581 Berx, B., Hansen, B., Østerhus, S., Larsen, K.M., Sherwin, T. & Jochumsen, K. (2013)
1582 Combining in situ measurements and altimetry to estimate volume, heat and salt transport
1583 variability through the Faroe–Shetland Channel, Ocean Sci., 9, 639–654, doi:10.5194/os-9-
1584 639-2013

1585 Binder, H., Boettcher, M., Grams, C. M., Joos, H., Pfahl, S., & Wernli, H. (2017).
1586 Exceptional air mass transport and dynamical drivers of an extreme wintertime Arctic warm
1587 event. Geophysical Research Letters, 44(23), 12-028, doi: 10.1002/2017GL075841

1588 Bjerknes, J. (1964) Atlantic Air-Sea Interaction, Editor(s): H.E. Landsberg, J. Van Mieghem,
1589 Advances in Geophysics, Elsevier,10, 1-82, doi:10.1016/S0065-2687(08)60005-9.

1590 Bjørk, A., Kjær, K., Korsgaard, N. et al. (2012) An aerial view of 80 years of climate-related
1591 glacier fluctuations in southeast Greenland. Nature Geosci 5, 427–432,
1592 doi:10.1038/ngeo1481

1593 Bleck, R., Rooth, C., Hu, D., & Smith, L. T. (1992) Salinity-driven Thermocline Transients
1594 in a Wind- and Thermohaline-forced Isopycnic Coordinate Model of the North Atlantic. J.
1595 Phys. Oceanogr., 22, 1486–1505, doi:10.1175/1520-0485(1992)0222.0.CO;2

1596 Böning C.W., & Bryan, F.O. (1996). Large-scale transport processes in high-resolution
1597 circulation models. in The Warmwatersphere of the North Atlantic Ocean, W. Krauss, Ed.,
1598 Gebrüder Borntraeger, 91–128.

1599 Brennan, M. K., Hakim, G. J., & Blanchard-Wrigglesworth, E. (2020). Arctic sea-ice
1600 variability during the instrumental era. Geophys. Res. Lett. 47, e2019GL086843,
1601 doi:10.1029/2019GL086843

1602 Bringedal, C., Eldevik, T., Skagseth, Ø., Spall, M., Østerhus, S. (2018). Structure and forcing
1603 of observed exchanges across the Greenland-Scotland Ridge. Journal of Climate, 31, 9881–
1604 9901, doi:10.1175/JCLI-D-17-0889.1

1605 Bryden, H. L. & Imawaki, S. (2001) Ocean Heat Transport. In Siedler G, Church J, Gould J
1606 (eds): Ocean circulation and climate: observing and modelling the global ocean, San Diego,
1607 USA. Academic Press, 455-474.

1608 Bueh, C., & Nakamura, H. (2007). Scandinavian pattern and its climatic impact. Quarterly
1609 Journal of the Royal Meteorological Society: A journal of the atmospheric sciences, applied
1610 meteorology and physical oceanography, 133(629), 2117-2131, doi:10.1002/qj.173

1611 Brakstad, A., Våge, K., Håvik, L., & Moore, G.W.K. (2019): Water Mass Transformation in
1612 the Greenland Sea during the Period 1986–2016. JPO, 49 (1), 121–140, doi:10.1175/JPO-D-
1613 17-0273.1

1614 Carmack, E., Yamamoto-Kawai, M., Haine, T, Bacon, S. (2016). Freshwater and its role in
1615 the Arctic Marine System: Sources, disposition, storage, export, and physical and
1616 biogeochemical consequences in the Arctic and global oceans. Journal of Geophysical
1617 Research Biogeoscience, 121, 675–717, doi:10.1002/2015JG003140

1618 Cassou, C., Terray, L., Hurrell, J. W., & Deser, C. (2004). North Atlantic winter climate
1619 regimes: Spatial asymmetry, stationarity with time, and oceanic forcing. Journal of Climate,
1620 17(5), 1055-1068, doi:10.1175/1520-0442(2004)017

1621 Chafik, L. & Rossby, T. (2019). Volume, heat, and freshwater divergences in the subpolar
1622 North Atlantic suggest the Nordic Seas as key to the state of the meridional overturning
1623 circulation. Geophys Res Lett, 46, 4799–4808, doi:10.1029/2019GL082110

1624 Chafik, L., Hátún, H., Kjellsson, J. et al. (2020) Discovery of an unrecognized pathway
1625 carrying overflow waters toward the Faroe Bank Channel. Nat Communications, 11, 3721,
1626 doi:10.1038/s41467-020-17426-8

1627 Chierici, M., Olsen, A., Johannessen, T., Trinañes, J., & Wanninkhof, R. (2009). Algorithms
1628 to estimate the carbon dioxide uptake in the northern North Atlantic using shipboard
1629 observations, satellite and ocean analysis data. Deep Sea Research Part II: Topical Studies in
1630 Oceanography, 56(8-10), 630-639, doi:10.1016/j.dsr2.2008.12.014

1631 Compo, G.P., Whitaker, J.S., Sardeshmukh, P.D., Matsui, N., Allan, R.J., Yin, X., Gleason,
1632 B.E., Vose, R.S., Rutledge, G., Bessemoulin, P., Brönnimann, S., Brunet, M., Crouthamel,
1633 R.I., Grant, A.N., Groisman, P.Y., Jones, P.D., Kruk, M.C., Kruger, A.C., Marshall, G.J.,
1634 Maugeri, M., Mok, H.Y., Nordli, Ø., Ross, T.F., Trigo, R.M., Wang, X.L., Woodruff, S.D.
1635 and Worley, S.J. (2011), The Twentieth Century Reanalysis Project. Q.J.R. Meteorol. Soc.,
1636 137: 1-28, doi:10.1002/qj.776

1637 Condron, A., & Renfrew, I. A. (2013). The impact of polar mesoscale storms on northeast
1638 Atlantic Ocean circulation. Nature Geoscience, 6(1), 34-37, doi:10.1038/ngeo1661

1639 Deser, C. (2000). On the teleconnectivity of the "Arctic Oscillation". Geophysical Research
1640 Letters, 27(6), 779-782, doi: 10.1029/1999GL010945

1641 DeVries, T., Holzer, M., & Primeau, F. (2017). Recent increase in oceanic carbon uptake
1642 driven by weaker upper-ocean overturning. Nature, 542(7640), 215-218,
1643 doi:10.1038/nature21068

1644 Dickson R. R. et al. (2000). The Arctic Ocean Response to the North Atlantic Oscillation. J.
1645 Clim, 13. 2671 – 2696, doi:10.1175/1520-0442(2000)013<2671:TAORTT

1646 Docquier D., Fuentes-Franco R., Koenigk T. & Fichefet T. (2020) Sea Ice-Ocean Interactions
1647 in the Barents Sea Modeled at Different Resolutions, Frontiers in Earth Science, 8,
1648 doi:10.3389/feart.2020.00172.

1649 Eldevik, T., Nilsen, J.E.Ø., Iovino, D., Olsson, K.A., Sandø, A.B., Drange,H. (2009)
1650 Observed sources and variability of Nordic seas overflow. Nature Geoscience 2, 405-409,
1651 doi:10.1038/ngeo518.

1652 Eldevik, T. & Nilsen, J. E. Ø. (2013). The Arctic–Atlantic thermohaline circulation. Journal
1653 of Climate, 26, 8698–8705, doi:10.1175/JCLI-D-13-00305.1

1654 Fan, S. M., Harris, L. M., & Horowitz, L. W. (2015). Atmospheric energy transport to the
1655 Arctic 1979–2012. Tellus A: Dynamic Meteorology and Oceanography, 67(1), 25482,
1656 doi:10.3402/tellusa.v67.25482

1657 Fanning, A. F. & Weaver, A. J. (1997). A Horizontal Resolution and Parameter Sensitivity
1658 Study of Heat Transport in an Idealized Coupled Climate Model. Journal of Climate, 10,
1659 2469–2478, doi:10.1175/1520-0442(1997)010<2469:AHRAPS>2.0.CO;2

1660 Fletcher, J., Mason, S., & Jakob, C. (2016). The climatology, meteorology, and boundary
1661 layer structure of marine cold air outbreaks in both hemispheres. Journal of Climate, 29(6),
1662 1999-2014, doi:10.1175/JCLI-D-15-0268.1

1663 Fransson, A., M. Chierici, I. Skjelvan, A. Olsen, P. Assmy, A. K. Peterson, G. Spreen, & B.
1664 Ward (2017), Effects of sea-ice and biogeochemical processes and storms on under-ice water
1665 fCO(2) during the winter-spring transition in the high Arctic Ocean: Implications for sea-air
1666 CO2 fluxes, J Geophys Res-Oceans, 122(7), 5566-5587, doi: 10.1002/2016jc012478.

1667 Friedlingstein, P. et al. (2019) Global Carbon Budget 2019, Earth Syst. Sci. Data, 11, 1783–
1668 1838, doi:10.5194/essd-11-1783-2019.

1669 Fröb, F., Olsen, A., Becker, M., Chafik, L., Johannessen, T., Reverdin, G., & Omar, A.
1670 (2019). Wintertime f CO2 Variability in the Subpolar North Atlantic Since 2004.
1671 Geophysical Research Letters, 46(3), 1580-1590, doi:10.1029/2018GL080554

1672 Ganachaud, A. & Wunsch, C. (2000) Improved estimates of global ocean circulation, heat
1673 transport and mixing from hydrographic data. Nature 408, 453–457 doi:10.1038/35044048

1674 Gebbie, G., & P. Huybers (2011) How is the ocean filled? *Geophys Res. Lett*, 38, L06604,
1675 doi:10.1029/2011GL046769

1676 Gillard, L. C., X. Hu, P. G. Myers, & J. L. Bamber (2016) Meltwater pathways from marine
1677 terminating glaciers of the Greenland ice sheet, Geophys. Res. Lett., 43, 10,873–10,882,
1678 doi:10.1002/2016GL070969
1679
1680 Glessmer, M. S., Eldevik, T., Våge, K. Nilsen, J. E. Ø. & Behrens, E. (2014) Atlantic origin
1681 of observed and modelled freshwater anomalies in the Nordic Seas, Nature Geoscience,
1682 doi:10.1038/NGEO2259
1683
1684 Graversen, R.G. & Burtu, M. (2016), Arctic amplification enhanced by latent energy
1685 transport of atmospheric planetary waves. Q.J.R. Meteorol. Soc., 142: 2046-2054,
1686 doi:10.1002/qj.2802

1687 Griffies, S. M., et al. (2016) OMIP contribution to CMIP6: experimental and diagnostic
1688 protocol for the physical component of the Ocean Model Intercomparison Project.
1689 Geoscientific Model Development, 3231-3296, doi:10.5194/gmd-9-3231-2016

1690 Hansen et al. (2016) A stable Faroe Bank Channel overflow 1995-2015. Ocean Science, 12,
1691 1205-1220, doi:10.5194/os-12-1205-2016

1692 Hattermann, T., Isachsen, P. E., von Appen, W.-J., Albretsen, J., & Sundfjord, A. (2016)
1693 Eddy driven recirculation of Atlantic Water in Fram Strait, Geophysical Research Letters, 43,
1694 3406–3414, doi:10.1002/2016GL068323.

1695 Hátún, H., Sandø, A. B., Drange, H., Hansen, B., & Valdimarsson, H. (2005). Influence of
1696 the Atlantic subpolar gyre on the thermohaline circulation. Science, 309(5742), 1841-1844,
1697 doi: 10.1126/science.1114777

1698 He, Y. C., Drange, H., Gao, Y., & Bentsen, M. (2016). Simulated Atlantic Meridional
1699 Overturning Circulation in the 20th century with an ocean model forced by reanalysis-based
1700 atmospheric data sets. Ocean Modelling, 100, 31-48 doi:10.1016/j.ocemod.2015.12.011

1701 Helland-Hansen, B., & Nansen, F. (1909). The Norwegian Sea: Its physical oceanography
1702 based upon the Norwegian researches 1900-1904. Kristiania: Det Mallingske bogtrykkeri.

1703 Hopkins, T. S. (1991) The GIN Sea - A synthesis of its physical oceanography and literature
1704 review 1972-1985. Earth-Sci. Rev., 3, 1, 175-318. doi:10.1016/0012-8252(91)90001-V

1705 Huang, J., Pickart, R.S., Huang, R.X., Lin, P., Brakstad, A. & Xu, F. (2020) Sources and
1706 upstream pathways of the densest overflow water in the Nordic Seas. Nature
1707 Communications 11, 5389, doi:10.1038/s41467-020-19050-y

1708 Hunke, E. C., Lipscomb, W. H., Turner, A. K., Jeffery, N., & Elliott, S. (2008). CICE: The
1709 Los Alamos sea ice model, documentation and software, version 4.0. Los Alamos National
1710 Laboratory Tech. Rep. Los Alamos, NM.

1711 Hurrell, J. W. (1995) Decadal Trends in the North Atlantic Oscillation: Regional
1712 Temperatures and Precipitation, Science, 269, doi:10.1126/science.269.5224.676

1713 Huth, R., & Beranová, R. (2021). How to recognize a true mode of atmospheric circulation
1714 variability. Earth and Space Science, 8(3), e2020EA001275, doi: 10.1029/2020EA001275

1715 ICES 2020, International Council for Exploration of the Seas, ICES report on Ocean climate,
1716 web: https://ocean.ices.dk/core/iroc

1717 Ilıcak, M. et al. (2016) An assessment of the Arctic Ocean in a suite of interannual CORE-II
1718 simulations. Part III: Hydrography and fluxes. Ocean Modelling 100, 141-161,
1719 doi:10.1016/j.ocemod.2016.02.004

1720 IHO (1953) International Hydrographic Organization, Limits of Oceans and Seas, Special
1721 Publication 28, 3'd edition.

1722 Ivanov, V., Alexeev, V., Koldunov, N. V., Repina, I., Sandø, A. B., Smedsrud, L. H. &
1723 Smirnov, A. (2016) Arctic Ocean heat impact on regional ice decay - a suggested positive

feedback , Journal of Physical Oceanography, 46, 1437-1456, doi: 10.1175/JPO-D-15-0144.1.

Jakhelln, A. (1936) The Water Transport of Gradient Currents. Geofys. Publ., Vol. XI, p. 11.

Jakobsson, M. & Macnab, R. (2006) A comparison between GEBCO Sheet 5.17 and the International Bathymetric Chart of the Arctic Ocean, Marine Geophysical Researches, 27: 35–48, doi 10.1007/s11001-005-7760-0

Jeansson, E., Olsen, A., Eldevik, T., Skjelvan, I., Omar, A., et al. (2011), The Nordic Seas carbon budget: Sources, sinks and uncertainties. Glob. Biogeochem. Cyc., 25, 4, doi:10.1029/2010GB003961

Jenkins, A. (2011): Convection-Driven Melting near the Grounding Lines of Ice Shelves and Tidewater Glaciers, J. Phys. Oceanogr., 41, 2279–2294, doi:10.1175/JPO-D-11-03.1.

Jochumsen et al. (2017) Revised transport estimates of the Denmark Strait overflow. Journal of Geophysical Research: Oceans, 122, 4, doi:10.1002/2017JC012803.

Johnson, H. L., Cornish, S. B., Kostov, Y., Beer, E. & Lique, C. (2018). Arctic Ocean freshwater content and its decadal memory of sea-level pressure. Geophysical Research Letters, 45, 4991–5001, doi:10.1029/2017GL076870

Jónsson & Valdimarsson (2004) A new path for the Denmark Strait overflow water from the Iceland Sea to Denmark Strait. Geophysical Research Letters, 31, L03305, doi:10.1029/2003GL019214

Karstensen et al., (2005). Water mass transformation in the Greenland Sea during the 1990s. Journal of Geophysical Research, 110, C7. doi:10.1029/2004JC002510

Kenigson, J. S., & Timmermans, M. L. (2021). Nordic Seas Hydrography in the Context of Arctic and North Atlantic Ocean Dynamics. Journal of Physical Oceanography, 51(1), 101-114, doi: 10.1175/JPO-D-20-0071.1

King, M.D., Howat, I.M., Candela, S.G. et al. (2020) Dynamic ice loss from the Greenland Ice Sheet driven by sustained glacier retreat. Commun Earth Environ 1, 1, doi:10.1038/s43247-020-0001-2

Kolstad, E. W., T. J.Bracegirdle, & I. A.Seierstad (2009) Marine cold-air outbreaks in the North Atlantic: Temporal distribution and associations with large-scale atmospheric circulation. Climate Dyn., 33, 187–197, doi:10.1007/s00382-008-0431-5.

L'Heureux, M. L., Kumar, A., Bell, G. D., Halpert, M. S., & Higgins, R. W. (2008). Role of the Pacific-North American (PNA) pattern in the 2007 Arctic sea ice decline. Geophysical Research Letters, 35(20), doi: 10.1029/2008GL035205

Large, W., Yeager, S., 2004. Diurnal to Decadal Global Forcing For Ocean and Sea-Ice Models: The Data Sets and Flux Climatologies. NCAR technical note NCAR/TN- 460+STR Technical Report, CGD Division of the National Center for Atmospheric Research, doi:10.5065/D6KK98Q6.

1761 Landschützer, P., Gruber, N., & Bakker, D. C. (2016). Decadal variations and trends of the
1762 global ocean carbon sink. Global Biogeochemical Cycles, 30(10), 1396-1417,
1763 doi:10.1002/2015GB005359

1764 Langehaug, H. R., Medhaug, I., Eldevik, T., & Otterå, O. H. (2012). Arctic/Atlantic
1765 exchanges via the subpolar gyre. Journal of Climate, 25(7), 2421-2439, doi: 10.1175/JCLI-D-
1766 11-00085.1

1767 Lannuzel, D., Tedesco, L., Van Leeuwe, M., Campbell, K., Flores, H., Delille, B., & Brown,
1768 K. (2020). The future of Arctic sea-ice biogeochemistry and ice-associated ecosystems.
1769 *Nature Climate Change*, 1-10, doi:10.1038/s41558-020-00940-4

1770 Latarius, K. & Quadfasel, D. (2016) Water mass transformation in the deep basins of the
1771 Nordic Seas: Analyses of heat and freshwater budgets, Deep Sea Research Part 1, 114, 23-42,
1772 doi:10.1016/j.dsr.2016.04.012

1773 Lauvset, S. K., Chierici, M., Counillon, F., Omar, A., Nondal, G., Johannessen, T., & Olsen,
1774 A. (2013). Annual and seasonal fCO2 and air–sea CO2 fluxes in the Barents Sea. Journal of
1775 Marine Systems, 113, 62-74, doi: 10.1016/j.jmarsys.2012.12.011

1776 Lauvset, S.K., Brakstad, A., Våge, K., Olsen, A., Jeansson, E., Mork, K.A. (2018) Continued
1777 warming, salinification and oxygenation of the Greenland Sea gyre. Tellus A 70, 1-9,
1778 doi:10.1080/16000870.2018.1476434.

1779 Levitus, S. (1998). World ocean database 1998.

1780 Lorenz, D. J., & Hartmann, D. L. (2003). Eddy–zonal flow feedback in the Northern
1781 Hemisphere winter. Journal of climate, 16(8), 1212-1227, doi: 10.1175/1520-0442(2003)16

1782 Lozier et al. (2019) A sea change in our view of overturning in the subpolar North Atlantic
1783 Science 363, 516–521, doi:10.1126/science.aau6592

1784 Li, C. & Born, A. (2019) Coupled atmosphere-ice-ocean dynamics in Dansgaard-Oeschger
1785 events, Quaternary Science Reviews 203, doi:10.1016/j.quascirev.2018.10.031

1786 Lique, C. & Thomas, M. D. (2018) Latitudinal shift of the Atlantic Meridional Overturning
1787 Circulation source regions under a warming climate. Nature Clim Change 8, 1013–1020,
1788 doi:10.1038/s41558-018-0316-5

1789 van der Linden, E. C., Le Bars, D., Bintanja, R. & Hazeleger, W. (2019) Oceanic heat
1790 transport into the Arctic under high and low CO2 forcing, Climate Dynamics (2019)
1791 53:4763–4780, doi:10.1007/s00382-019-04824-y

1792 Lindeman, M. R., Straneo, F.,Wilson, N. J., Toole, J. M.,Krishfield, R. A., Beaird, N. L., et
1793 al.(2020). Ocean circulation and variability beneath Nioghalvfjerdsbræ (79 North Glacier) ice
1794 tongue. Journal of Geophysical Research: Oceans, 125, e2020JC016091,
1795 doi:10.1029/2020JC016091

1796 Lundberg, L. & Haugan, P. M. (1996), A Nordic Seas Arctic Ocean carbon budget from
1797 volume flows and inorganic carbon data, Global Biogeochem Cy, 10(3), 493-510,
1798 doi:10.1029/96gb00359.
1799

1800 MacGilchrist, G. A., A. C. N. Garabato, T. Tsubouchi, S. Bacon, S. Torres-Valdes, & K.
1801 Azetsu-Scott (2014), The Arctic Ocean carbon sink, Deep-Sea Res Pt I, 86, 39-55, doi:
1802 10.1016/j.dsr.2014.01.002.

1803 Marshall, J. & Schott, F. (1999) Open - ocean convection: Observations, theory, and models.
1804 Reviews of Geophysics 37, 1-64, doi:10.1029/98RG02739.

1805 Mastropole, D., Pickart, R.S., Valdimarsson, H., Våge, K., Jochumsen, K., Girton, J. (2017)
1806 On the hydrography of Denmark Strait. Journal of Geophysical Research 122, 306-321,
1807 doi:10.1002/2016JC012007.

1808 Mauritzen, C. (1996) Production of dense overflow waters feeding the North Atlantic across
1809 the Greenland-Scotland Ridge. Part 1: Evidence for a revised circulation scheme. Deep Sea
1810 Res. Part I Oceanogr. Res. Pap. 43, 769-806, doi:10.1016/0967-0637(96)00037-4.

1811 Mayer, M., S. Tietsche, L. Haimberger, T. Tsubouchi, J. Mayer, & H. Zuo (2019): An
1812 Improved Estimate of the Coupled Arctic Energy Budget. J. Climate, 32, 7915–7934,
1813 doi:10.1175/JCLI-D-19-0233.1

1814 McKinley, G. A., Fay, A. R., Eddebbar, Y. A., Gloege, L., & Lovenduski, N. S. (2020).
1815 External forcing explains recent decadal variability of the ocean carbon sink. AGU Advances,
1816 1(2), e2019AV000149, doi:10.1029/2019AV000149

1817 Meier, W. N., et al. (2014), Arctic sea ice in transformation: A review of recent observed
1818 changes and impacts on biology and human activity, Rev. Geophys., 52, 185– 217,
1819 doi:10.1002/2013RG000431.

1820 Messori, G., Geen, R., & Czaja, A. (2017). On the spatial and temporal variability of
1821 atmospheric heat transport in a hierarchy of models. Journal of the Atmospheric Sciences,
1822 74(7), 2163-2189, doi:10.1175/jas-d-16-0360.1

1823 Messori, G., Woods, C., & Caballero, R. (2018). On the drivers of wintertime temperature
1824 extremes in the high Arctic. Journal of Climate, 31(4), 1597-1618, doi: 10.1175/jcli-d-17-
1825 0386.1

1826 Michel, C., Rivière, G., Terray, L., & Joly, B. (2012). The dynamical link between surface
1827 cyclones, upper-tropospheric Rossby wave breaking and the life cycle of the Scandinavian
1828 blocking. Geophysical research letters, 39 (10) doi:10.1029/2012GL051682

1829 Moore, R. W., Martius, O., & Spengler, T. (2010). The modulation of the subtropical and
1830 extratropical atmosphere in the Pacific basin in response to the Madden–Julian oscillation.
1831 Monthly Weather Review, 138(7), 2761-2779, doi: 10.1175/2010MWR3194.1

1832 Moore, G.W.K., Våge, K., Pickart, R. S., & Renfrew, I. A. (2015). Decreasing intensity of
1833 open-ocean convection in the Greenland and Iceland seas, Nature Climate Change, 5, 877-
1834 882, doi:10.1038/nclimate2688.

1835 Mork, K. A., Ø. Skagseth, V. Ivshin, V.Ozhigin,S. L. Hughes, & H. Valdimarsson (2014),
1836 Advective and atmospheric forced changes in heat and fresh water content in the Norwegian
1837 Sea, 1951–2010, Geophys. Res. Lett., 41, 6221–6228, doi:10.1002/2014GL061038.

1838 Mork, K. A., Skagseth, Ø. & Søiland, H. (2019) Recent warming and freshening of the
1839 Norwegian Sea observed by Argo data. J. Clim. 32, 3695–3705, doi:10.1175/JCLI-D-18-
1840 0591.1.

1841 Mouginot, J., Rignot, E., Scheuchl, B., Fenty, I., Khazendar, A., Morlighem, M.,…Paden, J.
1842 (2015). Fast retreat of Zachariæ Isstrøm, northeast Greenland. Science, 350(6266), 1357–
1843 1361, doi:10.1126/science.aac7111

1844 Mouginot, J., Rignot, E., Bjørk, A. A., van den Broeke, M., Millan, R., Morlighem, M., Noël,
1845 B., Scheuchl, B. & Wood, M. (2019) Forty-six years of Greenland Ice Sheet mass balance
1846 from 1972 to 2018, Proceedings of the National Academy of Sciences May 2019, 116 (19)
1847 9239-9244; doi: 10.1073/pnas.1904242116

1848 Mosby, H. (1962). Water, Salt and Heat Balance of the North Polar Sea and the Norwegian
1849 Sea. Vitenskapsakademiet.

1850 Muilwijk, M., Smedsrud, L. H., Ilicak, M.,& Drange, H. (2018). Atlantic Water heat transport
1851 variability in the 20th century Arctic Ocean from a global ocean model and observations.
1852 JGR Oceans, 123, 8159–8179, doi:10.1029/2018JC014327

1853 Muilwijk, M., Ilicak, M., Cornish, S. B., Danilov, S., Gelderloos, R., Gerdes, R., et al.
1854 (2019). Arctic Ocean response to Greenland Sea wind anomalies in a suite of model
1855 simulations. Journal of Geophysical Research: Oceans, 124, doi:10.1029/2019JC015101

1856 NCSC 2020, Norwegian Climate Service Centre, Observations and weather statistics, web:
1857 https://klimaservicesenter.no/observations/

1858 Nilsen, J. E. Ø., Y. Gao, H. Drange, T. Furevik, & M. Bentsen (2003) Simulated North
1859 Atlantic-Nordic Seas water mass exchanges in an isopycnic coordinate OGCM, Geophys.
1860 Res. Lett., 30(10), 1536, doi:10.1029/2002GL016597.

1861 Nguyen, A. T., Pillar, H., Ocaña, V., Bigdeli, A., Smith, T. A. & Heimbach, P. (2020) The
1862 Arctic Subpolar gyre sTate Estimate (ASTE): Description and assessment of a data-
1863 constrained, dynamically consistent ocean-sea ice estimate for 2002-2017, submitted to
1864 Journal of Advances in Modeling Earth Systems (JAMES), doi:10.1002/essoar.10504669.3

1865 Nilsen, J. E. Ø., Hátún, H., Mork, K. A., Valdimarsson, H. (2008). The NISE Dataset.
1866 Technical Report 08-01. Faroese Fisheries Laboratory, Box 3051, Tórshavn Faroe Islands.

1867 NMDC 2020, Norwegian Marine Data Centre, Data sets, web: https://nmdc.no/nmdc/datasets

1868 Notz, D. & Stroeve, J. (2016). Observed Arctic sea-ice loss directly follows anthropogenic
1869 CO2 emission. Science, 354, 747–750, doi:10.1126/science.aag2345

1870 Nøst, O. A., & Isachsen, P. E. (2003). The large-scale time-mean ocean circulation in the
1871 Nordic Seas and Arctic Ocean estimated from simplified dynamics. Journal of Marine
1872 Research, 61(2), 175–210, doi:10.1357/002224003322005069

1873 Madonna, E., Hes, G., Li, C., Michel, C., & Siew, P. Y. F. (2020). Control of Barents Sea
1874 wintertime cyclone variability by large-scale atmospheric flow. Geophysical Research
1875 Letters, 47, e2020GL090322. doi:10.1029/2020GL090322

1876 Ogawa, F., & Spengler, T. (2019). Prevailing surface wind direction during air–sea heat
1877 exchange. Journal of Climate, 32(17), 5601-5617, doi: 10.1175/JCLI-D-18-0752.1

1878 Olafsson, J., Olafsdottir, S. R., Takahashi, T., Danielsen, M., & Arnarson, T. S. (2021).
1879 Enhancement of the North Atlantic CO2 sink by Arctic Waters. Biogeosciences, 18(5), 1689-
1880 1701, doi:10.5194/bg-18-1689-2021

1881 Omar, A. M., T. Johannessen, A. Olsen, S. Kaltin, & F. Rey (2007), Seasonal and interannual
1882 variability of the air-seaCO(2) flux in the Atlantic sector of the Barents Sea, Mar Chem,
1883 104(3-4), 203-213, doi: 10.1016/j.marchem.2006.11.002.

1884 Onarheim, I.H., Eldevik, T., Smedsrud, L. H. & Stroeve, J. C. (2018). Seasonal and regional
1885 manifestation of Arctic sea ice loss. Journal of Climate, 31, 4917–4932, doi:10.1175/JCLI-D-
1886 17- 0427.1

1887 Orvik, K.A., Skagseth, Ø. & Mork, M. (2001) Atlantic inflow to the Nordic Seas: current
1888 structure and volume fluxes from moored current meters, VM-ADCP and SeaSoar-CTD
1889 observations, 1995–1999, Deep Sea Research Part I: Oceanographic Research Papers, 48, 4,
1890 937-957, doi:10.1016/S0967-0637(00)00038-8

1891 Orvik, K. A., & Niiler, P. (2002). Major pathways of Atlantic water in the northern North
1892 Atlantic and Nordic Seas toward Arctic. Geophysical Research Letters, 29(19), 2-1, doi:
1893 10.1029/2002GL015002

1894 Oudar, T., Cattiaux, J., & Douville, H. (2020). Drivers of the northern extratropical eddy-
1895 driven jet change in CMIP5 and CMIP6 models. Geophysical Research Letters, 47,
1896 e2019GL086695, doi:10.1029/2019GL086695

1897 Outten, S., Esau, I., & Otterå, O. H. (2018). Bjerknes compensation in the CMIP5 climate
1898 models. Journal of Climate, 31(21), 8745-8760, doi: 10.1175/JCLI-D-18-0058.1

1899 Overland, J. E., Turet, P., & Oort, A. H. (1996). Regional variations of moist static energy
1900 flux into the Arctic. Journal of Climate, 9, 54–65, doi:10.1175/1520-
1901 0442(1996)009<0054:RVOMSE>2.0.CO;2

1902 Papritz, L., & Grams, C. M. (2018). Linking low-frequency large-scale circulation patterns to
1903 cold air outbreak formation in the northeastern North Atlantic. Geophysical Research Letters,
1904 45(5), 2542-2553, doi:10.1002/2017GL076921

1905 Papritz, L., & Spengler, T. (2017). A Lagrangian climatology of wintertime cold air
1906 outbreaks in the Irminger and Nordic seas and their role in shaping air-sea heat fluxes.
1907 Journal of Climate, 30, 2717–2737, doi:10.1175/JCLI-D-16-0605.1

1908 Papritz, L. (2017). Synoptic environments and characteristics of cold air outbreaks in the
1909 Irminger Sea. International Journal of Climatology, 37, 193-207, doi:10.1002/joc.4991

1910 Papritz, L., Dunn-Sigouin, E. (2020). What configuration of the atmospheric circulation
1911 drives extreme net and total moisture transport into the Arctic. Geophysical Research Letters,
1912 47, e2020GL089769. doi:10.1029/2020GL089769

1913 Pemberton, P., Nilsson, J., Hieronymus, M., & Meier, H. E. M. (2015). Arctic Ocean Water
1914 Mass Transformation in S–T Coordinates, Journal of Physical Oceanography, 45(4), 1025-
1915 1050, doi:10.1175/JPO-D-14-0197.1

1916 Pérez-Hernández et al. (2019) Structure, Transport, and Seasonality of the Atlantic Water
1917 Boundary Current North of Svalbard: Results From a Yearlong Mooring Array. Journal of
1918 Geophysical Research: Oceans, 124, 3, doi:10.1029/2018JC014759

1919 Perovich, D. K., Light, B., Eicken, H., Jones, K. F., Runciman, K., Nghiem, S. V. (2007).
1920 Increasing solar heating of the Arctic Ocean and adjacent seas, 1979–2005: Attribution and
1921 role in the ice-albedo feedback. Geophysical Research Letters, 34, L19505,
1922 doi:10.1029/2007GL031480.

1923 Peixoto, J., & Oort, A. H. (1992). Physics of Climate: American Institute of Physics.

1924 Pipko, I., S. Pugach, I. Repina, O. Dudarev, A. Charkin, & I. Semiletov (2015), Distribution
1925 and air-sea fluxes of carbon dioxide on the Chukchi Sea shelf, Izvestiya, Atmospheric and
1926 Oceanic Physics, 51, 1088-1102, doi: 10.1134/S0001433815090133.

1927 Pithan, F., Mauritsen, T. (2014). Arctic amplification dominated by temperature feedbacks in
1928 contemporary climate models. Nature Geoscience, 7, 181–184, doi:10.1038/ngeo2071

1929 Pistone, K., Eisenman, I., & Ramanathan, V. (2019). Radiative heating of an ice-free Arctic
1930 Ocean. Geophysical Research Letters, 46, 7474–7480 doi:10.1029/2019GL082914

1931 Polyakov, I. V., G. V. Alekseev, L. a. Timokhov, U. S. Bhatt, R. L. Colony, H. L.Simmons,
1932 D. Walsh, J. E. Walsh, and V. F. Zakharov (2004), Variability of the Intermediate Atlantic
1933 Water of the Arctic Ocean over the Last 100 Years, Journal of Climate, 17(23), 4485–4497,
1934 doi:10.1175/JCLI-3224.1.

1935 Polyakov, I. V., V. a. Alexeev, U. S. Bhatt, E. I. Polyakova, & X. Zhang (2009), North
1936 Atlantic warming: patterns of long-term trend and multidecadal variability, Climate
1937 Dynamics, 34(2-3), 439–457, doi:10.1007/s00382-008-0522-3.

1938 Polyakov et al.(2017) Greater role for Atlantic inflows on sea-ice loss in the Eurasian Basin
1939 of the Arctic Ocean, Science doi:10.1126/science.aai8204.

1940 Rayner, N. A., Parker, D. E., Horton, E. B., Folland, C. K., Alexander, L. V., Rowell, D.
1941 P., Kent, E. C., & Kaplan, A. (2003), Global analyses of sea surface temperature, sea ice, and
1942 night marine air temperature since the late nineteenth century, *J. Geophys. Res.*, 108, 4407,
1943 doi:10.1029/2002JD002670, D14.

1944 Renwick, J. A., & Wallace, J. M. (1996). Relationships between North Pacific wintertime
1945 blocking, El Niño, and the PNA pattern. Monthly weather review, 124(9), 2071-2076,
1946 doi:10.1175/1520-0493(1996)124

1947 Rossby, T., Flagg, C., Chafik, L., Harden, B., & Søiland, H. (2018). A direct estimate of
1948 volume, heat, and freshwater exchange across the Greenland-Iceland-Faroe-Scotland Ridge.
1949 Journal of Geophysical Research: Oceans, 123, 7139–7153, doi:10.1029/2018JC014250

1950 Rossby, T., Chafik, L., & Houpert, L. (2020). What can hydrography tell us about the
1951 strength of the Nordic Seas MOC over the last 70 to 100 years?. Geophysical Research
1952 Letters, 47, e2020GL087456, doi:10.1029/2020GL087456

1953 Ruggieri, P., Alvarez-Castro, M. C., Athanasiadis, P., Bellucci, A., Materia, S., & Gualdi, S.
1954 (2020). North Atlantic circulation regimes and heat transport by synoptic eddies. Journal of
1955 Climate, 33(11), 4769-4785, doi:10.1175/JCLI-D-19-0498.1

1956 Rysgaard, S., Sogaard, D. H., Cooper, M., Pucko, M., Lennert, K., Papakyriakou, T. N.,
1957 Wang, F., Geilfus, N. X., Glud, R. N., Ehn, J., McGinnis, D. F., Attard, K., Sievers, J.,
1958 Deming, J. W., & Barber, D. (2013) Ikaite crystal distribution in winter sea ice and
1959 implications for CO2 system dynamics, The Cryosphere, 7, 707-718, doi:10.5194/tc-7-707-
1960 2013
1961
1962 Sampe, T., & Xie, S. P. (2007). Mapping high sea winds from space: A global climatology.
1963 Bulletin of the American Meteorological Society, 88(12), 1965-1978, doi:10.1175/BAMS-
1964 88-12-1965
1965
1966 Sandø, A. B., Nilsen, J. Ø., Eldevik, T., & Bentsen, M. (2012). Mechanisms for variable
1967 North Atlantic–Nordic seas exchanges. Journal of Geophysical Research: Oceans, 117(C12),
1968 doi: 10.1029/2012JC008177
1969
1970 Shaffrey, L., & Sutton, R. (2006). Bjerknes compensation and the decadal variability of the
1971 energy transports in a coupled climate model. Journal of Climate, 19(7), 1167-1181,
1972 doi:10.1175/JCLI3652.1
1973
1974 Schaffer, J., Kanzow, T. von Appen, W. et al. (2020) Bathymetry constrains ocean heat
1975 supply to Greenland's largest glacier tongue. Nat. Geosci, doi:10.1038/s41561-019-0529-x
1976
1977 Schauer, U., & Beszczynska-Möller, A. (2009). Problems with estimation and interpretation
1978 of oceanic heat transport–conceptual remarks for the case of Fram Strait in the Arctic Ocean.
1979 Ocean Science, 5(4), 487–494. https://doi.org/10.5194/os-5-487-2009
1980
1981 Schweiger, A.J., K.R. Wood, & J. Zhang (2019) Arctic Sea Ice Volume Variability over
1982 1901–2010: A Model-Based Reconstruction. J. Climate, 32, 4731–4752, doi:10.1175/JCLI-
1983 D-19-0008.1
1984
1985 Segtnan, O. H., T. Furevik, & A. D. Jenkins (2011), Heat and freshwater budgets of the
1986 Nordic seas computed from atmospheric reanalysis and ocean observations, J. Geophys. Res.,
1987 116, C11003, doi:10.1029/2011JC006939.
1988
1989 Seierstad, I. A., Stephenson, D. B., & Kvamstø, N. G. (2007). How useful are teleconnection
1990 patterns for explaining variability in extratropical storminess? Tellus A: Dynamic
1991 Meteorology and Oceanography, *59* (2), 170-181, doi:10.1111/j.1600-0870.2007.00226.x
1992
1993 Selyuzhenok, V., Bashmachnikov, I., Ricker, R., Vesman, A., & Bobylev, L. (2020) Sea ice
1994 volume variability and water temperature in the Greenland Sea. The Cryosphere, 14, 477-
1995 495, doi:10.5194/tc-14-477-2020

1996 Semper, S., Våge, K., Pickart, R.S., Valdimarsson, H., Torres, D.J. & Jónsson, S. (2019) The
1997 emergence of the North Icelandic Jet and its evolution from northeast Iceland to Denmark
1998 Strait. Journal of Physical Oceanography, doi:10.1175/JPO-D-19-0088.1.

1999 Semper, S., Pickart, R.S., Våge, K., Larsen, K.M.H., Hátún, H. & Hansen, B. (2020) The
2000 Iceland-Faroe Slope Jet: a conduit for dense water toward the Faroe Bank Channel overflow.
2001 Nature Communications 11, 5390, doi:10.1038/s41467-020-19049-5

2002 Serreze, M. C., A. P. Barrett, A. G. Slater, M. Steele, J. Zhang, & K. E. Trenberth (2007),
2003 The large-scale energy budget of the Arctic, J. Geophys. Res., 112, D11122,
2004 doi:10.1029/2006JD008230
2005
2006 Skagseth, Ø. T. Eldevik, M. Årthun, H. Asbjørnsen, V. Lien & L. H. Smedsrud (2020)
2007 Reduced efficiency of the Barents Sea cooling machine. Nature Climate Change, 2020,
2008 doi:10.1038/s41558-020-0772-6
2009
2010 Skjelvan, I., Johannesen, T. & Miller, L. A., (1999), Interannual variability of fCO2 in the
2011 Greenland and Norwegian Seas, Tellus, 51B, 477-489, doi:10.3402/tellusb.v51i2.16327
2012
2013 Skjelvan, I., et al. (2005) A review of the inorganic carbon cycle of the Nordic Seas and
2014 Barents Sea, 157-176 in The Nordic Seas: an integrated perspective, AGU Geophysical
2015 Monograph 158 (eds. H. Drange, T. Dokken, T. Furevik, R. Gerdes, and W. Berger), 2005
2016
2017 Slater, D. A., Straneo, F., Felikson, D., Little, C. M., Goelzer, H., Fettweis, X., & Holte, J.
2018 (2019) Estimating Greenland tidewater glacier retreat driven by submarine melting, The
2019 Cryosphere, 13, 2489–2509, doi:10.5194/tc-13-2489-2019.
2020
2021 Slater, D. A., Goldberg, D. N., Nienow, P. W., & Cowton, T. R. (2016): Scalings for
2022 submarine melting at tidewater glaciers from buoyant plume theory, J. Phys. Oceanogr., 46,
2023 1839–1855, doi:0.1175/JPO-D-15-0132.1.
2024
2025 Sorteberg, A., & Kvingedal, B. (2006). Atmospheric forcing on the Barents Sea winter ice
2026 extent. Journal of Climate, 19(19), 4772-4784, doi:10.1175/jcli3885.1
2027
2028 Steele, M., Morley, R., & Ermold, W. (2001). PHC: A global ocean hydrography with a high-
2029 quality Arctic Ocean. Journal of Climate, 14(9), 2079-2087, doi:10.1175/1520-
2030 0442(2001)014
2031
2032 Stigebrandt, A. (1981), A model for the thickness and salinity of the upper layer in the Arctic
2033 Ocean and the relationship between the ice thickness and some external parameters. J. Phys.
2034 Oceanogr., 11: 1407-1422, doi:10.1175/1520-0485(1981)011<1407:AMFTTA>2.0.CO;2
2035
2036 Simonsen, K., & P. M. Haugan (1996), Heat budgets for the Arctic Mediterranean and sea
2037 surface heat flux parameterizations for the Nordic Seas, J. Geophys. Res., 101, 6553–6576,
2038 doi:10.1029/95JC03305
2039
2040 Smedsrud, L. H., R. Ingvaldsen, J. E. Ø. Nilsen, & Ø. Skagseth (2010), Heat in the Barents
2041 Sea: Transport, storage and surface fluxes, Ocean Sci., 6(1), 219–234, doi:10.5194/os-6-219-
2042 2010
2043

2044 Smedsrud, L. H., et al. (2013), The role of the Barents Sea in the Arctic climate system, Rev.
2045 Geophys., 51, doi:10.1002/rog.20017.
2046
2047 Smedsrud, L.H., Halvorsen, M. H., Stroeve, J.C., Zhang, R., & Kloster, K. (2017)
2048 Fram Strait sea ice export variability and September Arctic sea ice extent over the last 80
2049 years. The Cryosphere (2017), 11, 65-79, doi:10.5194/tc-11-65-2017
2050
2051 Straneo, F., Sutherland, D.A., Holland, D., Gladish, C., Hamilton, G.S., Johnson, H.L.,
2052 Rignot, E., Xu, Y. & Koppes, M. (2012) Characteristics of ocean waters reaching Greenland's
2053 glaciers. *Annals of Glaciology*, *53*(60), 202-210, doi:10.3189/2012AoG60A059
2054
2055 Straneo, F. & Heimbach, P. (2013) North Atlantic warming and the retreat of Greenland's
2056 outlet glaciers. Nature 504, 36–43 doi:10.1038/nature12854
2057
2058 Stocker, A.N., Renner, A.H. & Knol-Kauffman, M., 2020. Sea ice variability and maritime
2059 activity around Svalbard in the period 2012–2019. *Scientific reports*, *10*(1), pp.1-12,
2060 doi:10.1038/s41598-020-74064-2

2061 Spall, M.A. (2004): Boundary Currents and Watermass Transformation in Marginal Seas. J.
2062 Phys. Oceanogr., 34, 1197–1213, doi:10.1175/1520-0485

2063 Sverdrup, H.U., Johnson, M.W., Fleming, R.H. (1942) The Oceans: Their Physics, Chemistry
2064 and General Biology. Prentice-Hall, New York, 1042 pp.

2065 Swift, J.H. & Aagaard, K. (1981) Seasonal transitions and water mass formation in the
2066 Iceland and Greenland seas. Deep-Sea Research A 28, 1107-1129, doi:10.1016/0198-
2067 0149(81)90050-9.
2068
2069 Takahashi, T., et al. (2009), Climatological mean and decadal change in surface ocean
2070 pCO(2), and net sea-air CO2 flux over the global oceans, Deep-Sea Res Pt Ii, 56(8-10), 554-
2071 577, doi: 10.1016/j.dsr2.2008.12.009.

2072 Takahashi, T., Olafsson, J., Goddard, J. G., Chipman, D. W., & Sutherland, S. C. (1993)
2073 Seasonal-Variation of Co2 and Nutrients in the High-Latitude Surface Oceans - a
2074 Comparative-Study, Global Biogeochem Cy, 7, 843-878, doi:10.1029/93GB02263

2075 Terpstra, A., Renfrew, I. A., & Sergeev, D. E. (2021). Characteristics of Cold-Air Outbreak
2076 Events and Associated Polar Mesoscale Cyclogenesis over the North Atlantic Region. Journal
2077 of Climate, 34(11), 4567-4584, doi:10.1175/JCLI-D-20-0595.1

2078 Timmermans, M.-L., & Marshall, J. (2020) Understanding Arctic Ocean circulation: A
2079 review of ocean dynamics in a changing climate. Journal of Geophysical Research: Oceans,
2080 125, e2018JC014378, doi:10.1029/2018JC014378

2081 Tsujino, Hiroyuki, et al. (2018) JRA-55 based surface dataset for driving ocean–sea-ice
2082 models (JRA55-do), Ocean Modelling 130, 79-139, doi:10.1016/j.ocemod.2018.07.002

2083 Trenberth, K. E., & Shea, D. J. (2006). Atlantic hurricanes and natural variability in 2005.
2084 Geophysical Research Letters, 33, L12704, doi:10.1029/2006GL026894

2085 Trenberth, K. E., & Fasullo, J. T. (2017). Atlantic meridional heat transports computed from
2086 balancing Earth's energy locally. Geoph. Res. Lett., 44(4), 1919-1927,
2087 doi:10.1002/2016GL072475

2088 Trenberth, K. E., Zhang, Y., Fasullo, J. T., & Cheng, L. (2019). Observation-based estimates
2089 of global and basin ocean meridional heat transport time series. J. Climate, 32, 4567-4583,
2090 doi:10.1175/JCLI-D-18-0872.1

2091 Trigo, R.M., Valente, M.A., Trigo, I.F., Miranda, P.M.A., Ramos, A.M., Paredes, D. &
2092 García-Herrera, R. (2008). The Impact of North Atlantic Wind and Cyclone Trends on
2093 European Precipitation and Significant Wave Height in the Atlantic. Annals of the New York
2094 Academy of Sciences, 1146: 212-234, doi:10.1196/annals.1446.014

2095 Tsubouchi, T. et. al (2020) Increased ocean heat transport into the Nordic Seas and Arctic
2096 Ocean over the period 1993-2016. Nature Climate Change, doi:10.1038/s41558-020-00941-3

2097 Vikebø, F. et al. (2003) Wave height variations in the North Sea and on the Norwegian
2098 Continental Shelf, 1881–1999, Continental Shelf Research 23 (2003) 251–263,
2099 doi:10.1016/S0278-4343(02)00210-8

2100 Visbeck et al., 1995. Preconditioning the Greenland Sea for deep convection: ice formation
2101 and ice drift. Journal of Geophysical Research: Oceans, 100, C9, doi: 10.1029/95JC01611.

2102 Våge, K., Pickart, R.S., Spall, M.A., Valdimarsson, H., Jónsson, S., Torres, D.J., Østerhus,
2103 S., Eldevik, T. (2011) Significant role of the North Icelandic Jet in the formation of Denmark
2104 Strait overflow water. Nature Geoscience 4, 723-727, doi:10.1038/ngeo1234.

2105 Våge, K. et al. (2015) Water mass transformation in the Iceland Sea, Deep Sea Research,
2106 101, 98-109, doi:10.1016/j.dsr.2015.04.001.

2107 Våge K., L. Papritz, L. Håvik, M.A. Spall, & G.W.K. Moore (2018) Ocean convection linked
2108 to the recent ice edge retreat along east Greenland. Nature Communications, 9,
2109 doi:10.1038/s41467-018-03468-6

2110 Walsh, J. E. F. Fetterer, J. S. Stewart, & W. L. Chapman (2017) A database for depicting
2111 Arctic sea ice variations back to 1850. Geogr. Rev., 107, 89–107, doi:10.1111/j.1931-
2112 0846.2016.12195.x.

2113 Watson, A.J., P.D. Nightingale, & D. J. Cooper (1995) Modelling atmosphere-ocean CO2
2114 transfer, Phil. Trans. R. Soc. Lond. B, 348, 125-132, doi:10.1098/rstb.1995.0054

2115 Wernli, H. & C. Schwierz (2006) Surface Cyclones in the ERA-40 Dataset (1958–2001). Part
2116 I: Novel Identification Method and Global Climatology. J. Atmos. Sci., 63, 2486–2507,
2117 doi:10.1175/JAS3766.1

2118 Werenskiold, W. (1935) Coastal Currents. Geofys. Publ., Vol. X, p. 13.

2119 Wettstein, J. J., & Wallace, J. M. (2010). Observed patterns of month-to-month storm-track
2120 variability and their relationship to the background flow. Journal of the Atmospheric
2121 Sciences, 67(5), 1420-1437, doi:10.1175/2009JAS3194.1

2122 Wilson, N. J. & F. Straneo (2015), Water exchange between the continental shelf and the
2123 cavity beneath Nioghalvfjerdsbræ (79 North Glacier), Geophys. Res. Lett., 42, 7648–7654,
2124 doi:10.1002/2015GL064944

2125 Woodgate, R. A., Aagaard, K., Weingartner, T. J. (2006). Interannual changes in the Bering
2126 Strait fluxes of volume, heat and freshwater between 1991 and 2004. Geophysical Research
2127 Letters, 33, L15609, doi:10.1029/2006GL026931

2128 Woods, C., Caballero, R., & Svensson, G. (2013). Large-scale circulation associated with
2129 moisture intrusions into the Arctic during winter. Geophysical Research Letters, 40(17),
2130 4717-4721, doi: 10.1002/grl.50912

2131 Woollings, T., Hannachi, A., & Hoskins, B. (2010). Variability of the North Atlantic eddy-
2132 driven jet stream. Quarterly Journal of the Royal Meteorological Society, 136(649), 856-868,
2133 doi:10.1002/qj.625Woollings, T., Czuchnicki, C., & Franzke, C. (2014). Twentieth century
2134 North Atlantic jet variability. Quarterly Journal of the Royal Meteorological Society,
2135 140(680), 783-791, doi:10.1002/qj.2197

2136 Wunsch, C., 2020: Is the Ocean Speeding Up? Ocean Surface Energy Trends. J. Phys.
2137 Oceanogr., 50, 3205–3217, doi:10.1175/JPO-D-20-0082.1.

2138 Yashayaev, I. & Seidov, D. (2015) The role of the Atlantic Water in multidecadal ocean
2139 variability in the Nordic and Barents Seas. Prog. Oceanogr. 132, 68–127,
2140 doi:10.1016/j.pocean.2014.11.009

2141 Yasunaka, S., et al. (2018) Arctic Ocean CO2 uptake: an improved multiyear estimate of the
2142 air–sea CO2 flux incorporating chlorophyll a concentrations, Biogeosciences, 15, 1643–1661,
2143 doi:10.5194/bg-15-1643-2018.

2144 Young, I. R. & Ribal, A. (2019) Multiplatform evaluation of global trends in wind speed and
2145 wave height, Science, Vol. 364, Issue 6440, pp. 548-552, doi: 10.1126/science.aav9527

2146 Zhang, J., Steele, M., Rothrock, D. A., & Lindsay, R. W. (2004). Increasing exchanges at
2147 Greenland-Scotland Ridge and their links with the North Atlantic Oscillation and Arctic sea
2148 ice. Geophysical research letters, 31(9), doi: 10.1029/2003GL019304

2149 Østerhus, S. et al. (2019) Arctic Mediterranean exchanges: a consistent volume budget and
2150 trends in transports from two decades of observations, Ocean Sci., 15, 379-399,
2151 doi:10.5194/os-15-379-2019

2152 Årthun, M., Eldevik, T., Smedsrud, L. H., Skagseth, Ø., & Ingvaldsen, R. (2012),
2153 Quantifying the influence of Atlantic heat on Barents Sea ice variability and retreat, J. Clim.,
2154 25, 4736–4743, doi:10.1175/JCLI-D-11-00466.1.

2155 Årthun, M. & Eldevik, T. (2016) On Anomalous Ocean Heat Transport toward the Arctic and
2156 Associated Climate Predictability, J.lim. 29(2), 689–704, doi:10.1175/JCLI-D-15-0448.1